POLITECNICO DI TORINO

Corso di Laurea Magistrale
in INGEGNERIA MECCANICA

Tesi di Laurea Magistrale

A linear approach to the fluid-dynamic solution of large district heating networks

Case study: Turin network

Relatore

prof. Vittorio Verda

Correlatrice

ing. Elisa Guelpa

Candidato

Riccardo Papacchini

A.A. 2017/2018

To my parents Wilma&Gianni.

Index

Abstract

District heating is one of the most efficient and environmentally friendly ways to satisfy heat demand in densely populated areas. It allows reducing the global fuel consuption for heating purposes thanks to a centralized production. In these systems, thermal energy is sent to users through an underground network that provides hot water to the users. This paper has been developed in collaboration with IREN s.p.a. and it deal with Turin district heating network, that is, with its 5700 m^3 of heated volume, Italy's biggest network. Thermo-fluid-dynamic simulations of such large networks usually require large computational resources becouse of the complex topology that also involved loops.

The main novelty of this work is the possibility of simulating the thermal-fluid-dynamic quantity in large networks through a very fast model. Having such compact model is useful to analyse the way extensions and alternative management strategies affect the thermal load evolution. In this respect, peak shaving strategies are adopted to reduce the thermal energy that must be provide during the morning peak, by modifying the start-up schedule at the users. These strategies also allow a better and cheaper operation of the thermal plants. For that reason, an efficient numeric scheme is required to evaluate the effectiveness of these strategies.

This proposed model takes advantage of the simplicity of the fluid dynamics solution of tree-shape networks, to modify the topology of the Turin network, moving from the resolution of a nonlinear problem to a linear one.

Introduction

The case study is the Turin District Heating System that provides heat through a double pipe network with an extension of 528 km. It is mainly divided into two parts directly connected: the transport network and the distribution networks. The first expands across the city area and links the thermal plants to the distribution networks; the seconds link a group of buildings to the transport network. There are many distribution networks as the group of buildings are and have typically a tree-shape configuration. The trasport network, instead, is unique, is characterized by large mass flow rates and shows close path, aimed at guarantee service reliability in case of pipes failures.

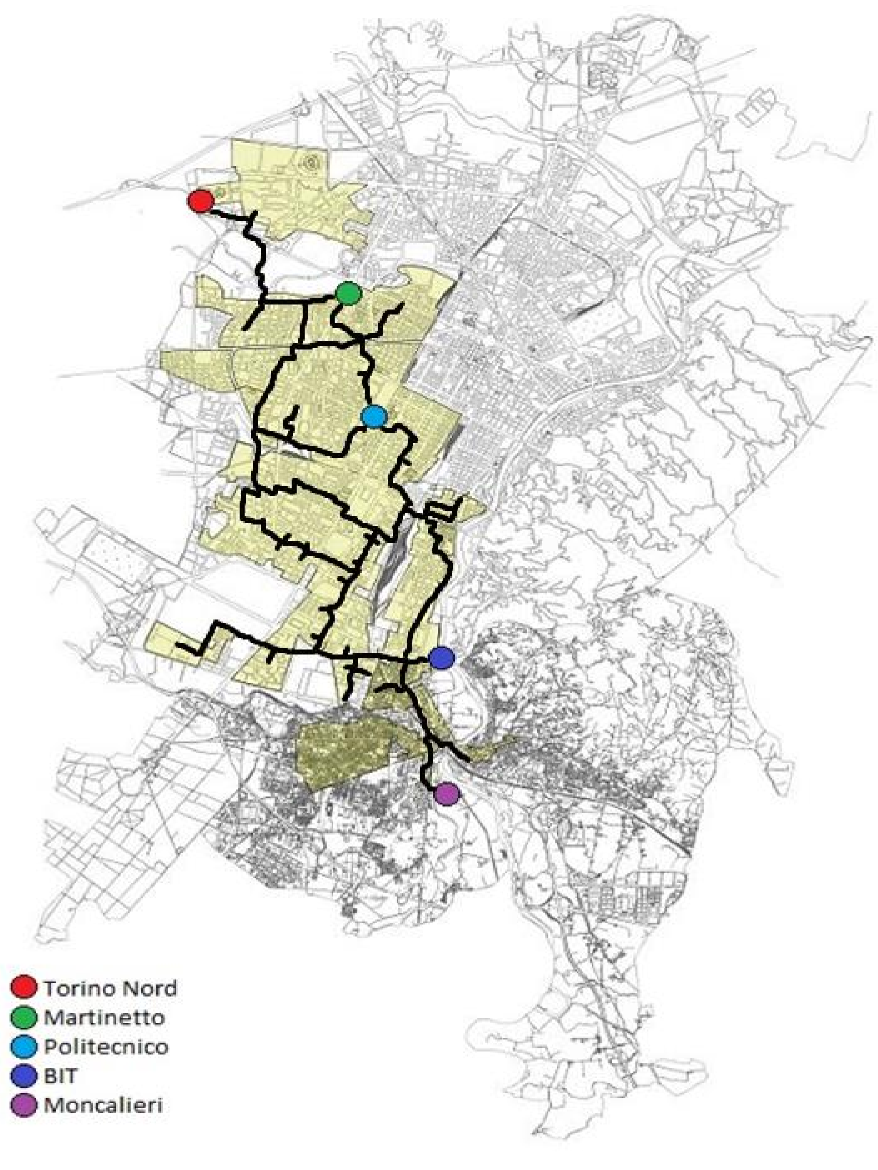

Figure 1 The Turin transport network (Iren Energia, s.d.)

Calculation of mass flow rates in a tree-shape networks is agile and implies only the solution of the continuity equation, which means that a linear system has to be solved.

If loops are considered, solution became more complex and implies combined calculation of mass flow rates and pressures, i.e. the solution of the continuity equation and the momentum equation. The algebraic system derived from the two relations has as many equations as the unknown are, but its solution is not as easy as it seems, because of three reasons:

- Continuity and momentum equations are coupled, hence have to be solved simultaneously
- The momentum equation is nonlinear

As shown in the following, a robust solution to this type of problems is the SIMPLE[1] algorithm, which is an iterative strategy based on a "guess and correct" procedure. However, if the number of nodes becomes large, this approach causes computational time to increase significantly.

In this paper, an alternative approach is proposed to the solution of the fluid-dynamic of the transport network (network henceforth), in order to reduce computational time in case of common computation frequencies.

The complexity of the solution is closely linked to the network topology, hence the idea of modifing the transport network so that its description doesn't match to the real topology but to a tree-shape ones.

This approach implies that some branches have to be removed in order to modify the topology of fluid network and new mass flow rates boundary conditions has to be applied in their place. Such new boundary conditions are evaluated through a multilinear regression, whose coefficients are calculated on simulations done using the SIMPLE strategy, as a function of mass flow rates at the power plants.

In order to perform an analysis of the accuracy of this type of model, mass flow rates and temperatures are evaluated and a comparizon is made with respect to results coming from the nonlinear fluid dynamic model (Guelpa et. al., 2017), which is assume as the most reliable model. Different scenarios are proposed in the end to appreciate the variation in the accuracy with the global load.

[1]Semi-Implicit Method for Pressure Linked Equations - Patankar and Splanding (1980)

1.0 The Thermo fluid dynamic model

The network fluid dynamic simulation consists in evaluating mass flow rates in each branch. In case of tree-shape networks, this goal requires the continuity equation to be solved. If the network has loops, a solution of the momentum equation is also required to evaluate the pressure in each node. Once mass flow rates are known, the energy equation has to be solved to evaluate temperatures in each node of the network.

The theoretical basis of the thermo-fluid dynamic model is mentioned hereafter, in order to introduce conserved and nonconserved quantities that are involved in the calculation.

Further details on the conservation laws are available in (Sciacovelli et. al., 2015).

1.1 The continuity equation

The differential three-dimensional expression of the continuity equation can be written as the sum of partial derivatives with respect to time and respect to the spatial coordinates:

$$\frac{\partial \rho}{\partial t} + \nabla \cdot \rho \boldsymbol{v} = 0 \qquad (1.1)$$

Or, using the definition of substantial derivative:

$$\frac{D\rho}{Dt} + \rho \nabla \cdot \boldsymbol{v} = 0 \qquad (1.2)$$

where ρ is the volumetric mass density and v is a vector whose elements are the velocities along the three axis.

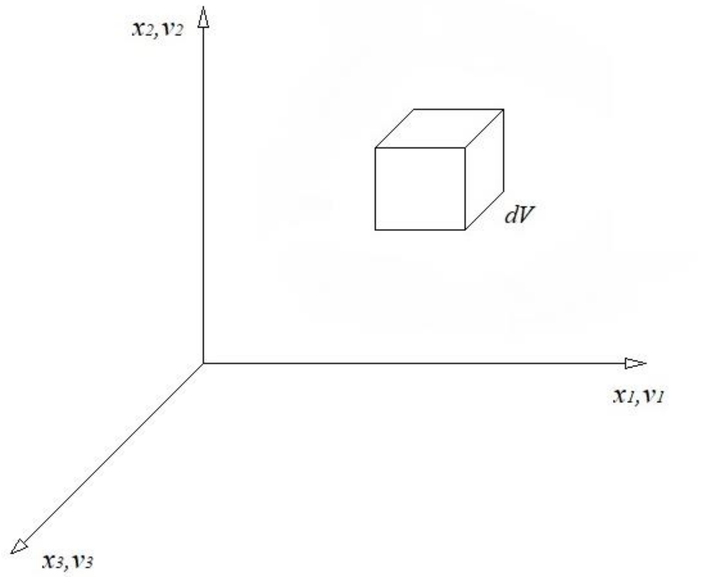

Figure 2 The volume element ΔV of a coninuum body (Sciacovelli, 2015)

1.2 The momentum equation

The rate of change of momentum of a fluid can be expressed as the sum of a contribution of momentum due to convection plus the external forces.

Referring to a generic control volume CV, the first contribution is the net rate of momentum across the boundary of the control the volume, while external forces are the summation of surface forces (pressure and viscous forces) and body forces, such as gravity.

The differential formulation[2] of the momentum equation can be written using the vector notation as:

$$\frac{\partial \rho \boldsymbol{v}}{\partial t} = -\nabla \cdot \rho \boldsymbol{v}\boldsymbol{v} - \nabla p - \nabla \cdot \boldsymbol{\tau} + \rho \boldsymbol{g} \qquad (1.3)$$

where p is the static pressure, $\boldsymbol{g}$ is the gravitational field and $\boldsymbol{\tau}$ is the viscous stress tensor, whose expression (Batchelor, 1967) is formulated in the case of a Newtonian fluid; according to this model

[2] Augustin-Louis Cauchy (1789-1857)

stresses at the boundary of the control volume are proportional to the velocity field in the following way:

$$\boldsymbol{\tau} = -\mu(\nabla \boldsymbol{v} + \nabla \boldsymbol{v}^T) + \left(\frac{2}{3}\mu - k\right)(\nabla \cdot \boldsymbol{v})\boldsymbol{I} \qquad (1.4)$$

Where μ is the viscosity, k is the dilatational viscosity and $\boldsymbol{I}$ the identity matrix.

1.3 The energy equation

In order to perform an energy analysis of the network, the energy equation is now introduced. Its expression can be derived by considering an energy balance on a generic control volume, without taking into account nuclear, chemical or radiative energy.

$$\frac{\partial}{\partial t}\left(\rho u + \frac{1}{2}\rho v^2\right) dV = -\nabla \cdot (\rho \boldsymbol{e} v) dV - \nabla \cdot \boldsymbol{q} dV - \nabla \cdot p \boldsymbol{v} dV - \nabla(\boldsymbol{\tau} \cdot \boldsymbol{v}) dV + \rho \boldsymbol{g} \cdot \boldsymbol{v} dV \qquad (1.5)$$

The term on the left hand side is the net rate of change of the total energy, expressed as the variation in time of the internal energy and kinetic energy

The first term on the right hand side is the net convective flow rate of the total energy.

The second term on the right hand side is the net heat flux, where $\boldsymbol{q}$ is the heat flux which can be formulated through Fourier's Law[3].

The third term on the right hand side is the rate of work done by pressure

The fourth term on the right hand side is the rate of work done by viscous stresses, expressed as product between the stress tensor $\boldsymbol{\tau}$ (Eq. (1.4)) and the velocity vector $\boldsymbol{v}$.

The fifth term on the right hand side is the rate of work done by gravity.

In order to achieve a more suitable formulation of the energy equation, expressions of non-conserved quantities have to be expressed.

---

[3] $\boldsymbol{q} = -k\nabla T$, where k is the conductivity and T temperature.

The Mechanical Energy can be obtained by multiplying Eq. (1.3) by the velocity vector $\boldsymbol{v}$:

$$\frac{\partial}{\partial t}\left(\frac{1}{2}\rho v^2\right) = -\nabla \cdot \left(\frac{1}{2}\rho \boldsymbol{v} v^2\right) - \boldsymbol{v} \cdot \nabla p - \boldsymbol{v} \cdot \nabla \cdot \boldsymbol{\tau} + \rho \boldsymbol{v} \cdot \boldsymbol{g} \tag{1.6}$$

The second and the third term on the right hand side of Eq. (1.6) can be rewrite according to the differential operators property[4]:

$$\frac{\partial}{\partial t}\left(\frac{1}{2}\rho v^2\right) = -\nabla \cdot \left(\frac{1}{2}\rho \boldsymbol{v} v^2\right) - \nabla \cdot p\boldsymbol{v} + p\nabla \cdot \boldsymbol{v} - \nabla \cdot (\boldsymbol{\tau v}) + \boldsymbol{\tau}: \nabla \boldsymbol{v} + \rho \boldsymbol{v} \cdot \boldsymbol{g} \tag{1.7}$$

Internal Energy instead result from the subtraction between Eq. (1.7) and the Mechanical energy equation:

$$\frac{\partial}{\partial t}(\rho u) = -\nabla \cdot (\rho u \boldsymbol{v}) - \nabla \cdot \boldsymbol{q} - p\nabla \cdot \boldsymbol{v} - \boldsymbol{\tau}: \nabla \boldsymbol{v} \tag{1.8}$$

If the substantial derivative definition[5] is used, Eq.(1.8) can be rewrite to obtain:

$$\rho \frac{Du}{Dt} = -\nabla \cdot \boldsymbol{q} - p\nabla \cdot \boldsymbol{v} - \boldsymbol{\tau}: \nabla \boldsymbol{v} \tag{1.9}$$

Using the thermodynamic definition of enthalpy[6], Eq. (1.9) can be rewrite as the Enthalpy equation:

$$\rho \frac{Dh}{Dt} = -\nabla \cdot q - \tau: \nabla v + \frac{Dp}{Dt} \tag{1.10}$$

Where continuity Eq. (1.2) has been applied.

If enthalpy term mechanic equation[7] is introduced:

$$\rho c_p \frac{DT}{Dt} = \nabla \cdot (k\nabla T) - \boldsymbol{\tau}: \nabla \boldsymbol{v} + \beta T \frac{Dp}{Dt} \tag{1.11}$$

---

4 $\nabla \cdot (a\boldsymbol{b}) = \boldsymbol{b} \cdot a + a\nabla \cdot \boldsymbol{b}$ and $\nabla \cdot (\boldsymbol{A} \cdot \boldsymbol{b}) = \boldsymbol{b} \cdot \nabla \cdot (A^T) + \boldsymbol{A}: \nabla \boldsymbol{b}$

5 $\rho \frac{DZ}{Dt} = \frac{\partial(\rho Z)}{\partial t} + \nabla \cdot (\rho \boldsymbol{v} Z)$

6 $h = u + (1/\rho)p \rightarrow \frac{Dh}{Dt} = \frac{Du}{Dt} + \frac{1}{\rho}\frac{Dp}{Dt} - \frac{p}{\rho^2}\frac{D\rho}{Dt}$

7 $dh = c_p dT + \frac{1}{\rho}(1 - \beta T)dp$, where $\beta \doteq -\frac{1}{\rho}\left(\frac{\partial \rho}{\partial T}\right)_p$ is the thermal expantion coefficient

where the first term on the right-hand side is the conductive term resulting from the Fourier's formulation.

Eq. (1.11) is a linear relation that express the definitive form of the energy equation, useful to temperatures calculation.

2.0 Physical approach and assumptions

A one-dimensional model has been used to simulate the fluid dynamic behavior of this district heating network (DHN). The prevalence of the pipes length respect to the other two dimensions allows one to neglect velocity and temperature variation along the radius and to substitute them with average values in order to reduce computational efforts.

2.1 The continuity equation

The mass conservation has to be applied in each node of the network, as a balance between mass flow rates that crosses the boundary of the specific control volume, and can be expressed by integrating continuity equation over a control volume CV that involve such node:

$$\int_{CV} \frac{\partial \rho}{\partial t} dV + \int_{CV} \frac{\partial \rho v_1}{\partial x_{\mathbf{1}}} dV = 0 \tag{2.1}$$

If an incompressible fluid and a fixed CV are considered, Eq. (2.1) can be rewritten as:

$$\frac{d}{dt}\rho \int_{CV} dV + \rho \int_{CA} v_1 \cdot \boldsymbol{n} \, dA = 0 \tag{2.2}$$

where the Gauss theorem has been used in order to reduce the second term into a surface integral.

From this integration derive the final expression of the continuity equation, in witch external mass flow rates can be can isolated in order to considered those flows that has to be set as a fluid dynamic boundary condition in each junction (i.e. mass flow rates exchanged with users).

$$\frac{d\,M}{dt} + \sum_j \rho_j v_{1,j} A_j + G_{ext} = 0 \tag{2.3}$$

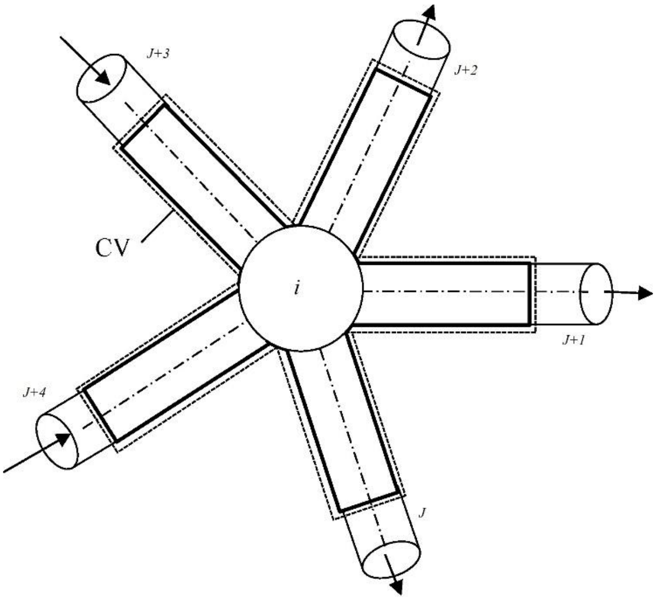

Figure 3 Control volume for the continuity equation applied to a junction (Sciacovelli, 2015)

$$\rho_j v_{1,j} A_j + \rho_{j+1} v_{1,j+1} A_{j+1} + \rho_{j+2} v_{1,j+2} A_{j+2} - \rho_{j+3} v_{1,j+3} A_{j+3} - \rho_{j+4} v_{1,j+4} A_{j+4} + G_{ext\,i} = 0 \quad (2.4)$$

2.2 The momentum equation

In the same way, assumptions are introduced for the momentum equation.

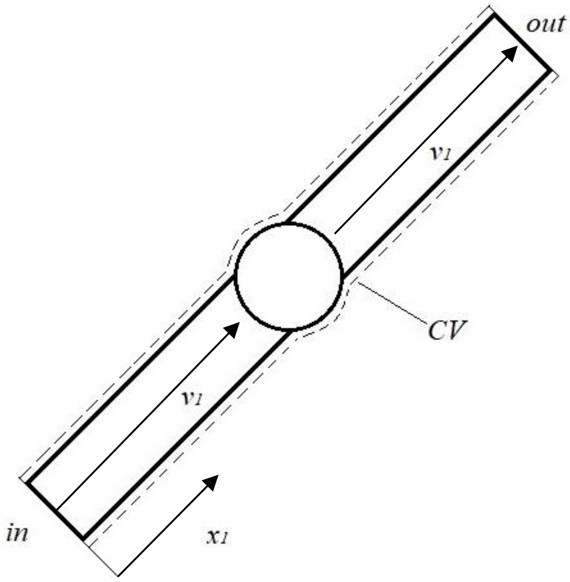

Figure 4 Network branch (Sciacovelli, 2015)

Eq (1.3) can be integrated over the control volume CV using the one-dimensional formulation:

$$\int_{CV} \rho \frac{\partial v_1}{\partial t} dV = -\int_{CV} \rho v_1 \frac{\partial v_1}{\partial x_1} dV - \int_{CV} \frac{\partial p}{\partial x_1} dV - \int_{CV} F_{FRICT}\, dV + \int_{CV} F_{x_1}\, dV \qquad (2.5)$$

Where the contribution of the viscous forces F_{FRICT} has been modeld through semi-empirical correlation. A momentum source term is introduced in order to collect local effects contributions due to pumps or junctions, in addition to gravity:

$$F_{x_1} = F_{PUMP} + F_{LOCAL} + \rho g_{x_1} \qquad (2.6)$$

If an incompressible fluid is considered, integration of the steady state formulation of the Eq. (2.5) leads to:

$$\rho\frac{(v_{1,in})^2-(v_{1,out})^2}{2}S+(p_{in}-p_{out})S-\rho g(z_{out}-z_{in})S-\Delta P_{FRICT}\,S-\Delta P_{LOCAL}S+ \qquad (2.7)$$

$$+\Delta P_{PUMP}\,S=0$$

Where:

- ΔP_{FRICT} pressure difference due to friction;
- ΔP_{LOCAL} pressure difference due to local losses;
- ΔP_{PUMP} pressure difference related with the work pumps and fans;
- $\rho g(z_{out}-z_{in})$ gravitational term difference
- $\rho\frac{(v_{1,in})^2-(v_{1,out})^2}{2}$ kinetic energy difference

Or equivalently:

$$(P_{in}-P_{out})-\Delta P_{FRICT}-\Delta P_{LOCAL}+\Delta P_{PUMP}=0 \qquad (2.8)$$

Where the definition of total pressure[8] P has been used.

Unsteady terms for both continuity and momentum equation are assumed negligible in fact the fluid-dynamic perturbations travel the entire network in a period of time of few seconds, smaller than time steps adopted in the numeric scheme.

Using the characteristic equations for friction and local losses (Appendix A), Eq. (2.8) can be written as:

$$P_{in}-P_{out}=-\frac{1}{2}\frac{G^2}{\rho\,S^2}\left(f\frac{L}{D_h}+\sum_k\beta_k\right)-\Delta P_{PUMP} \qquad (2.9)$$

[8] $P\doteq p+\rho\frac{v^2}{2}+\rho gz$

2.3 The energy equation

Eq. (1.11) is not directly useful to the thermal analysis of the network. A useful formulation is the so called "temperature" formulation of the energy equation:

$$\frac{\partial(\rho c_p T)}{\partial t} + \nabla \cdot (\rho c_p \boldsymbol{v} T) = k\nabla^2 T - \varphi_l \tag{2.10}$$

Where a negative source term has been introduced to include thermal losses through the ground.

Eq. (2.10) is a specific formulation of the enthalpy equation in which some simplifying assumptions has been carried out (constant thermal conductivity k, negligible viscous term, and negligible compressibility effects).

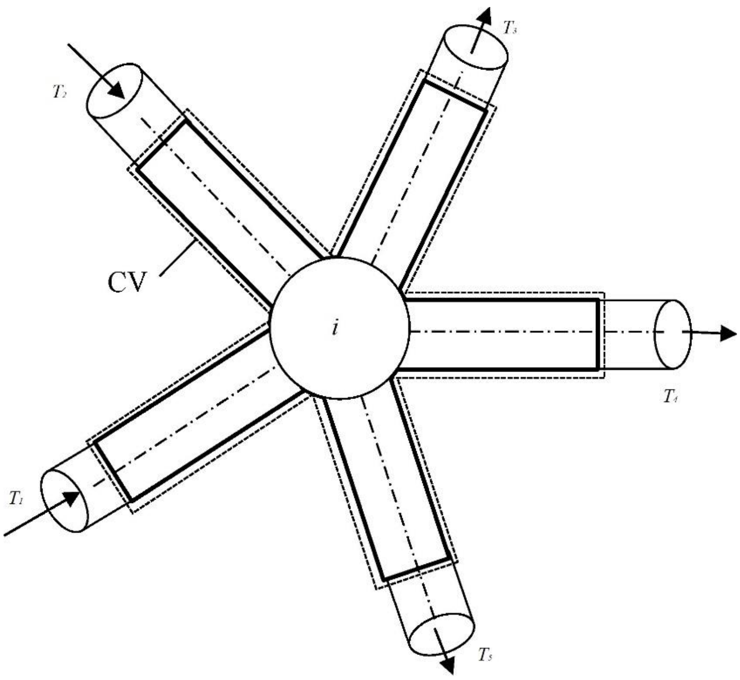

Figure 5 Control volume for the energy equation applied to a junction

The integration of Eq. (2.10) over the CV leads to the energy equation for the i-th node (junction):

$$\int_{CV} \frac{\partial(\rho c_p T)}{\partial t} dV + \int_{CV} \frac{\partial(\rho c_p v_1 T)}{\partial x_1} dV = \int_{CV} k \frac{\partial^2 T}{\partial x_1^2} dV - \int_{CV} \varphi_l \, dV \tag{2.11}$$

$$\frac{\partial\left(\rho c_p T\right)}{\partial t}\Delta V + \sum_j \rho_j c_{p,j} v_{1,j} T_j A_j = -\,\varphi_{l,i} \tag{2.12}$$

where the conductive term has been neglect respect to the convective one.

Density is also assumed as a contant.

In this section a steady state analysis is reported, so the unsteady term in Eq. (2.12) is neglected:

$$\sum_j \rho_j c_p v_{1,j} T_j A_j = -\,\varphi_{l,i} \tag{2.13}$$

Furthermore, a proper heat transfer correlation has to be introduce to consider heat losses towards the environment:

$$\sum_j c_p T_j G_j = -\sum_j \frac{L_j}{2}\Omega_j U_j (T_i - T_\infty) \tag{2.14}$$

Where Ω_j is the perimeter, U_j is the global heat transfer coefficient, and T_∞ is the environment temperature.

3.0 Numerical approach

3.1 One-Dimensional modeling of tree-shape fluid networks

The first issue is to apply continuity equation to the whole network, so a proper topological description of the network is required.

To have this, the *Graph Theory*[9] has been used. According to this theory, the network topology is expressed by the *Incidence Matrix A*, that is characterized by a number of rows that is equal to the number of nodes and a number of columns equal to the number of branches. The generic element $A_{i,j}$ is equal to 1 if the i-th node is the inlet node of the j-th branch, while it is -1 if the i-th node is an outlet node of the j-th branch and it is 0 in all the other cases.

A progressive notation has to be assigned to nodes and branches separately.

A=

	j-1	j	j+1	j+2	j+3
i-2	+1	0	0	0	0
i-1	-1	+1	0	0	0
i	0	-1	+1	-1	+1
i+1	0	0	-1	0	0
i+2	0	0	0	+1	0
i+3	0	0	0	0	-1

Figure 6 The *Incidence* Matrix

According to the continuity equation, such networks require the solution of a linear system:

$$\mathbf{A} \cdot \mathbf{G} = \mathbf{G}_{ext} \tag{3.1}$$

where **G** is a 1-by-NB vector whose elements are the unknown mass flow rates that flows in each branch of the network. Column vector $\mathbf{G_{ext}}$ has as many elements as the nodes are and contain the external mass flow rates exchanged (extracted or injected) at the i-th node; if no exchange occurs, the i-th value will be zero.

[9] Deo (2004); Chandrashekar and Wong (1982)

3.2 One-Dimensional modeling of fluid networks (with loops) – The *Full Model*

The fluid dynamic solution of networks that show close paths requires the combined solution of both continuity and momentum equation.

In order to cast a suitable matrix form of the momentum equation, hydraulic Resistance (Appendix B) can be introduced in Eq. (2.9) so that:

$$P_{in} - P_{out} = R \cdot \, G - \Delta P_{PUMP} \tag{3.2}$$

The right-hand side of Eq. (3.2) can be expressed in each branch using the incidence matrix:

$$\Delta P_j = \boldsymbol{A}^T \cdot P_j \tag{3.3}$$

Hence the matrix form of the momentum equation can be write as:

$$\boldsymbol{A}^T \cdot \boldsymbol{P} = \boldsymbol{R} \cdot \boldsymbol{G} - \boldsymbol{t} \tag{3.4}$$

Where the conductance matrix $\boldsymbol{Y} = \boldsymbol{1}/\boldsymbol{R}$ as been introduced.

Vector $\boldsymbol{G}$, whose elements are the mass flow rates flowing in each branch of the network, is obtained as:

$$\boldsymbol{G} = \boldsymbol{Y} \cdot \boldsymbol{A}^T \cdot \boldsymbol{P} - \boldsymbol{Y} \cdot \boldsymbol{t} \tag{3.5}$$

Most of the critical issues are related to the momentum equation, particularly in the hidden dependence in the conductance due to the advective term, that ends up with a nonlinear relation; furthermore, mass flow rates appear in both continuity and momentum equation, hence a simultaneous solution has to be reached.

3.2.1 The SIMPLE algorithm

A way to solve these problems is to adopt a combined application of two algorithms: the SIMPLE and the fixed point algorithm. The SIMPLE[10] is an iterative strategy based on a "guess and correct" procedure that allows one to have a simultaneous solution of both continuity and momentum equation.

The "true" value of mass flow rate and pressure can be expressed as the sum of a guess value (*) and a correction ('):

$$\boldsymbol{G} = \boldsymbol{G}^* + \boldsymbol{G}' \tag{3.6}$$

$$\boldsymbol{P} = \boldsymbol{P}^* + \boldsymbol{P}' \tag{3.7}$$

If the guess momentum equation is considered:

$$\boldsymbol{G}^* = \boldsymbol{A}^{\boldsymbol{T}} \cdot \boldsymbol{Y}^* \cdot \boldsymbol{P}^* - \boldsymbol{Y}^* \cdot \boldsymbol{t} \tag{3.8}$$

a new relation can be expressed as the difference between the true momentum equation (Eq. (3.5)) and the guess momentum equation:

$$\boldsymbol{G} - \boldsymbol{G}^* = \boldsymbol{A}^{\boldsymbol{T}} \cdot (\boldsymbol{Y} \cdot \boldsymbol{P} - \boldsymbol{Y}^* \cdot \boldsymbol{P}^*) + \boldsymbol{t} \cdot (\boldsymbol{Y} - \boldsymbol{Y}^*) \tag{3.9}$$

Assuming weak nonlinearities and $\boldsymbol{Y} = \boldsymbol{Y}^*$**,** the right-hand side of the Eq. (3.9) can be modified, so that:

$$\boldsymbol{G} - \boldsymbol{G}^* = \boldsymbol{A}^{\boldsymbol{T}} \cdot \boldsymbol{Y}^* \cdot (\boldsymbol{P} - \boldsymbol{P}^*) = \tag{3.10}$$

$$\boldsymbol{G}' = \boldsymbol{A}^{\boldsymbol{T}} \cdot \boldsymbol{Y}^* \cdot \boldsymbol{P}' \tag{3.11}$$

At this point Eq. (3.1) can be written using the guessed-correction decomposition and substitute in Eq. (3.11), so that:

$$\boldsymbol{A} \cdot \boldsymbol{Y}^* \cdot \boldsymbol{A}^{\boldsymbol{T}} \cdot \boldsymbol{P}' = -\boldsymbol{A} \cdot \boldsymbol{G}^* - \boldsymbol{G}_{\boldsymbol{ext}} \tag{3.12}$$

Eq. (3.12) can be rewrite as:

$$\boldsymbol{H} \cdot \boldsymbol{P}' = \boldsymbol{b} \tag{3.13}$$

[10] Semi-Implicit Method for Pressure Linked Equations - Patankar and Splanding (1980)

Where $\boldsymbol{H} \doteq \boldsymbol{A} \cdot \boldsymbol{Y}^{*} \cdot \boldsymbol{A}^{\boldsymbol{T}}$.

Once the guess **P*** and **G*** are set, Eq. (3.8) can be solved and P' and G' can be evalueted through Eq. (3.13) and Eq. (3.11) respectively. Nevertheless, the resulting "true" values of P and G are not consistent with the real ones because of the assumption $\boldsymbol{Y} = \boldsymbol{Y}^{*}$ made in Eq. (3.11).

As a consequence, an iteration strategy as to be applied in order to recover the initial guess values **P*** and **G*** and reach the exact ones. This strategy is illustrated in *Figure 7*.

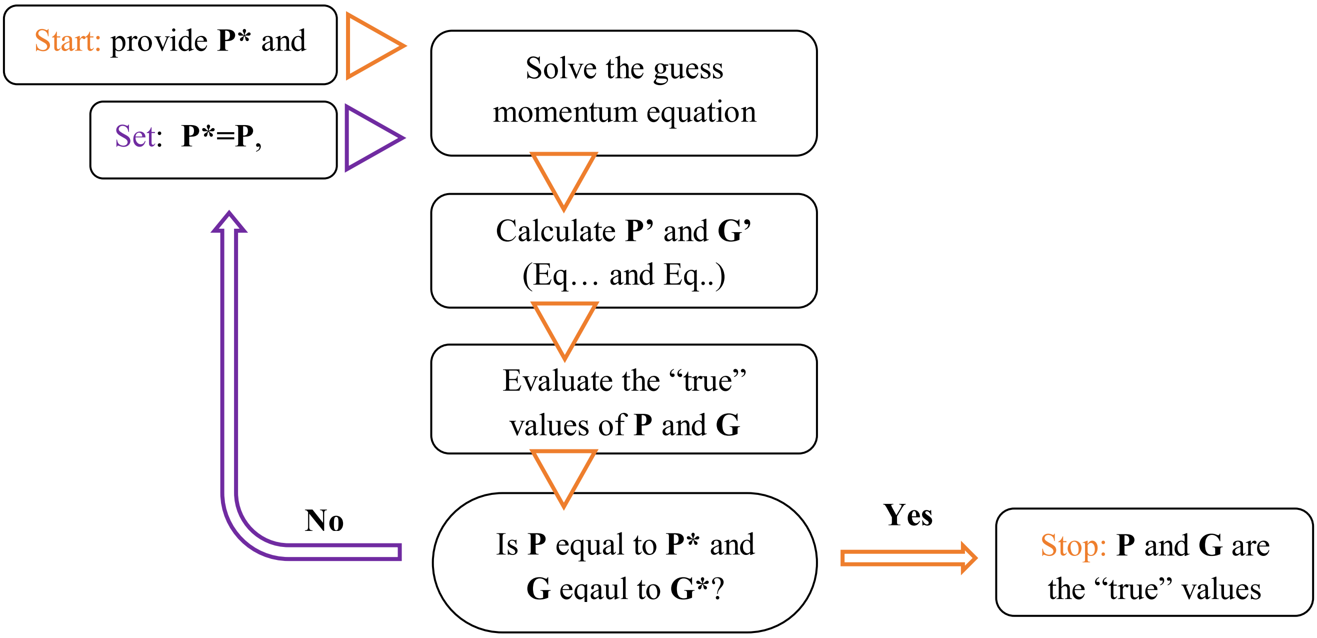

***Figure** 7* The SIMPLE algorithm

Despite the assumption of weak nonlinearity, the momentum Eq. (3.9) is still nonlinear, so a proper numerical scheme has to be use to handle it. To do this, fixed point method is adopted.

This iterative method provides the guess value G* in order to assure the convergence.

According to the conductance definition, Eq. (3.8) can be reformulated as:

$$G^{*} = \boldsymbol{\Lambda}(G^{*}) \tag{3.14}$$

Where $\boldsymbol{\Lambda}(\boldsymbol{G}^{*}) = \boldsymbol{Y}(\boldsymbol{G}^{*}) \cdot \boldsymbol{A}^{\boldsymbol{T}} \cdot \boldsymbol{P}^{*} + \boldsymbol{Y}(\boldsymbol{G}^{*}) \cdot \boldsymbol{t}$

In each iteration, the updated guess value can be expressed as a function of the previous guess value:

$$\boldsymbol{G}^{*}_{(k+1)} = \boldsymbol{\Lambda}\left(\lambda_1 \cdot \boldsymbol{G}^{*}_{(k)} + \lambda_2 \cdot \boldsymbol{G}^{*}_{(k-1)}\right) \tag{3.15}$$

Where λ_1 and λ_2 are under-relaxation coefficents, chose so that $\lambda_1+\lambda_2 = 1$.

The update of G* stops when the difference between $G^*_{(k+1)}$ and $G^*_{(k)}$ is below a set tollerance.

Figure 8 shows the full numeric scheme in which the fixed point algorithm has been highlighted in red.

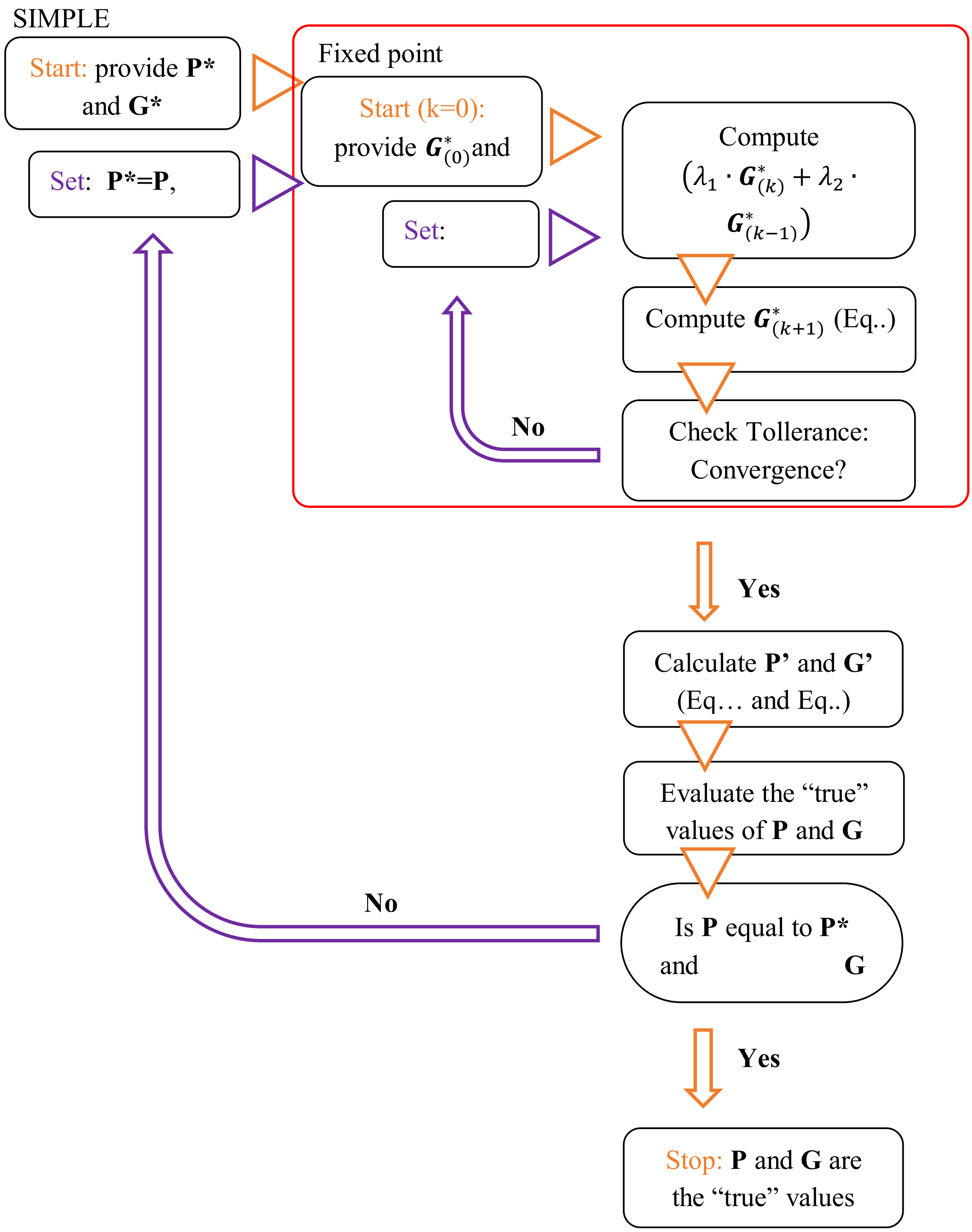

Figure 8 The algorithm for the solution of the momentum equation

Reference to this section can be find in (Sciacovelli, 2015)

3.3 The thermal model

The thermal problem requires that the energy equation (Eq. (2.14)) has to be solved in each *i-th* node of the network.

In order to apply Eq. (2.14) in every node of the network, the set of equations is expressed in matrix form:

$$\boldsymbol{K} \cdot \boldsymbol{T} = \boldsymbol{f} \tag{3.16}$$

where $\boldsymbol{T}$ is a 1-by-NN vector unknown temperatures, $\boldsymbol{f}$ is a 1-by-NN vector of known values and $\boldsymbol{K}$ is the so called Stiffness Matrix (a NN-by-NN matrix). To assemble System (3.16), temperature boundary conditions have to be applied first. According to Eq. (2.14), a proper strategy has to be adopt in order to evaluate temperatures T_j at the boundary of the control volume CV.

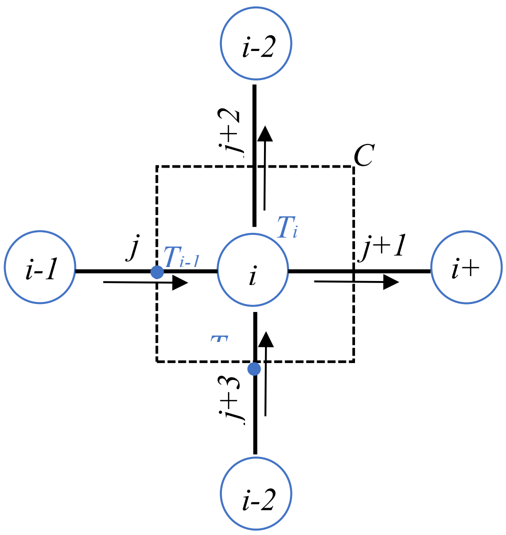

Figure 9 Energy conservation for the *i*-th node

A solution to this type of problems, where convective phenomenon prevails, is the Upwind Scheme, a simple strategy in which boundary temperatures T_j are assume equal to the temperatures in the upstream nodes, respectivly.

Eq. (2.14) for the *i*-th row (node) of System (3.16) becomes:

$$\left(c_p\left(G_{j+1}+G_{j+3}\right)+\frac{1}{2}\left(L_j\Omega_jU_j+L_{j+1}\Omega_{j+1}U_{j+1}+L_{j+2}\Omega_{j+2}U_{j+2}+L_{j+3}\Omega_{j+3}U_{j+3}\right)\right)T_i - c_pG_jT_{i-1} - c_pG_{j+2}T_{i+2} = \frac{1}{2}\left(L_j\Omega_jU_j+L_{j+1}\Omega_{j+1}U_{j+1}+L_{j+2}\Omega_{j+2}U_{j+2}+L_{j+3}\Omega_{j+3}U_{j+3}\right)T_\infty \tag{3.17}$$

If the *i-th* node is a boundary node (i.e. node where temperature is a constrain), the *i*-th element of vector ***f*** is replaced with the corresponding temperature value and its constant term moves from matrix ***K*** to vector ***f***.

In this paper, an application of this model is used in section 9.0 to analyse the accuracy of the *Compact Model.*

Further details in assembling System (3.16) can be found in (Sciacovelli et. al., 2015)

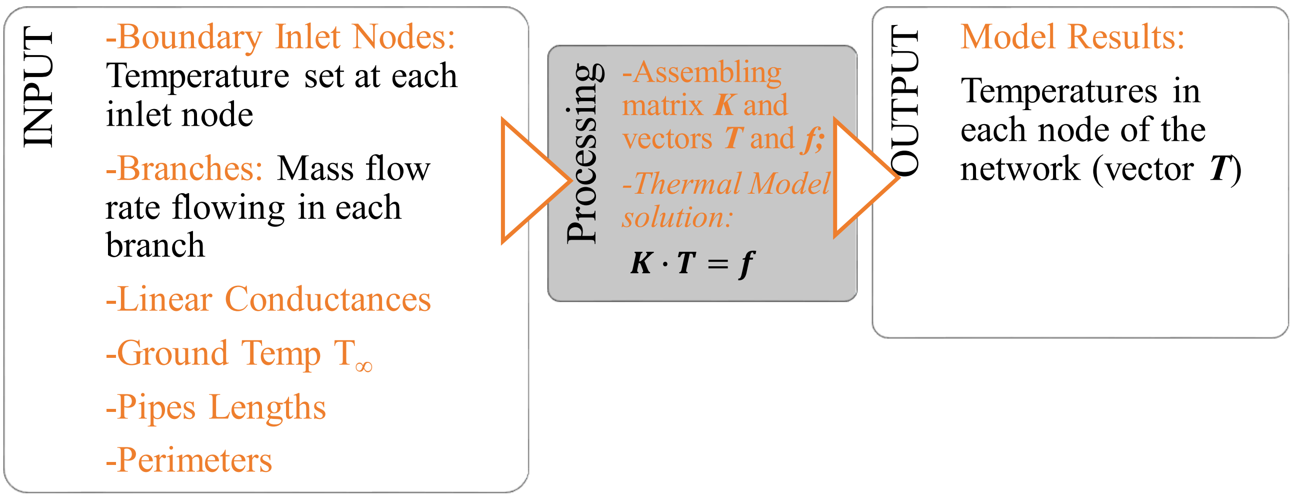

Figure 10 The *Thermal Model*

4.0 Mapping the network

In approaching this topic, one of the first issues was to have an analytic description of the network useful to creates plots that can easily show the evidences of the achieved results and also to identify errors in the codes compilation. Particularly, the goal is to have a plot of the DHN as a result of a Matlab® code that can be used to depict mass flow rates distribution.

As first step, nodes coordinates are collected from a 2-D CAD provided by IREN District Heating Team (Appendix C).

Nodes coordinates list (containing the name and the x and y-position of each node) is extracted and examined in order to collect those nodes where only junctions, barycenter or power plants are. This is possible thanks to an existing name list.

This task results in the following code lines.

```
function [x,y] = OrdinaNodi_Return( NodiCodice,NodiDaOrdinare,Ascisse,Ordinate )

%OrdinaNodi_Return recive as inputs the reference list of nodes names
%and the string containing nodes names and coordinates from the 2-D plot
%that as to be sort, respectively.

%nodes coordinates are the outputs.

for j=1:length(NodiCodice)

    for i=1:length(NodiDaOrdinare)

        if strcmp(NodiDaOrdinare(i),NodiCodice(j))==1
            NodiOrdinati(j).nome=NodiDaOrdinare(i);
            NodiOrdinati(j).ascissa=Ascisse(i);
            X(j)=Ascisse(i);
            NodiOrdinati(j).ordinata=Ordinate(i);
```

```
                Y(j)=Ordinate(i);
                 x(j)=NodiOrdinati(j).ascissa;
                 y(j)=NodiOrdinati(j).ordinata;
            end
      end
end

end
```

Once nodes coordinates are collected, a map of the network can be plot.

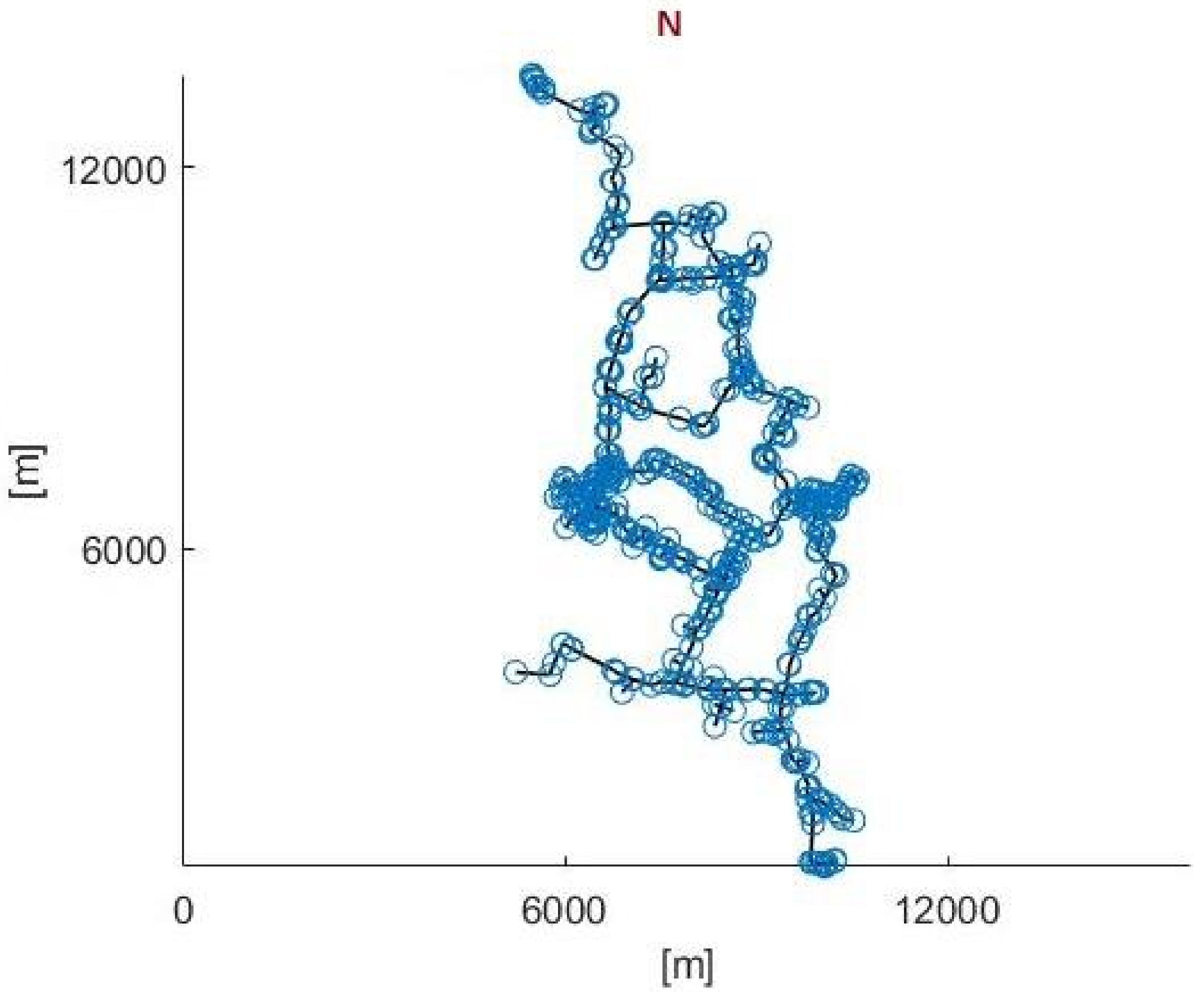

Figure 11 Network map: blue circles includes both junctions and barycenter nodes

5.0 Acquired tools

As said, this project set as goal the construction of a simplified, linear fluid dynamic model (*Compact Model* henceforth) from a more complex one, that is the result of academic development on the Turin DHN. This last model (*Full Model* henceforth*)* is already developed in a Matlab® code and simulate the fluid dynamic behaviour of the Turin DHN using monitored data as boundary conditions. An algorithm is also available to perform the energy analysis of the network through the *Thermal Model*.

Figure 12 shows the schematic of *Full* and *Thermal Model* used in this dissertation.

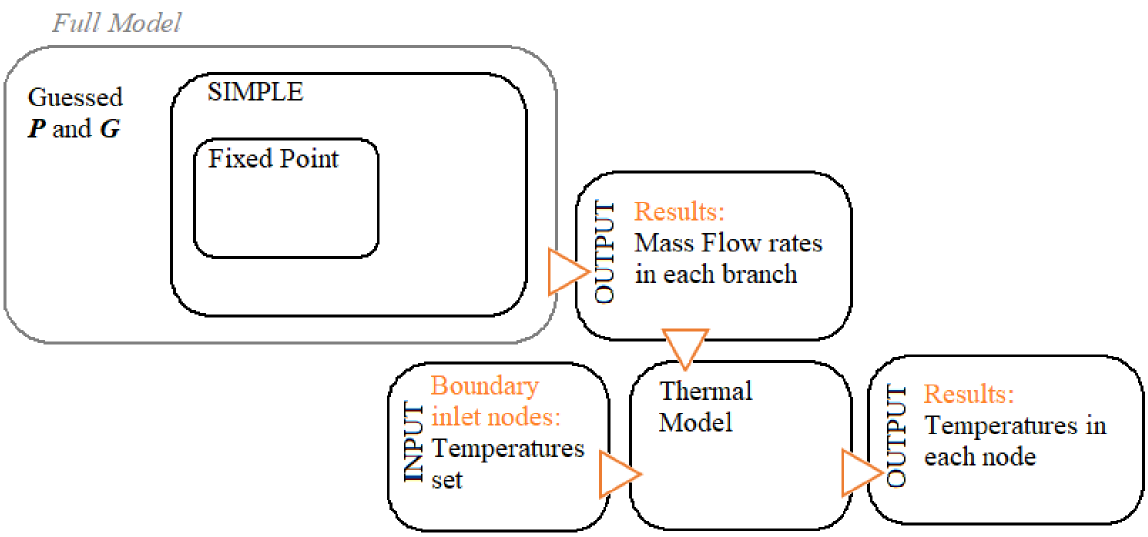

Figure 12 The *Full* and *Thermal Model*

The *Full Model* section has been used to create a mass flow rates database useful to describe the fluid dynamic behaviour of the network; these data, collected as a function of the global mass flow rates, are then used to build the *Compact Model*. The thermal section instead, is used to appreciate the difference in thermal power at the power stations, due to the linear model.

A in-depth dissertation on the *Full Model* and its accuracy is available in (Guelpa et. al., 2017).

6.0 Boundary conditions

As anticipated in section 5, in order to collect data useful to achieve the linear fluid-dynamic model, the whole network has to be simulated through the *Full Model.*

To do this, some boundary conditions have to be expressed in order to reproduce different fluid flow distribution as a function of the global mass flow rate extracted/injected in the network.

Starting from the initial time, is typically required to provide increasing rates of fluid to the network, accordingly with the morning increasing heat demand. This means that each power plant has to inject increasing value of mass flow rate to satisfy the increasing heat demand.

The boundary conditions that have to be set are:

- Power plants nodes
- Barycenter nodes (users)

These two type of boundary conditions can be collect in two matrices named $\boldsymbol{G_{pp\_gen}}$ and $\boldsymbol{G_{bar\_gen}}$ respectively.

Matrix $\boldsymbol{G_{pp\_gen}}$ is built so that each row has to receive a number of elements *pp* equal to the number of power stations; each row-element represents the mass flow rate that is flowing through the j-th[11] power plant; $\boldsymbol{G_{pp\_gen}}$ has as many rows as the observations are.

Once the structure of $\boldsymbol{G_{pp\_gen}}$ is defined, a proper logic scheme has to be identified in order to set mass flow rates values at each power station.

In each observation, the global mass flow rate G_{Tot} is set as a percentage of the total network capacity (that is about 5000 kg/s) and increase with increasing of i[12], from a minimum of 500 kg/s to a maximum of 5000 kg/s .

$$G_{Tot} = \sum_{i=1}^{pp} Gpp_{max_i} \tag{6.1}$$

[11] Column index
[12] Row index

Where pp is the number of power plants and Gpp_{max} is maximum mass flow rates of each, whose values are reported in *Appendix D*.

G_{Tot} is then distributed to the singles power plants through a random thermal load coefficient according to a priority order.

The sum of the elements of each row of $\boldsymbol{G_{pp\_gen}}$ correspond to the global mass flow rate that is provided to the network and so to the users.

The function for the calculation of the $\boldsymbol{G_{pp\_gen}}$ matrix is reported here below:

```
function [BCdata] = BCcreation_PowerPlants(z,BCdata)

 for z=1:length(t)
   BCdata.priorita                                                        =
BCdata.priorita(randperm(length(BCdata.priorita)));
 BCdata.priorital(z,:)=BCdata.priorita;

  for y=1:length(BCdata.priorita)




       BCdata.flag=0
      if
BCdata.G_globale(z)*BCdata.CoeffCarico(BCdata.priorita(y))<...
             BCdata.G_centrMax(BCdata.priorita(y))

BCdata.G_centrModello(z,BCdata.priorita(y))=BCdata.G_globale(z)*..
.
             BCdata.CoeffCarico(BCdata.priorita(y))

      else
      BCdata.G_centrModello(z,BCdata.priorita(y))=
BCdata.G_centrMax(BCdata.priorita(y))
      BCdata.flag=1
```

```
    end


    if sum(BCdata.G_centrModello(z,:))>BCdata.G_globale(z)
       if BCdata.flag==1

BCdata.G_centrModello(z,BCdata.priorita(y))=BCdata.G_globale(z)-
...

sum(BCdata.G_centrModello(z,:))+BCdata.G_centrMax(BCdata.priorita(
y))

       else

BCdata.G_centrModello(z,BCdata.priorita(y))=BCdata.G_globale(z)-
...
       sum(BCdata.G_centrModello(z,:))+BCdata.G_globale(z)*...
       BCdata.CoeffCarico(BCdata.priorita(y))
       end
       break
    end

end

if sum(BCdata.G_centrModello(z,:))<BCdata.G_globale(z)
         BCdata.G_diff=BCdata.G_globale(z)-
sum(BCdata.G_centrModello(z,:))
         BCdata.G_disponibilita=BCdata.G_centrMax-
BCdata.G_centrModello(z,:)
         for i=1:length(BCdata.priorita)

             if
BCdata.G_disponibilita(BCdata.priorita(i))>BCdata.G_diff
                 BCdata.G_centrModello(z,BCdata.priorita(i))=...
```

```
BCdata.G_centrModello(z,BCdata.priorita(i))+BCdata.G_diff
                  BCdata.G_diff==0
                  break
              else
                  BCdata.G_centrModello(z,BCdata.priorita(i))=...
                   BCdata.G_centrMax(BCdata.priorita(i))
                   BCdata.G_diff=BCdata.G_diff-...
                   BCdata.G_centrMax(BCdata.priorita(i))+...
                   BCdata.G_centrModello(z,BCdata.priorita(i))
              end
          end
  end
   if sum(BCdata.G_centrMax)<BCdata.G_globale(z)
       fprintf('[WARNING] The global load exceeds the limit valaue')
   end

 end

end
```

Matrix $\boldsymbol{G_{bar\_gen}}$ includes the observed data related to the mass flow rates extracted/injected through the barycenter nodes. As anticipated, these mass flow rates are evaluated through a α coefficient calculated as:

$$\alpha_j = \frac{Gb_{max\,j}}{\sum_{i=1}^{NB} Gb_{max\,i}} \tag{6.2}$$

where *NB* is the number of barycenter nodes, and Gb_{max} is the limit mass flow rate flowing through th *j*-th barycenter node, whose values are available in *Appendix D*.

The mass flow rate extracted/injected in each observation is evaluated as:

$$Gb_j = G_{Tot} \cdot \alpha_j \tag{6.3}$$

The function for the calculation of the G_{bar_gen} matrix is reported here below:

```
function [  BCdata ] = BCcreation_bar(NetData,BCdata,A,t)
    %Assegno le portate per sostituirle nel BC
    BCdata.G_centrModelloExtended=zeros(length(t),length(A(:,1)));
    for i=1:length(NetData.PowerPlants.Nodes)

BCdata.G_centrModelloExtended(:,NetData.PowerPlants.Nodes(i))=...
             BCdata.G_centrModello(:,i)
    end


    BCdata.G_barModelloExtended=zeros(length(t),length(A(:,1)));
    for z=1:length(t)
    for i=1:length(NetData.bar(:,3))
    BCdata.G_barModelloExtended(z,NetData.bar(i,1))=
BCdata.AlfaGbar(i)*...
        sum(BCdata.G_centrModello(z,:))
    end
    end


end
```

In the return network, mass flow rate flows from barycenter node (where users are) to the power stations. Therefore, according to fluid dynamic signs convention, a negative sign has to be considered for mass flow rates extracted at power plants nodes.

```
% Inlet Mass flow rates (Gpp_gen)
    BC.bin=-BCdata.G_barModelloExtended;
% Outlet Mass flow rates (Gbar_gen)
    BC.bout=BCdata.G_centrModelloExtended;
```

The number of observations n is set equal to t for both matrices, that is the number of observations chose to describe thermal transient. Higher values of this number are recommended because the higher the number of observations is, the best is for the accuracy of the *Compact Model*.

7.0 Linear approach

As said, the aim is to compile a model that simulate the network fluid dynamic behaviour with a less complex numeric scheme, on the basis of mass flow rates data collected using the *Full Model*. The construction of this model starts defining the evolution of the fluid dynamic transient that occurs during the simulation. This means that mass flow rates[13] have to be set in the power plants nodes and in the barycenter nodes and the *Full Model* has to be used to evaluate mass flow rates in each branch of the *DHN*. At this stage, a linear relation is investigated to directly link the mass flow rate flowing in each power plant to the mass flow rate flowing in such branches that are removed (*LTTB* henceforth) in order to reduce the DHN into an equivalent tree-shape network. Once this linear relation is known, mass flow rate in each *LTTB* can be expressed as an exclusive function of the mass flow rate flowing in each power stations. Mass flow rates values in these branches are then set, with the proper sign, as additional boundary conditions to the equivalent tree-shape network, in the end-nodes of each removed branch (i.e. *LTTB*).

Finally, the fluid dynamic of the equivalent tree-shape network can be evaluated through the continuity equation (3.1).

7.1 The equivalent tree-shape network

As said, Turin *DHN* shows close paths that improve the reliability of the system in case of pipes failure.

Each loop has to be identified in order to modify the topological description of the network into a tree-shape configuration.

Euler's law is used to calculate the number of these close paths:

$$NL = NB - NN + 1 \tag{7.1}$$

[13] Section 6.0 Boundary Condition

Where *NL* is the number of loops (close paths), *NB* is the number of branches and *NN* the number of nodes.

As shown in *Figure 13*, Turin network has 9 loops with various size that are constituted by many branches. In each loop, one of these branches, the so called '*Loop to Tree Branch*', is selected in order to remove it from the *Incidence Matrix A* and obtain the equivalent tree-shape configuration depicted in *Figure 14*.

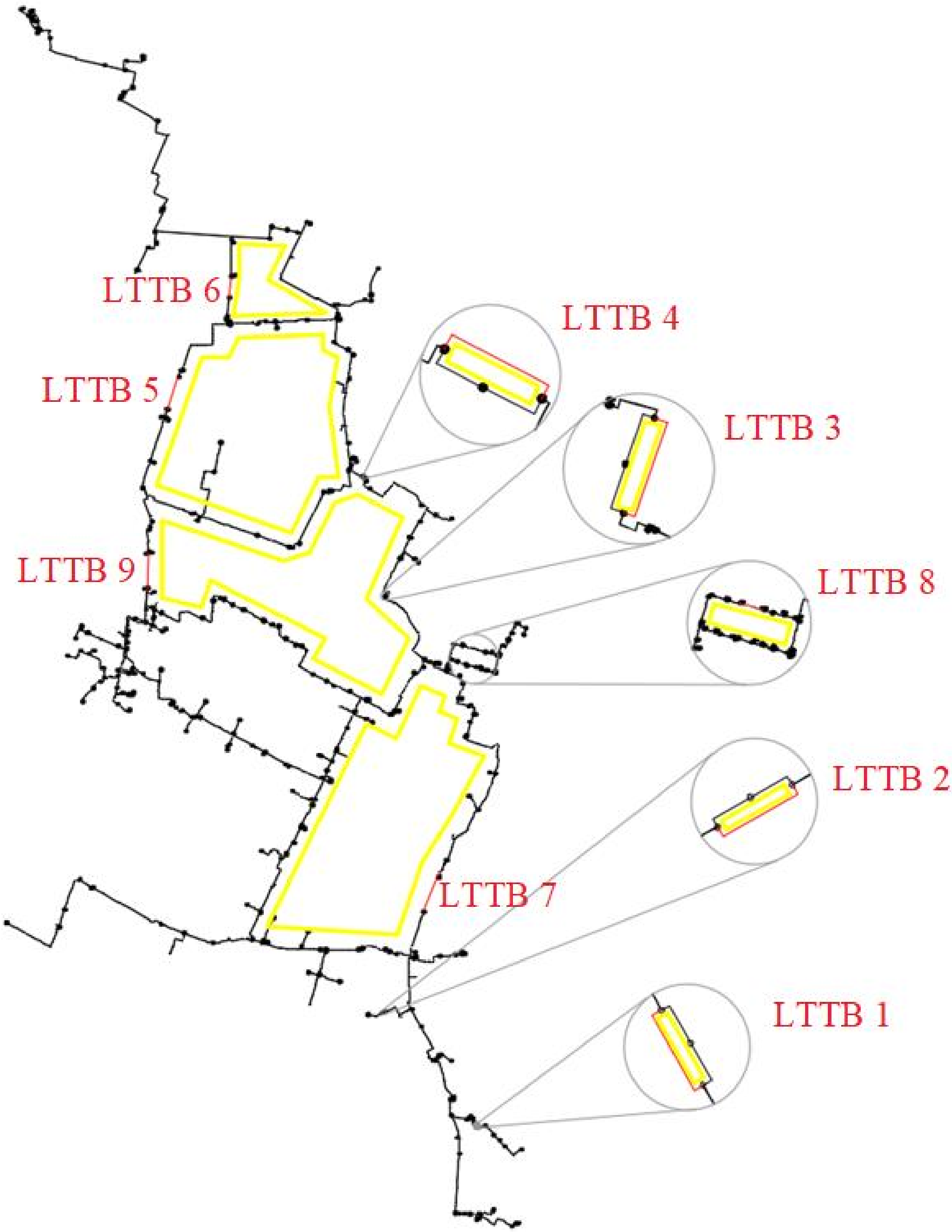

Figure 13 Turin District Heating Network: close paths in yellow, *LTTBs* in red.

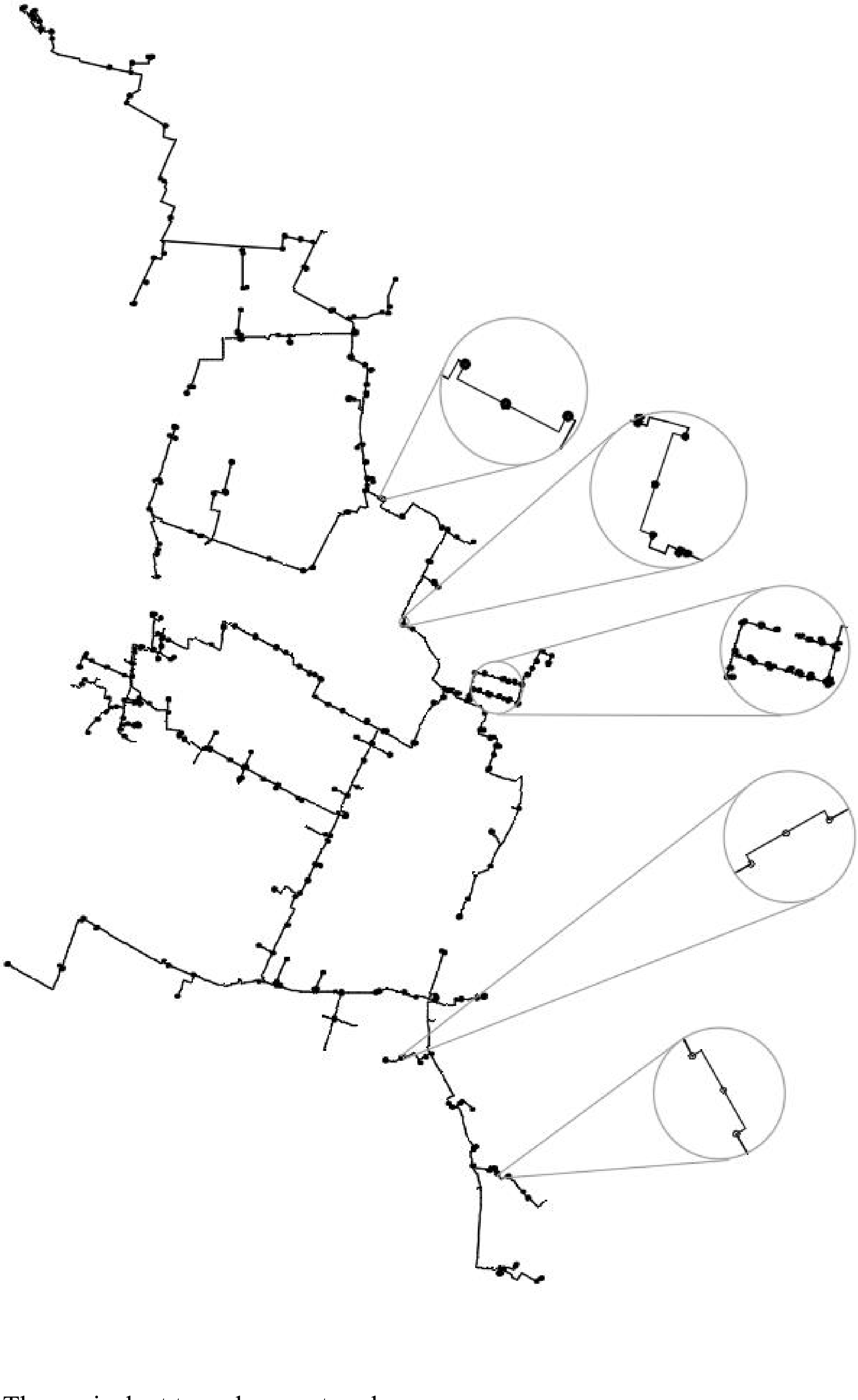

Figure 14 The equivalent tree-shape network

To do this, each loops is identified on the *2D-cad* and an *NL*-by-2 table is expressed in order to collect the name of the end-nodes of each *LTTB* (*Boundary Nodes* henceforth).

Branches	***Boundary Nodes* - name**	
LTTB_1	CA051	NS007
LTTB_2	CA055	CA056
LTTB_3	CA065	CA066
LTTB_4	CA082	CA083
LTTB_5	CA079	NC040
LTTB_6	NN038	NN039
LTTB_7	CA009	NS019
LTTB_8	NS039	NS040
LTTB_9	NS155	NS156

Table 1 End nodes of the *LTTBs* - Nomenclature

According to the numeric order of the branches, each row of *Table 1* corresponds to a column index in the incidence matrix *A*, so that

$$\boldsymbol{LTTB_{pos}} = \begin{bmatrix} 104 \\ 108 \\ 115 \\ 132 \\ 258 \\ 335 \\ 377 \\ 413 \\ 594 \end{bmatrix}$$

Vector $\boldsymbol{LTTB_{pos}}$ express the positions of the LTTBs in matrix *A*. A *for cycle* can be implemented in order to obtain the incidence matrix of the equivalent tree-shape network.

```
    A_tree=A;
for i=1:length(Maglie)
    Descend=1:length(Maglie);
    Descend=sort(Descend,'descend') ;
    A_tree(:,Maglie(Descend(i)))=[];
end
```

It is important to stress that, unlike branches, the number of nodes doesn't change, hence nodes collect in *Table 1* are still part of the tree-shape network.

7.2 Data generation – *LTTB* mass flow rates

The solution of the continuity equation implies that additional boundary conditions have to be set in the *Boundary Nodes* of the *LTTBs*. Evaluation of these new boundary conditions can be made by considering the fact that mass flow rates flowing in the *LTTBs* are a function of the mass flow rates at the power plants. A linear relation between these two sets of mass flow rates can be investigate using the Matlab® *Regress* function, so that the boundary condition at each *LTTB* can be estimated as an exclusive (linear) function of the mass flow rates at the power plants. Expression of this linear function will be illustrated hereafter. First, a sufficient amount of data has to be produced to have a complete description of the network fluid dynamic behaviour, when the global load varies. To do this mass flow rates in *LTTB* are computed using the *Full Model* in which matrices $\boldsymbol{G_{pp\_gen}}$ and $\boldsymbol{G_{bar\_gen}}$ are set as boundary conditions.

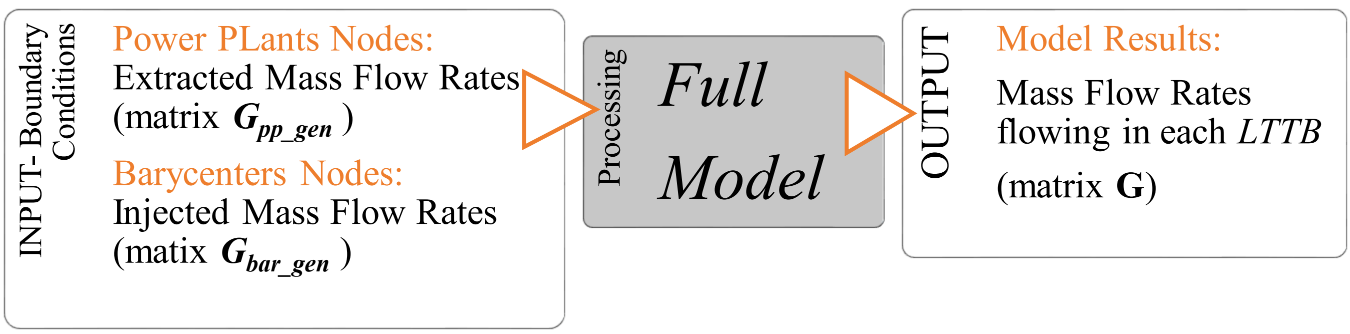

Figure 15 The *Full Model*

The fluid dynamic model receives as inputs matrix $\boldsymbol{G_{pp\_gen}}$ and matrix $\boldsymbol{G_{bar\_gen}}$ expressing the boundary conditions as a variation of the global load. After running the full model, real mass flow rates in each branch are collect in an output matrix **G**, which has as many columns as the branches. Each row of matrix **G** results from a global load setting G_{Tot} , that can be expressed as a percentage of the total capacity.

If a row vector $\boldsymbol{G_{full}}$ is isolated from matrix ***G***, it is possible to plot a map of the network at a prescribed load, in which each branch is depicted according to the corresponding mass flow rate. *Figure 16* show the mass flow rates distribution when G_{Tot} is equal to a 50% of the total capacity.

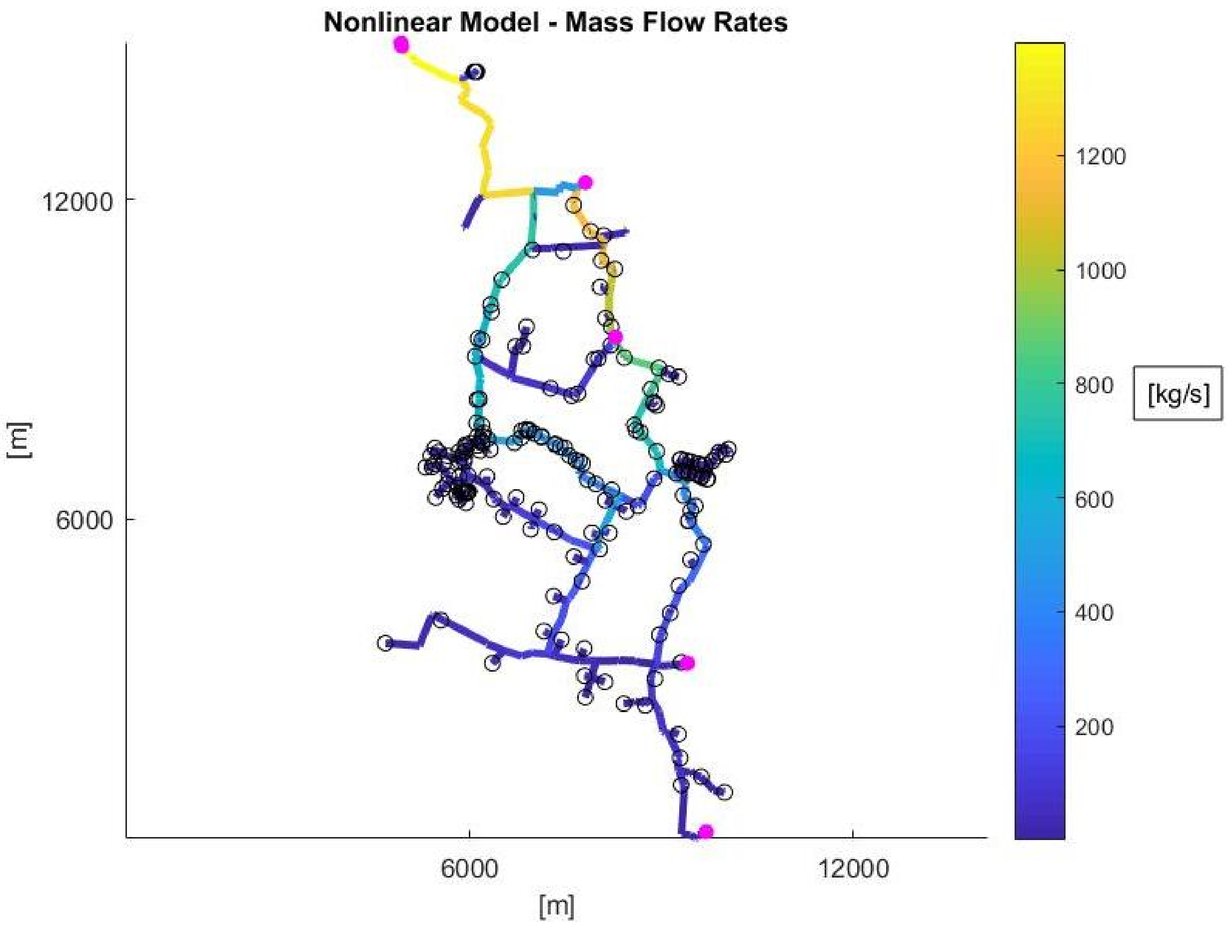

Figure 16 Mass flow rates resulting from the *Full Model*

In order to collect the mass flow rates in each $LTTB$, column vectors corresponding to these branches are isolated from matrix **G** and a new n-by-NL matrix, named $\boldsymbol{G_{LTTB\_n}}$, is defined:

$$\boldsymbol{G_{LTTB\_901}} = \begin{vmatrix} G_{1,1} & G_{1,2} & G_{1,3} & G_{1,4} & G_{1,5} & G_{1,6} & G_{1,7} & G_{1,8} & G_{1,9} \\ . & & & & . & & & & . \\ . & & & & . & & & & . \\ . & & & & . & & & & . \\ . & & & & . & & & & . \\ . & & & & . & & & & . \\ G_{t,1} & G_{t,2} & G_{t,3} & G_{t,4} & G_{t,5} & G_{t,6} & G_{t,7} & G_{t,8} & G_{t,9} \\ . & & & & . & & & & . \\ . & & & & . & & & & . \\ . & & & & . & & & & . \\ . & & & & . & & & & . \\ . & & & & . & & & & . \\ . & & & & . & & & & . \\ G_{n,1} & G_{n,2} & G_{n,3} & G_{n,4} & G_{n,5} & G_{n,6} & G_{n,7} & G_{n,8} & G_{n,9} \end{vmatrix} \tag{7.2}$$

This matrix contains mass flow rate in each LTTB as a function of the global load G_{Tot} (25% to 100%) and will be useful in following chapter in order to build the linear model.

7.3 Multilinear Regression

7.3.1 The Linear Model

The network topology modification process from the real shape into a tree-shape requires that boundary conditions have to be applied where $LTTBs$ where.

As said, the aim is to find a linear relation that allows one to evaluate the additional boundary conditions as an exclusive function of the mass flow rates at the power plants, so that:

$$\boldsymbol{G_{pp}} \cdot \boldsymbol{B} = \boldsymbol{G_{LTTB\_linear}} \tag{7.3}$$

where:

- $\boldsymbol{G_{pp}}$ is a 1-by-pp vector whose elements are the mass flow rates at each power plants
- $\boldsymbol{G_{LTTB\_linear}}$ is a 1-by-NL matrix containing estimated mass flow rates values in each $LTTB$

- ***B*** is a *pp*-by-*NL* matrix of constant coefficients

Mass flow rates at power plants is considered as an input information, hence, once matrix ***B*** is evaluated, vector $\boldsymbol{G_{LTTB\_linear}}$ can be used to set the additional boundary condition in the tree-shape network.

Calculation of ***B*** is performed using the Matlab Multilinear Regress Function.

The function accepts as input two arrays:

- an *n*-by-*p* matrix of *p* predictors at each of *n* observations
- an *n*-by-1 vector of observed responses

where *p* is equal to *pp* (number of power stations).

In that case, predictors are the mass flow rates at the power plants, collected in each row of matrix $\boldsymbol{G_{pp\_gen}}$, whereas the vector of observed responses is equal to each column of matrix $\boldsymbol{G_{LTTB\_n}}$ that collects the real mass flow rates values as a function of the global load.

The Regress Function returns a *pp*-by-1 vector ***b*** of coefficients, estimates for the multilinear regression of the responses related to a single *LTTB*. Hence a *for cycle* has to be implemented to recalls the Regress function for each of the nine *LTTBs*. Each calls generate a ***b*** vector that will constitutes the ***B*** matrix.

```
function [ ModelResults ] = RegressCoeffGeneration(
BCdata,NetData,ModelResults )


 for i=1:length(NetData.LoopToTreeBranches)
  ModelResults.LinearRegress.RegressCoeff(:,i)=regress...

(ModelResults.G_LoopToTreeBranches(:,i),BCdata.G_centrModello);
 end


end
```

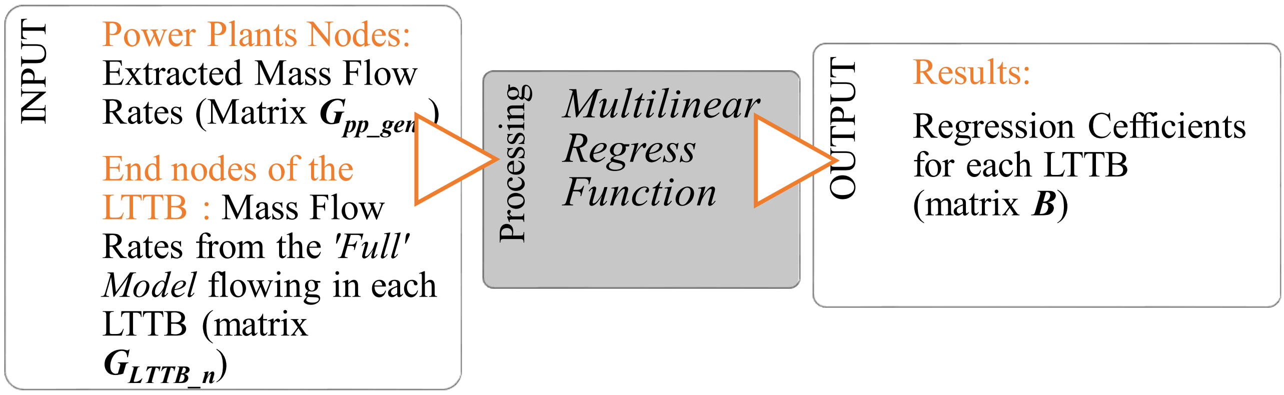

Figure 17 The linear regression

Matrix $\boldsymbol{B}$ is evaluated, saved and no longer updated since matrix $\boldsymbol{G_{pp\_gen}}$ and matrix $\boldsymbol{G_{bar\_gen}}$ are not modified.

$$\boldsymbol{B} = \begin{vmatrix} 0.001263 & -0.00109 & 0.141262 & -0.09931 & 0.032535 & 0.023408 & 0.38251 & 0.008372 & 0.093729 \\ 0.001263 & -0.00109 & -0.16068 & 0.202635 & -0.31561 & -0.37444 & -0.08772 & 0.008372 & -0.30229 \\ 0.001263 & -0.00109 & -0.17179 & 0.213738 & -0.08952 & 0.006588 & -0.08534 & 0.008372 & -0.28039 \\ 0.001263 & -0.00109 & -0.16253 & 0.204483 & -0.28719 & -0.29032 & -0.07546 & 0.008372 & -0.29782 \\ 0.001263 & -0.00109 & -0.16054 & 0.202496 & -0.31956 & -0.378 & -0.09063 & 0.008372 & -0.30343 \\ 0.001263 & -0.00109 & 0.144394 & -0.10244 & 0.031394 & 0.019543 & 0.378414 & 0.008372 & 0.087545 \end{vmatrix}$$

Figure 18 Coefficients for the linear regression

At this stage, we are able to evaluate a set of estimated mass flow rates in each LTTB as the product between a generic vector $\boldsymbol{G_{pp}}$ and the matrix $\boldsymbol{B}$, so that:

$$\begin{bmatrix} G_{pp1} \\ G_{pp2} \\ G_{pp3} \\ G_{pp4} \\ G_{pp5} \\ G_{pp6} \end{bmatrix} \cdot \begin{bmatrix} B_{11} & B_{12} & B_{13} & B_{14} & B_{15} & B_{16} & B_{17} & B_{18} & B_{19} \\ B_{21} & B_{22} & B_{23} & B_{24} & B_{25} & B_{26} & B_{27} & B_{28} & B_{29} \\ B_{31} & B_{32} & B_{33} & B_{34} & B_{35} & B_{36} & B_{37} & B_{38} & B_{39} \\ B_{41} & B_{42} & B_{43} & B_{44} & B_{45} & B_{46} & B_{47} & B_{48} & B_{49} \\ B_{51} & B_{52} & B_{53} & B_{54} & B_{55} & B_{56} & B_{57} & B_{58} & B_{59} \\ B_{61} & B_{62} & B_{63} & B_{64} & B_{65} & B_{66} & B_{67} & B_{68} & B_{69} \end{bmatrix} = \begin{bmatrix} G_{LTTB\_linear_1} \\ G_{LTTB\_linear_2} \\ G_{LTTB\_linear_3} \\ G_{LTTB\_linear_4} \\ G_{LTTB\_linear_5} \\ G_{LTTB\_linear_6} \\ G_{LTTB\_linear_7} \\ G_{LTTB\_linear_8} \\ G_{LTTB\_linear_9} \end{bmatrix} \tag{7.4}$$

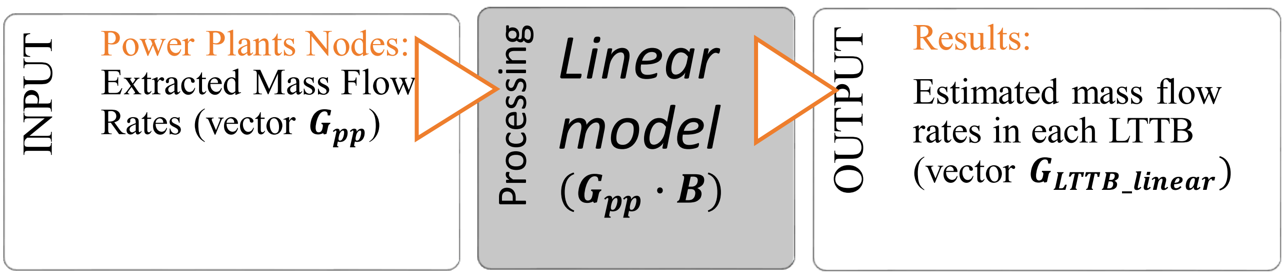

Figure 19 The *Linear Model*

8.0 The *Compact Model*

The algorithm presented till now is able to:

- evaluate the topology of the equivalent tree-shape network
- evaluate a vector $\boldsymbol{Gb}$ whose elements are the mass flow rates injected at the barycenters nodes (Eq. (6.2) and Eq. (6.3))
- estimates a vector $\boldsymbol{G_{LTTB\_linear}}$ of mass flow rates from an input vector $\boldsymbol{G_{pp}}$, through a linear regression

In order to solve the fluid dynamic model of the equivalent tree-shape network, boundary condition has to be applied and the follow linear system has to be solved:

$$\mathbf{A_{tree}} \cdot \mathbf{G}_{\boldsymbol{linear}} = \mathbf{G}_{\boldsymbol{ext}} \tag{8.1}$$

where $\mathbf{A_{tree}}$ is the Incidence matrix expressed in section 7.1 , $\mathbf{G}_{\boldsymbol{linear}}$ is a 1-by-*NB* vector of unknown mass flow rates and $\mathbf{G}_{\boldsymbol{ext}}$ is a 1-by-*NN* vector containing the external mass flow rates.

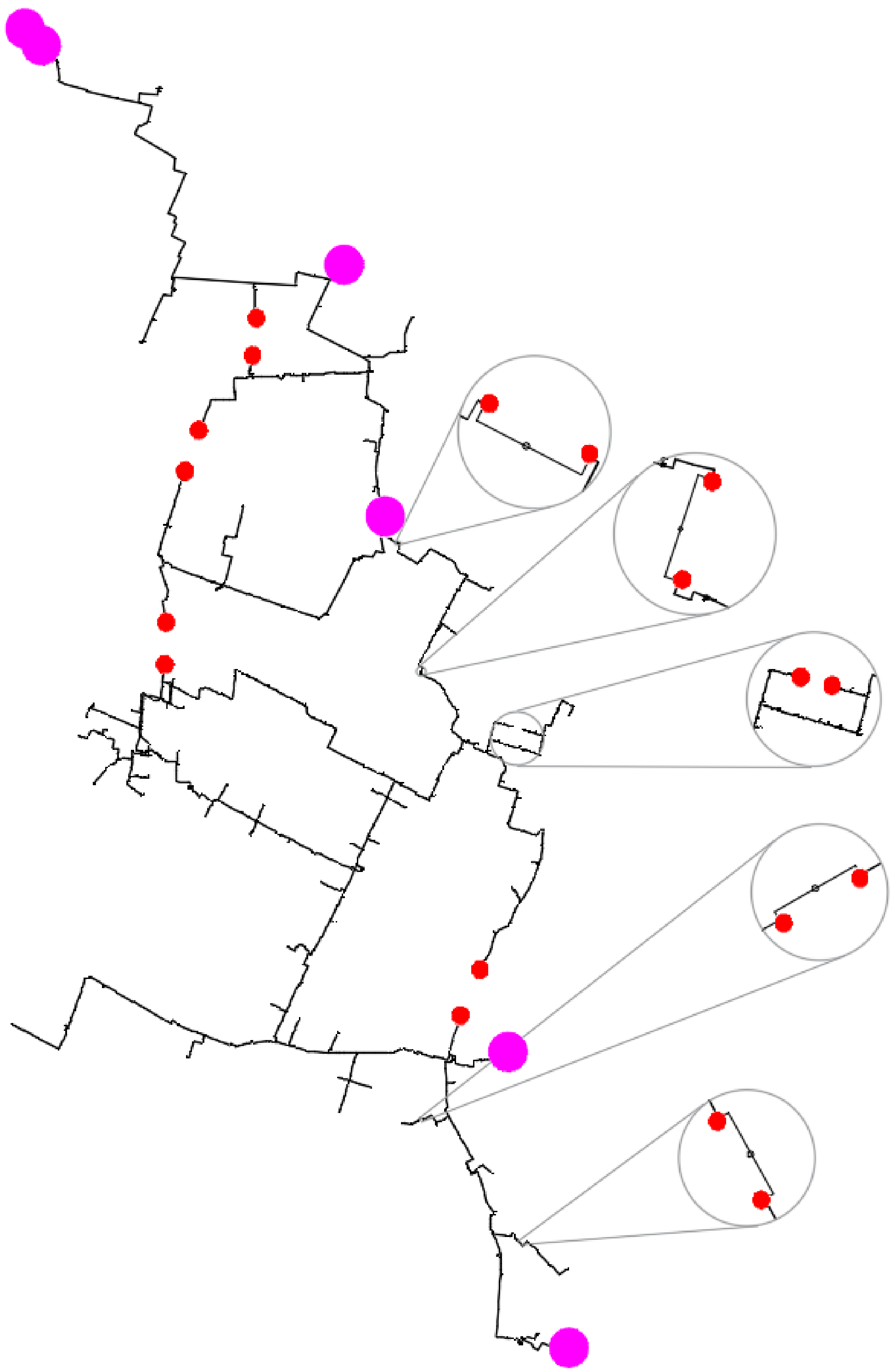

Figure 20 The equivalent tree-shape network: *Boundary Nodes* in red, power plants in magenta

According to *Figure 20*, the number NB of nodes in which extraxtions/injections occurs is equal to:

$$NB = pp + NB + 2(NL) \qquad (8.2)$$

where:

- pp is the number of power stations
- NB is the number of barycenters nodes
- NL is the number of LTTBs

Appling boundary conditions in each nodes means that vector $\mathbf{G}_{ext}$ has to contain the mass flow rates exchanged toward environment, with the proper sign. If no fluid exchange occurs in a *NB* node, the corrisponding element of $\mathbf{G}_{ext}$ is zero.

In the return network, fluid flows from the barycenters nodes to the power plants, determining a flow direction in each branch of the network. Therefore, according to the sign convencions, mass flow rates extracted at the power plants shall be positive, while those injected in the barycenters nodes negative.

This two type of boundary conditions are evaluated with the same criteria used to expressed matrix $\boldsymbol{G}_{pp\_gen}$ and $\boldsymbol{G}_{bar\_gen}$:

1. mass flow rates at each power plants is set according to a priority order
2. mass flow rates at each barycenter nodes is set according Eq.(6.2) and Eq. (6.3)

In order to expressed vector $\mathbf{G}_{ext}$, these two type of boundary conditions can be collect in a 1-by-*NN* vector ***BC.b***, using data in (Appendix F) to determin the indices and completed with boundary conditions at the end-nodes of *LTTBs*.

First, the numeric indices of the *Boundary Nodes* has to be identified using vector $\boldsymbol{LTTB}_{pos}$ (section 7.1) and matrix $\boldsymbol{A}$.

```
function [ NetData ] = Find_LTTBNodes( NetData,A )

for i=1:length(NetData.Maglie)

NetData.Nodi_LoopToTreeBranches(i,:)=find(A(:,NetData.Maglie(i)))

    end
end
```

Function 'Find_LTTBnodes' collects each nodes in a *NL*-by-2 matrix so that each row of that matrix contains the end-nodes of a *LTTB*. The elements of this matrix ('NetData.Nodi_LoopToTreeBranches' in the function) is reported in *Table 2*.

Removed Branches ($LTTB_{pos}$)	***Boundary Nodes***	
LTTB_1 (115)	104	370
LTTB_2 (132)	107	108
LTTB_3 (104)	113	114
LTTB_4 (108)	129	130
LTTB_5 (335)	127	299
LTTB_6 (413)	357	358
LTTB_7 (258)	75	382
LTTB_8 (594)	402	403
LTTB_9 (377)	515	516

Table 2 End nodes of the *LTTBs* - numbering

In each *LTTB* flows a mass flow rate, according to vector $\boldsymbol{G_{LTTB\_linear}}$; this means that the same mass flow rates is exchanged in each of the two *Boundary Nodes*, but with opposite signs.

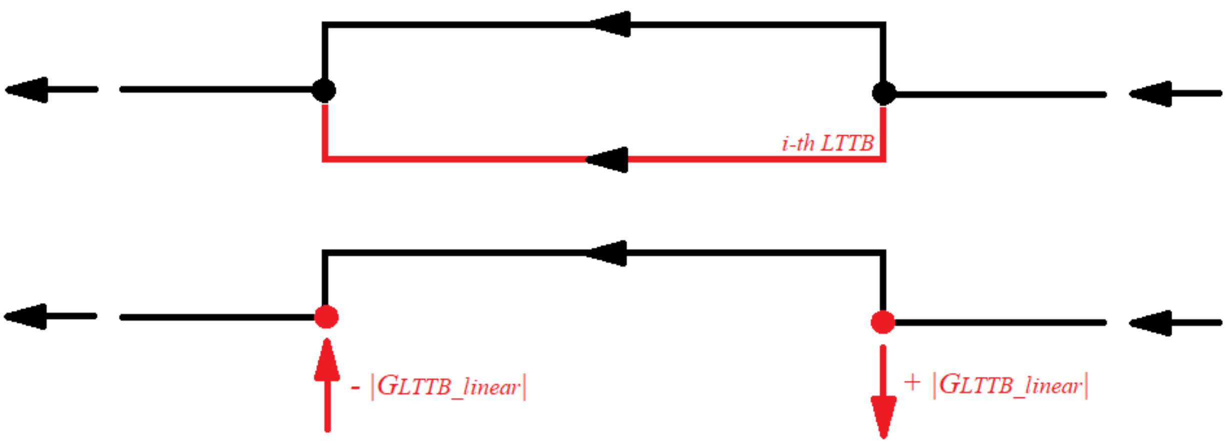

Figure 21 Example of a loop – topology processing

According to *Figure 21*, sign assignment comply the flow direction in the *i*-th *LTTB*. The correct sign can be assigns using the matrix *A*.

To do this, function 'BCLinearModelCreation_LTTBnodes' receive as inputs vector ***BC.b***, incidence matrix $\boldsymbol{A}$ and vector $\boldsymbol{G_{LTTB\_linear}}$, and return as output vector $\mathbf{G}_{ext}$, resulting from the integration of the mass flow rates at the *Boundary Nodes*.

```
function [ BC ] = BCLinearModelCreation_LTTBnodes...
( NetData,ModelResults,BC,A,t)

          for i=1:length(NetData.Maglie)
      for j=1:2

        BC.b_1test(NetData.Nodi_LoopToTreeBranches(i,j))=...

(ModelResults.LinearRegress.G_LoopToTreeBranches(z,i))*...

A(NetData.Nodi_LoopToTreeBranches(i,j),NetData.Maglie(i));

        if
((ModelResults.LinearRegress.G_LoopToTreeBranches(z,i))*...

A(NetData.Nodi_LoopToTreeBranches(i,j),NetData.Maglie(i))>0

BC.boutTreeNet(z,NetData.Nodi_LoopToTreeBranches(i,j))=...

(ModelResults.LinearRegress.G_LoopToTreeBranches(z,i))*...

A(NetData.Nodi_LoopToTreeBranches(i,j),NetData.Maglie(i))
        else

BC.binTreeNet(z,NetData.Nodi_LoopToTreeBranches(i,j))=...

(ModelResults.LinearRegress.G_LoopToTreeBranches(z,i))*...

A(NetData.Nodi_LoopToTreeBranches(i,j),NetData.Maglie(i))
        end
      end
    end

end
```

Once vector $\mathbf{G}_{ext}$ is obtained, the linear System 8.1 can finally be solved and mass flow rates in each branch of the network can be collect in vector $\mathbf{G}_{linear}$.

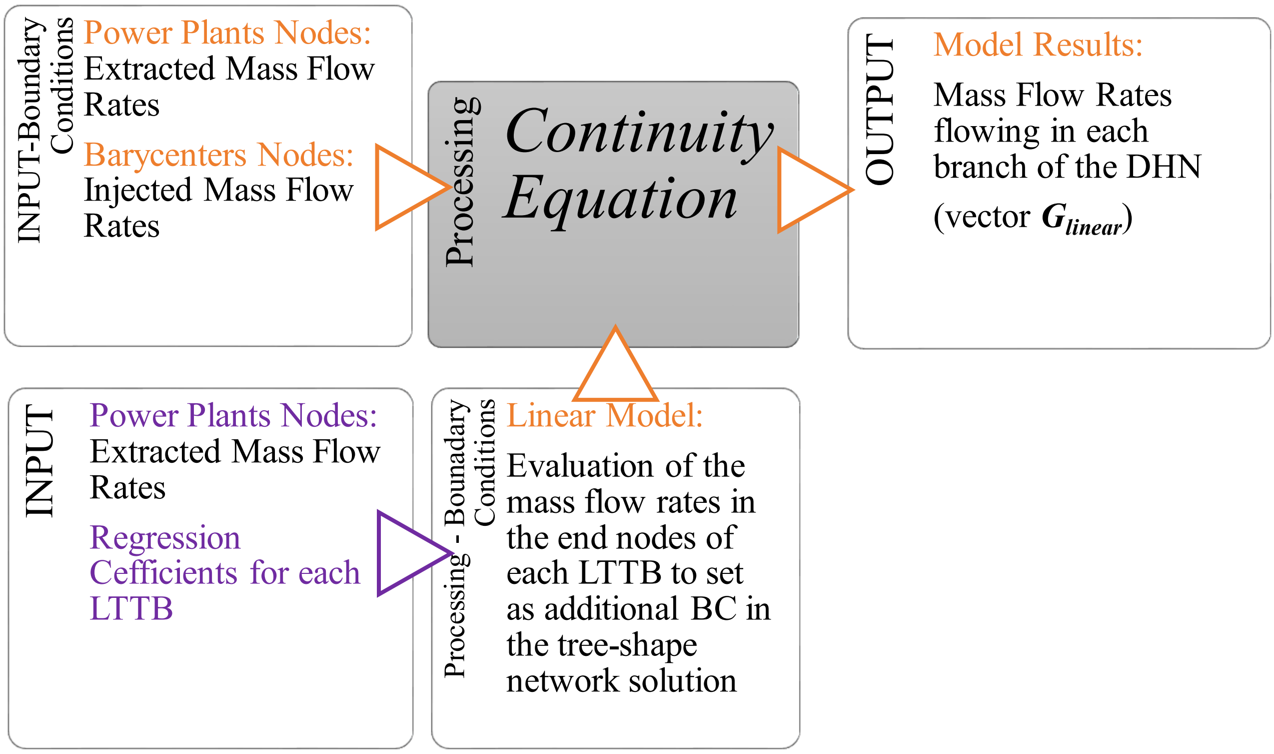

Figure 22 The *Compact Model*

9.0 Results and discussions

Results on the accuracy of the *Compact Model* will be presented in this chapter. Mass flow rates evaluated through this model are compared to the ones elaborated with the *Full Model,* in order to estimates errors that occurs if the linear approach is adopted. To have such type of comparison, common boundary conditions are expressed for both models, using functions presented in section 6.

Once the two models are run, errors can be evaluated immediately as the difference between vectors **G** and $\mathbf{G}_{\mathbf{linear}}$. However, the accuracy of the *Compact* M*odel* is mainly influenced by the linear model, therefore errors related to the evaluation of vector $\boldsymbol{G_{LTTB\_linear}}$ are calculated first, in order to analyse the way the boundary conditions at the *Boundary Nodes* influence the whole network.

Comparison between vectors **G** and $\mathbf{G}_{\mathbf{linear}}$ is then carried out by selecting four different scenarios in which the two vectors are evaluated from different values of the global load G_{tot}. For each scenario, increasing values of the global load G_{tot} are selected as a percentage of the total capacity. The prescribed load G_{tot} is then distributed to each power plant according to a resonable priority order: Moncalieri and TN are switched on first, as they are cogeneration plants; storages are used to cover the peak requests; while boilers provides heat during peak and off-peak hours, when the load exceeds a prescribed value.

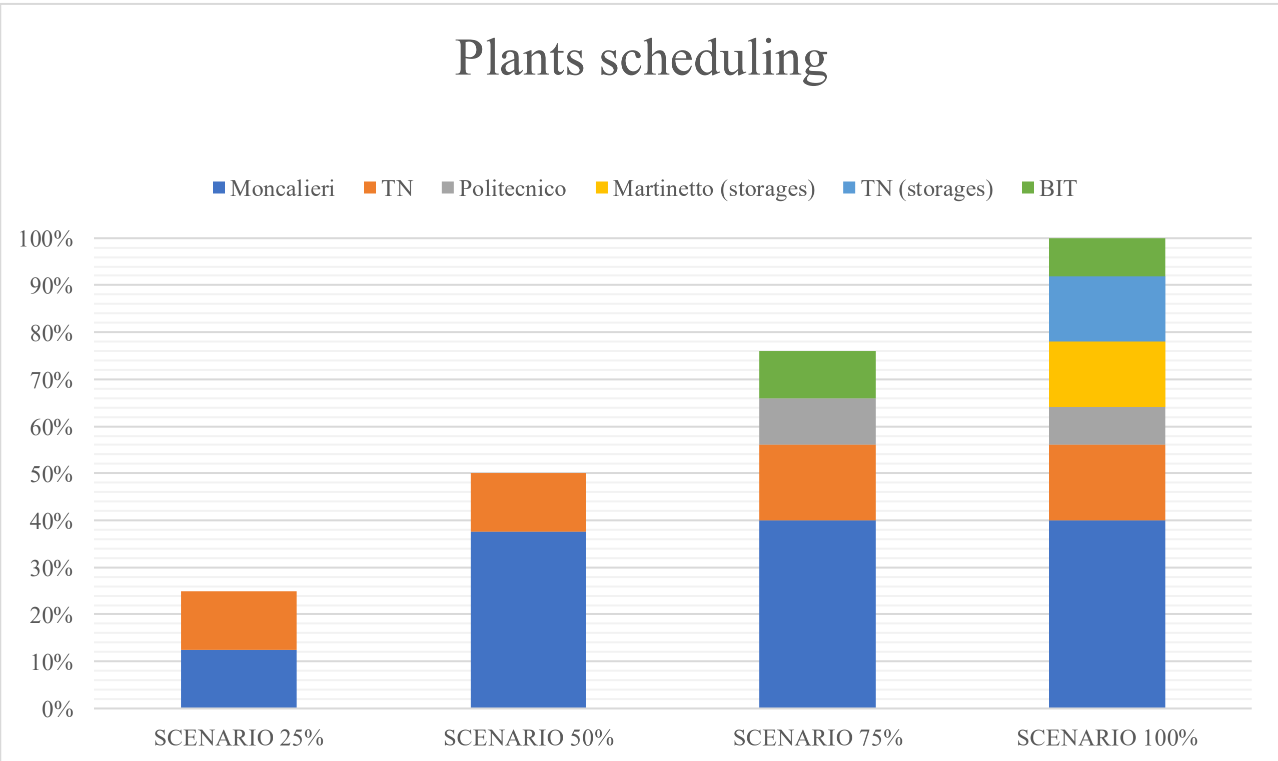

Figure 23 Power plants scheduling depending on the global thermal request

A thermal analysis is finally performed to analyse the relevance of the fluid dynamic errors in terms of thermal power at each power plants.

9.1 The linear model

Accuracy in mass flow rates evaluation is mainly due to boundary conditions sets in each *Boundary Node* and collected in vector $\boldsymbol{G_{LTTB\_linear}}$. As seen in section 7.3 , this vector results from a linear regression of data collected in matrix $\boldsymbol{G_{LTTB\_901}}$.

In order to evaluate the accuracy of the linear model, vector $\boldsymbol{G_{LTTB\_linear}}$ is evaluated in each scenario using the corresponding boundary condition: in each scenario, vector $\boldsymbol{G_{pp}}$ is set to the corrisponding power plants schedule illustrated in *figure 23* and System 7.3 is solved, as illustrated in section 7.3.1. The resulting output vector $\boldsymbol{G_{LTTB\_linear}}$ is then compared to vector $\boldsymbol{G_{LTTB}}$ to stress the errors due to the Linear Model.

The following plots shows a comparison of the mass flow rates between the two models, in each *LTTB*, from 25% to 100% of the total capacity.

From a quick examination of these graphs it can be noticed that mass flow rate in a single *LTTB* doesn't necessarily increase with increasing values of the total load. That's because the fluid flows along different paths, according to the number and the position of the power plants involved, where the least resistances occurs. For that reason, there are no generalizations at all on the accuracy respect to the global load, outside of the singles start up schedules shown in *Figure 23.* Moreover, in a single loop, no relation between the accuracy of the compact model and its mass flow rates can be stress, since there are mutual dependences between loops. This leads to conclude that any loop can't be analysed independently.

Nevertheless, combined observation of the graphs and the map in *Figure 13* allows one to notice that the bigger is the loop to witch *LTTB* belongs, the larger is the difference between the two mass flow rates; evidences of that can be noticed in *LTTB_1* and *LTTB_2* respect to *LTTB_7* and *LTTB_9*. Differences below the 0.01% can be noticed in *LTTB_1, LTTB_2* and *LTTB_8* ; such low values occur because the branches of each loop cause drag and the upstream flow splits equally on the two paths. Moreover, these differences are not affected by alterations coming from the bigger loops because they are located in terminal branch.

Differences in the accuracy of *Compact Model* also occurs between loops that are in terminal paths, respect to those who are distributed in the inner areas of the network, such as *LTTB_3* and *LTTB_4* respect to *LTTB_8* (where no sensible differences occur between the two models). In this case, on the contrary, the difference between the two mass flow rates is larger in *LTTB_3* and *LTTB_4*, despite their dimensions.

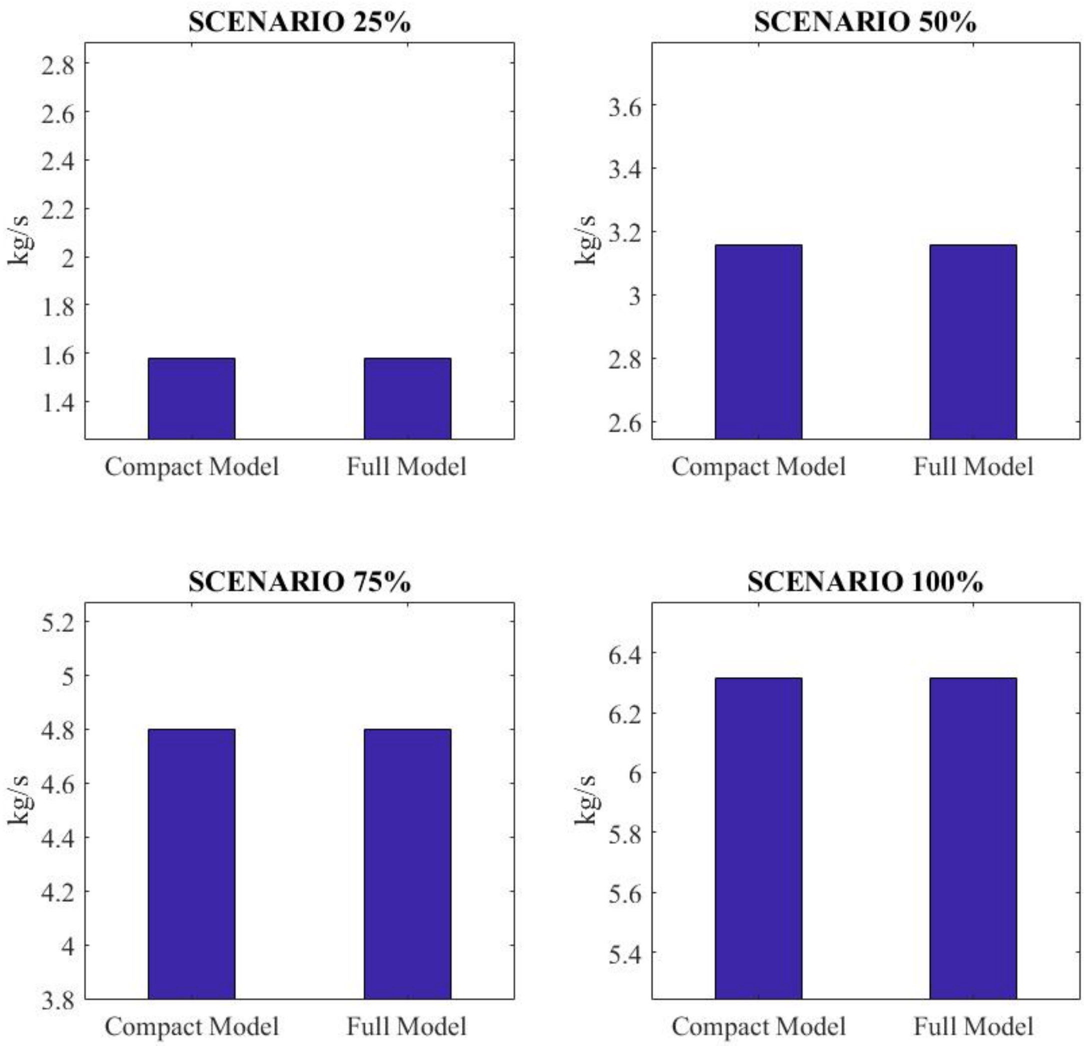

Figure 24 *LTTB_1*: comparison of mass flow rates

LTTB_1	SCENARIO 25%	SCENARIO 50%	SCENARIO 75%	SCENARIO 100%
Error% *Compact* vs. *Full model*	**<0.01**	**<0.01**	**<0.01**	**<0.01**

Table 3 Relative errors from the C*ompact Model*

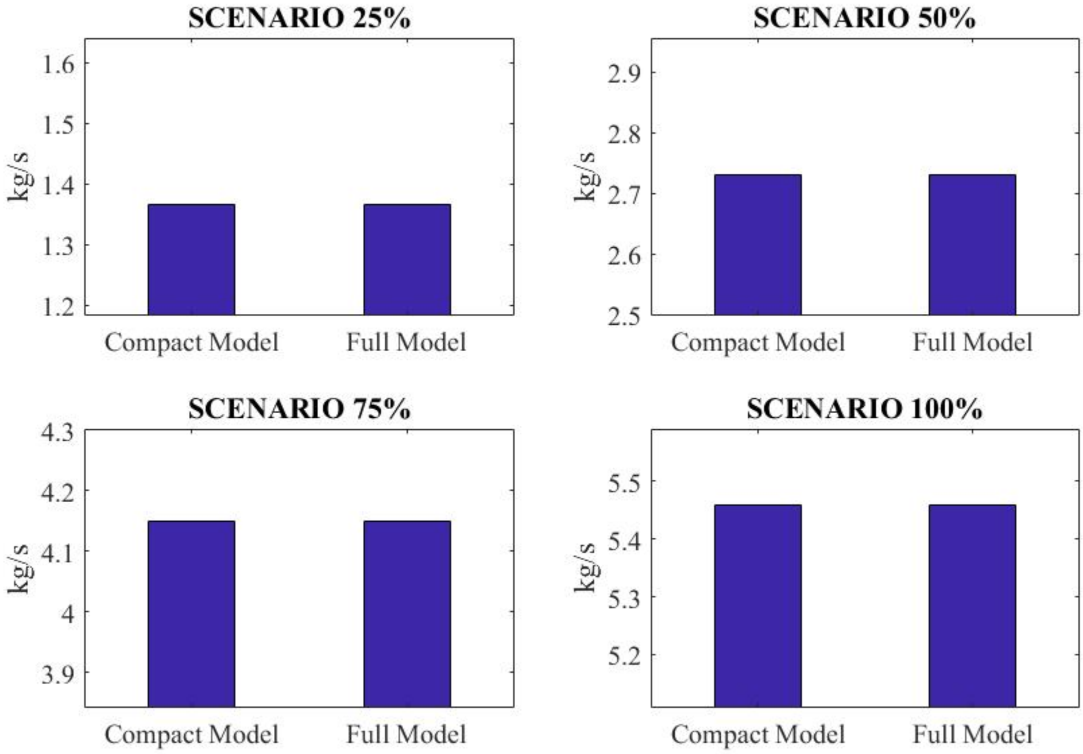

Figure 25 *LTTB_2*: comparison of mass flow rates

LTTB_2	SCENARIO 25%	SCENARIO 50%	SCENARIO 75%	SCENARIO 100%
Error% *Compact* vs. *Full model*	**<0.01**	**<0.01**	**<0.01**	**<0.01**

Table 4 Relative errors from the C*ompact Model*

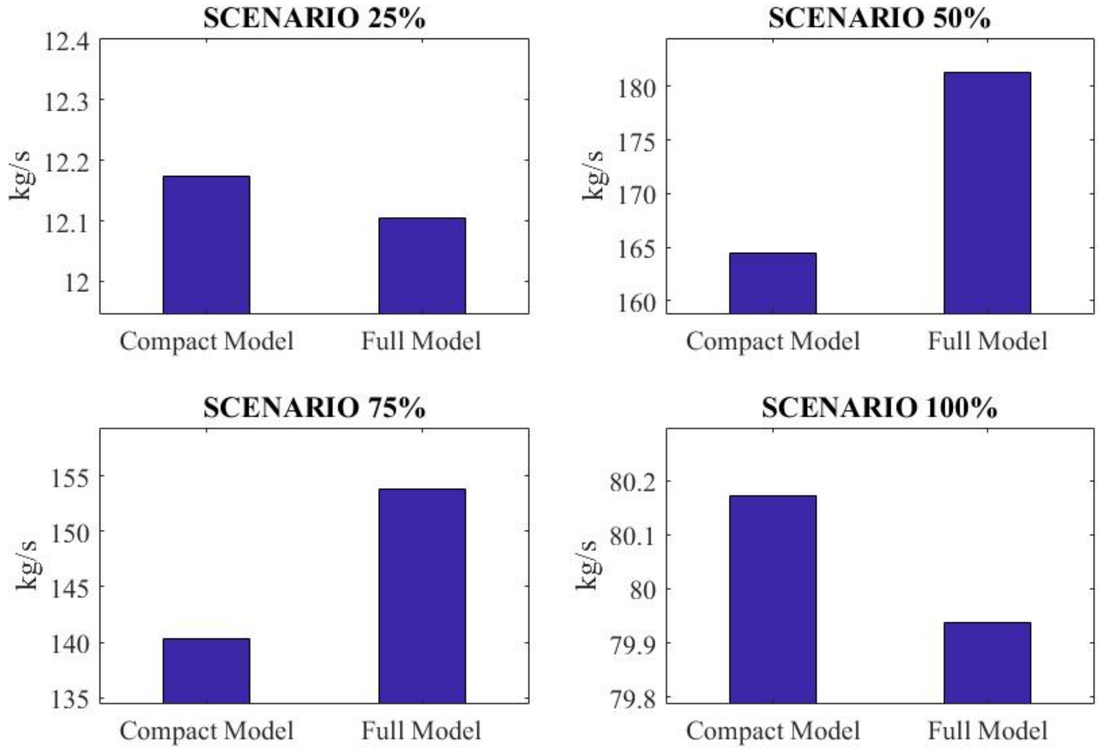

Figure 26 *LTTB_3*: comparison of mass flow rates

LTTB_3	SCENARIO 25%	SCENARIO 50%	SCENARIO 75%	SCENARIO 100%
Error% *Compact* vs. *Full model*	***0.57***	***9.31***	***8.85***	***0.29***

Table 5 Relative errors from the C*ompact Model*

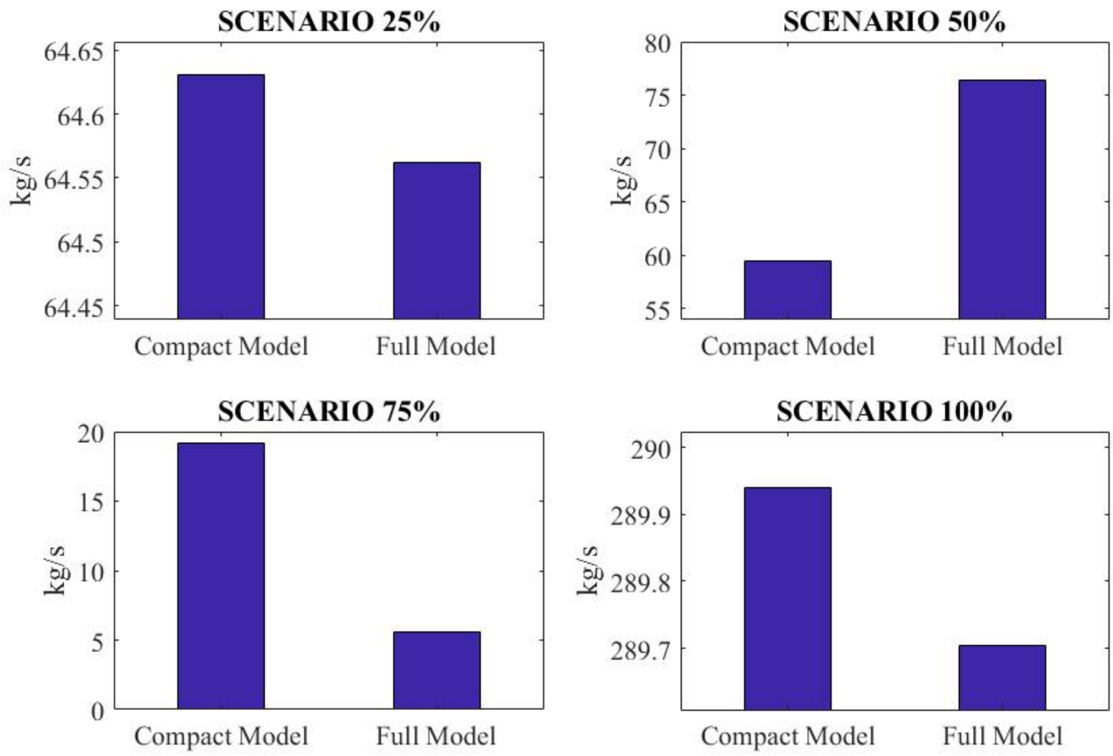

Figure 27 *LTTB_4*: comparison of mass flow rates

LTTB_4	SCENARIO 25%	SCENARIO 50%	SCENARIO 75%	SCENARIO 100%
Error% *Compact* vs. *Full model*	***0.11***	***22.11***	***245.2***	***0.08***

Table 6 Relative errors from the C*ompact Model*

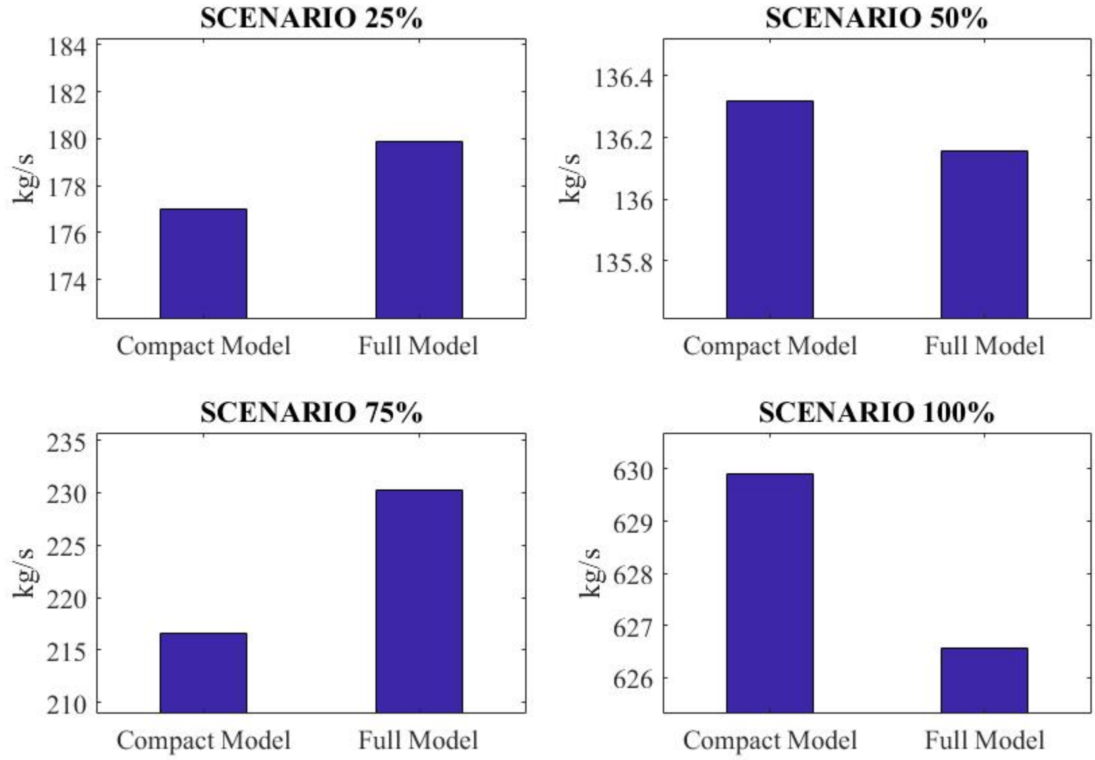

Figure 28 *LTTB_5*: comparison of mass flow rates

LTTB_5	SCENARIO 25%	SCENARIO 50%	SCENARIO 75%	SCENARIO 100%
Error% *Compact* vs. *Full model*	***1.61***	***0.12***	***5.98***	***0.53***

Table 7 Relative errors from the C*ompact Model*

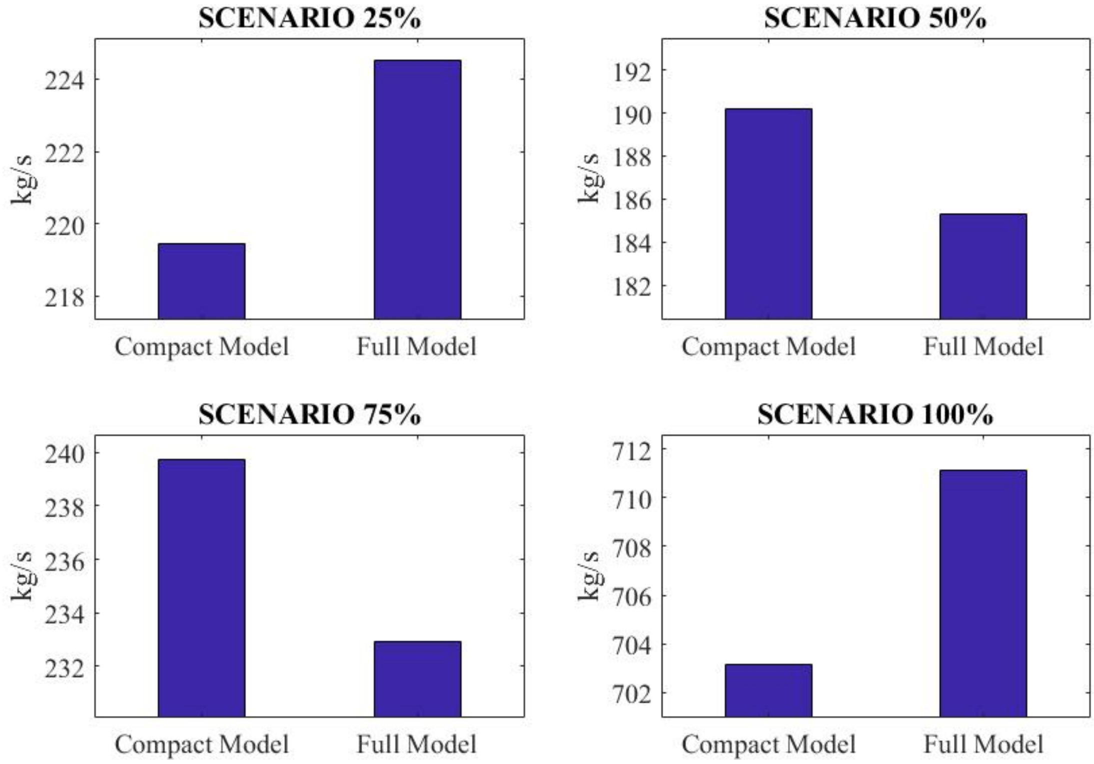

Figure 29 *LTTB_6*: comparison of mass flow rates

LTTB_6	SCENARIO 25%	SCENARIO 50%	SCENARIO 75%	SCENARIO 100%
Error% *Compact* vs. *Full model*	***2.26***	***2.64***	***2.93***	***1.12***

Table 8 Relative errors from the C*ompact Model*

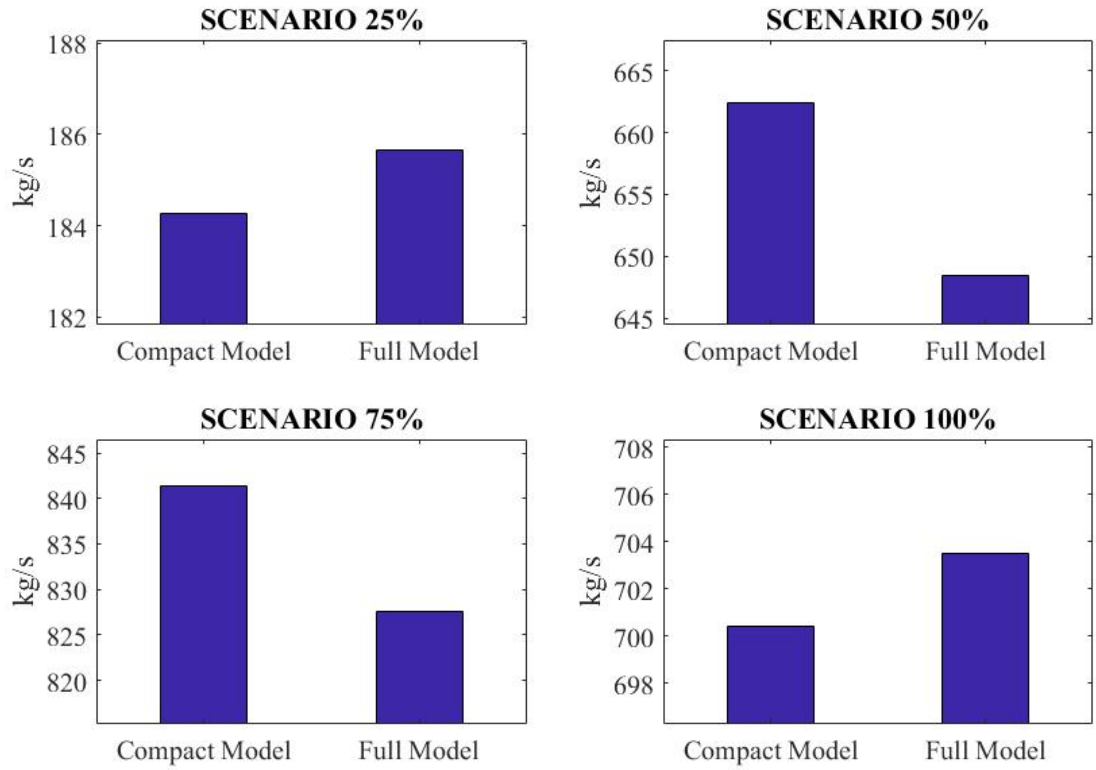

Figure 30 *LTTB_7*: comparison of mass flow rates

LTTB_7	SCENARIO 25%	SCENARIO 50%	SCENARIO 75%	SCENARIO 100%
Error% *Compact* vs. *Full model*	***0.75***	***2.15***	***1.67***	***0.43***

Table 9 Relative errors from the C*ompact Model*

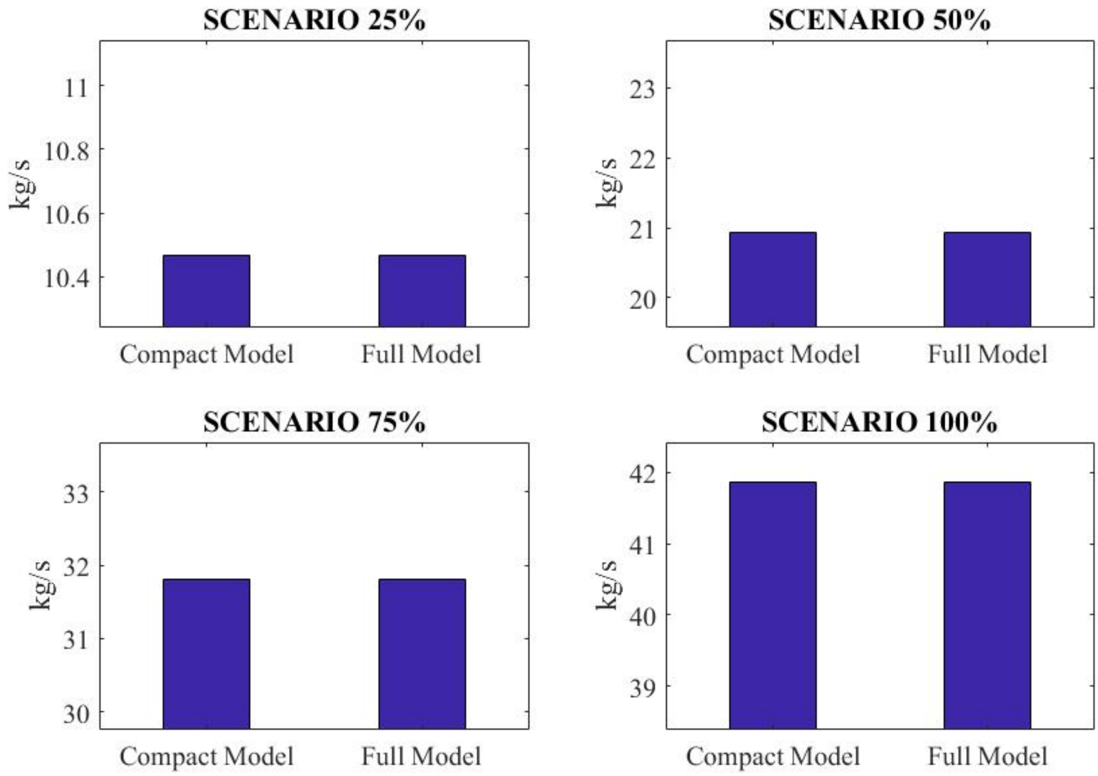

Figure 31 *LTTB_8*: comparison of mass flow rates

LTTB_8	SCENARIO 25%	SCENARIO 50%	SCENARIO 75%	SCENARIO 100%
Error% *Compact* vs. *Full model*	**<0.01**	**<0.01**	**<0.01**	**<0.01**

Table 10 Relative errors from the C*ompact Model*

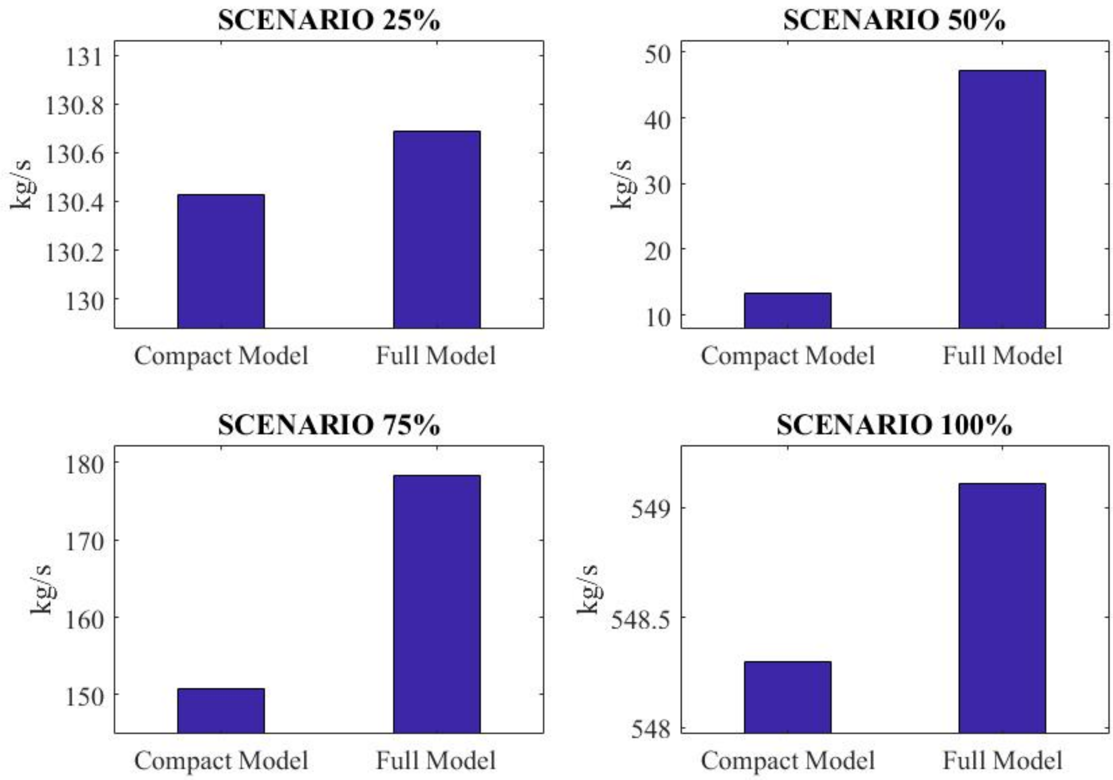

Figure 32 *LTTB_9*: comparison of mass flow rates

LTTB_9	SCENARIO 25%	SCENARIO 50%	SCENARIO 75%	SCENARIO 100%
Error% *Compact* vs. *Full model*	***0.19***	***71.91***	***15.40***	***0.14***

Table 11 Relative errors from the C*ompact Model*

9.2 The *Compact Model*

Evaluation of mass flow rates is now performed along the network using the *Compact Model*. In the following, boundary conditions expressed in *Figure 23* are used in order to simulate the fluid dynamic behaviour of the DHN and compare it to results coming from the *Full Model*. In each scenario, plots of the network show the mass flow rates derived from the *Compact Model*, as well as absolute and relative errors, evaluated to the comparison with the *Full Model* in each branch of the tree-shape network.

Examination of these errors proves a very good accuracy of the new model along the fluid network. Absolute errors illustrated in the previous section in fact, tend to spread only in the loop of origin, causing alteration on its own circulating flow. This behaviour is evident in SCENARIO 25%, 50%, and 75% (*Figures 34, 38, 42*) where higher values occur in branches that are common paths for several loops. Relative error instead shows the impact that absolute errors have relative to the reference mass flow rate coming from the *Full Model*. If a single branch is considered, fluid dynamic errors can be expressed as:

$$Err\%_k = \frac{\left|G_{full_k}\right| - \left|G_{linear_k}\right|}{\left|G_{full_k}\right|} 100 \tag{9.1}$$

where $\boldsymbol{G_{full}}$ is a vector expressed according Section 7.2 that contains mass flow rates from the *Full Model*, while $\boldsymbol{G_{linear}}$ contains mass flow rates from the *Compact Model.* A compared observation of the first and the third graph of each scenario shows large relative errors where low mass flow rates occur: this means that the impact of these alterations on the overall fluid dynamic is limited, particularly respect to the flow handle by power plants.

An energy analysis is also performed in each scenario using the *Thermal Model*. The temperatures evaluation in each node of the equivalent tree-shape network is crucial to understand what impact the use of the *Compact Model* could have on the heat fluxes, particularly where power plants are. For that reason, these temperatures are compared to those evaluated using mass flow rates from the *Full Model*, in order to differentiate heat fluxes from the *Full+Thermal Model* to those from the *Compact+Thermal Model*. To do that, inlet temperatures has to be set in all the inlet nodes: if the real DHN (with loops) is considered, temperature boundary conditions has to be set in all the barycentre nodes, while, in the tree-shape network, also *Boundary Nodes* have to be considered. As in the fluid dynamic simulation in fact, a higher number of boundary conditions is required to solve the thermal problem in the equivalent tree-shape network: the number of boundary conditions in the tree-shape case increases from *NB* to *NB+NL* due to the removal of the *LTTBs.* Temperature in the inlet *Boundary Nodes* are set equal to those evaluated using the *Full+Thermal Model*, while temperatures at barycenter nodes can be found in Appendix F.

Temperatures coming from the *Compact+Thermal Model* are evaluated in each node and depicted according to the topology of the network in *Figures 37, 41, 45 and 49*. In these plots a temperature decreasing can be observed in moving from the centre to the outside of the network. This phenomenon is due to thermal losses that occur along paths, from the inlet points to the power plants; however, it tends to be less evident on higher global load levels. Moving from SCENARIO 25% to SCENARIO 100% in fact, a more homogenous temperature distribution can be noted as a consequence of the increasing fluid velocities. Cooler nodes instead, can be noted where no mass flow rate flows, such as disabled power stations or users.

Temperatures coming from the *Full+Thermal Model* are only evaluated in power plants nodes: in each power station, inlet temperature is compared to the corresponding temperature from the C*ompact Model* and thermal powers are evaluate in the two cases using a fixed supply temperature.

9.2.1 SCENARIO 25%

Power plants mass flow rate [kg/s]	***Moncalieri***	***TN***	***Politecnico***	***Martinetto (storages)***	***TN (storages)***	***BIT***
SCENARIO 25%	625	625	0	0	0	0

Table 12 Mass flow rates at the power plants

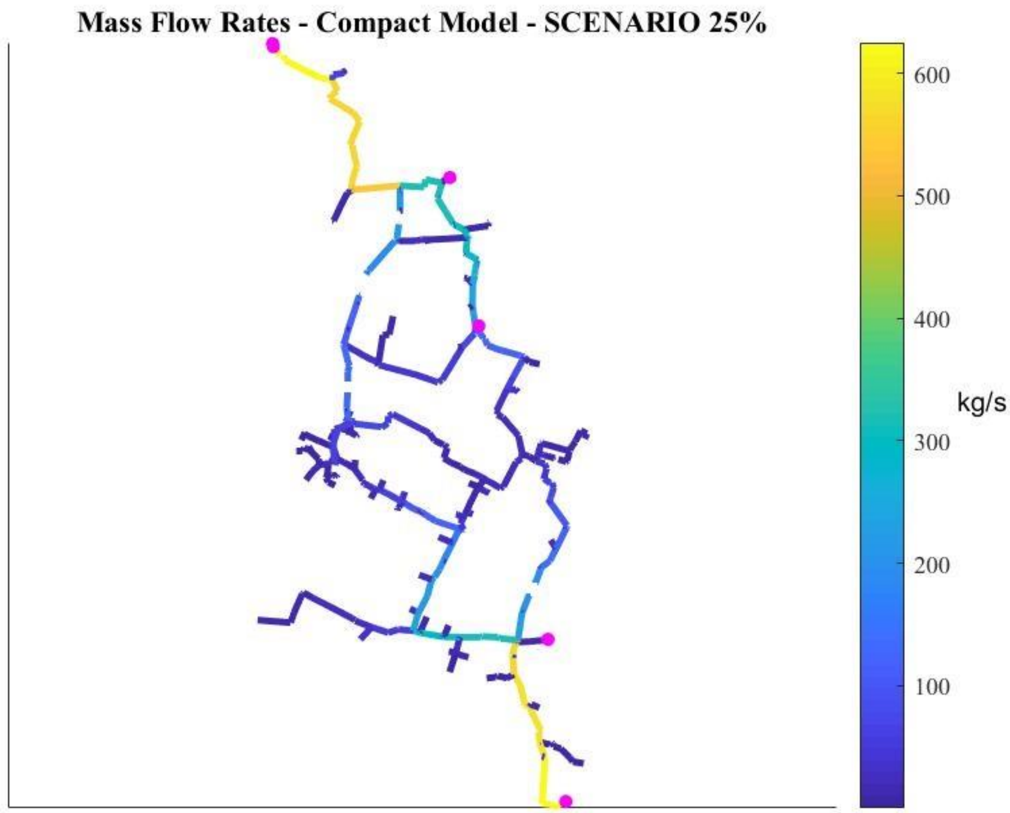

Figure 33 Mass flow rates, SCENARIO 25%. Power plants nodes in magenta.

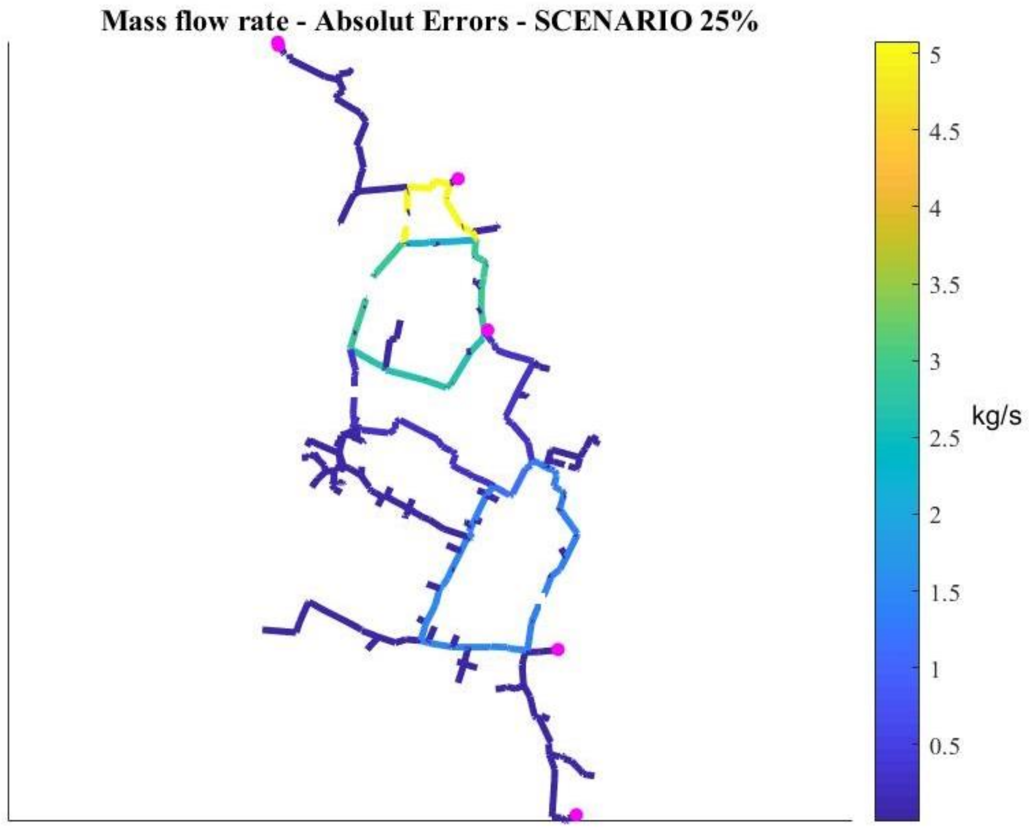

Figure 34 Absolute errors ***ErrAbs***, SCENARIO 25%. Power plants nodes in magenta.

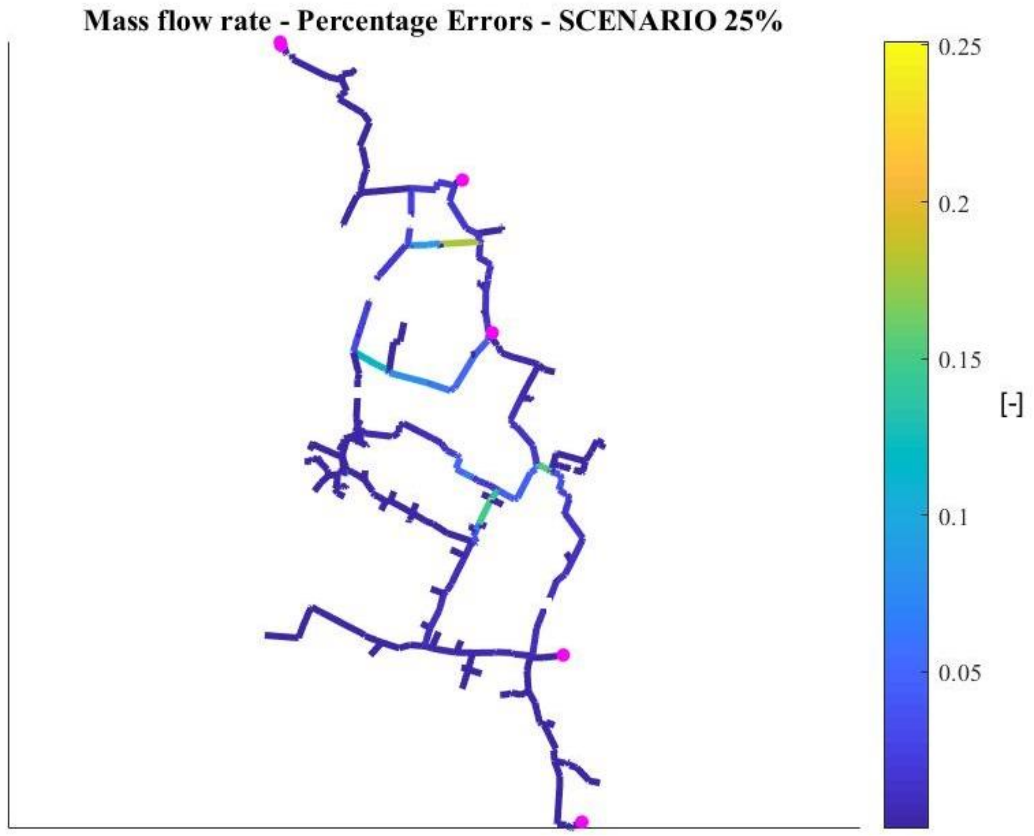

Figure 35 Relative errors ***Err%***, SCENARIO 25%. Power plants nodes in magenta.

Power Plants	**Temp. [K]** *Compact+ Thermal Model*	**Temp. [K]** *Full+Thermal Model*	**Temp. Errors %**	**Heat Flux[14] [MW]** *Compact+ Thermal Model*	**Heat Flux[15] [MW]** *Full+Thermal Model*
Moncalieri	319,7	319,5	0,06	191,80	192,30
TN	298,4	300,9	0,85	247,50	240,95
Politecnico	319,0	304,9	4,61	-	-
Martinetto (storages)	299,8	299,3	0,16	-	-
TN (storages)	299,8	300,5	0,23	-	-
BIT	319,6	319,5	0,03	-	-

Table 13

[14] Constants specific heat and supply temperature (Appendix G)

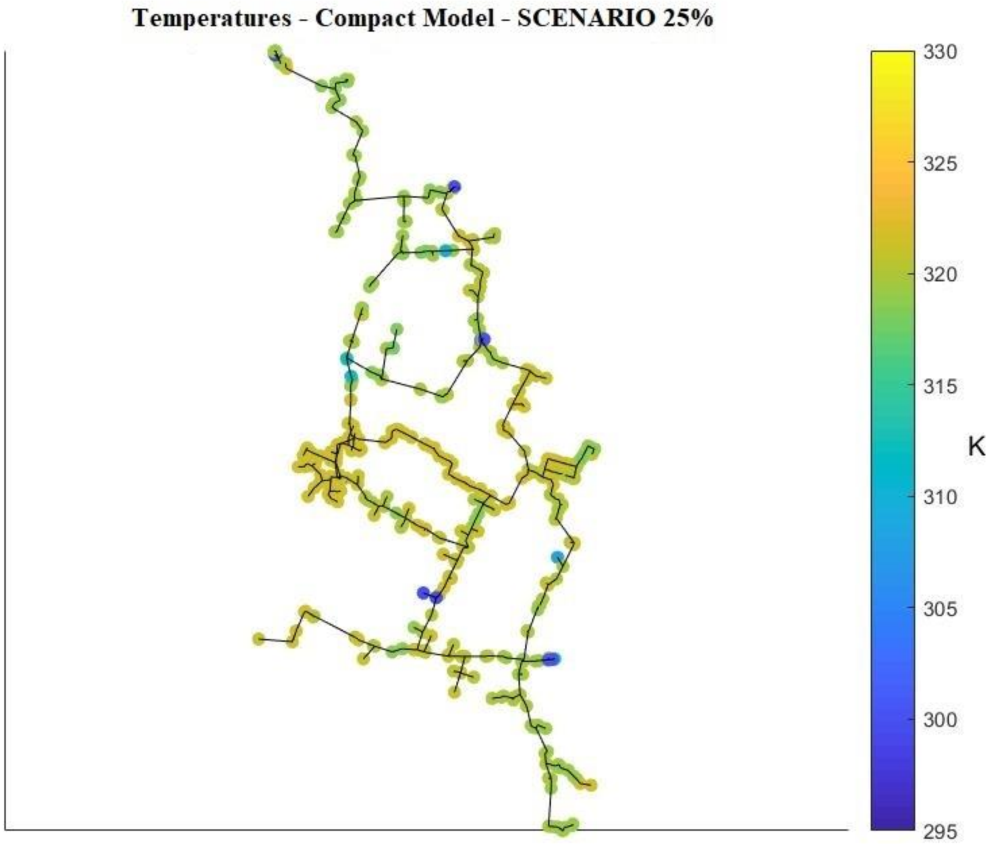

Figure 36 Temperature distribution from the *Compact+Thermal Model*

9.2.2 SCENARIO 50%

Power plants mass flow rate [kg/s]	***Moncalieri***	***TN***	***Politecnico***	***Martinetto (storages)***	***TN (storages)***	***BIT***
SCENARIO 50%	1875	625	0	0	0	0

Table 14 Mass flow rates at the power plants

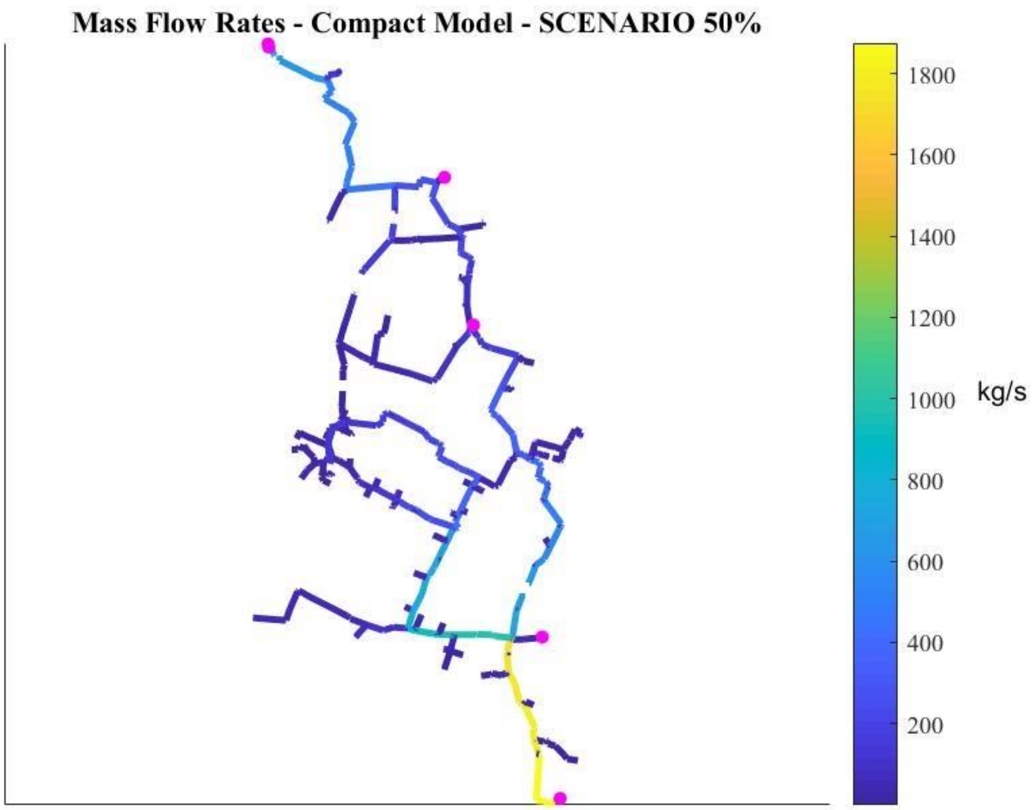

Figure 3735 Mass flow rates, SCENARIO 50%. Power plants nodes in magenta.

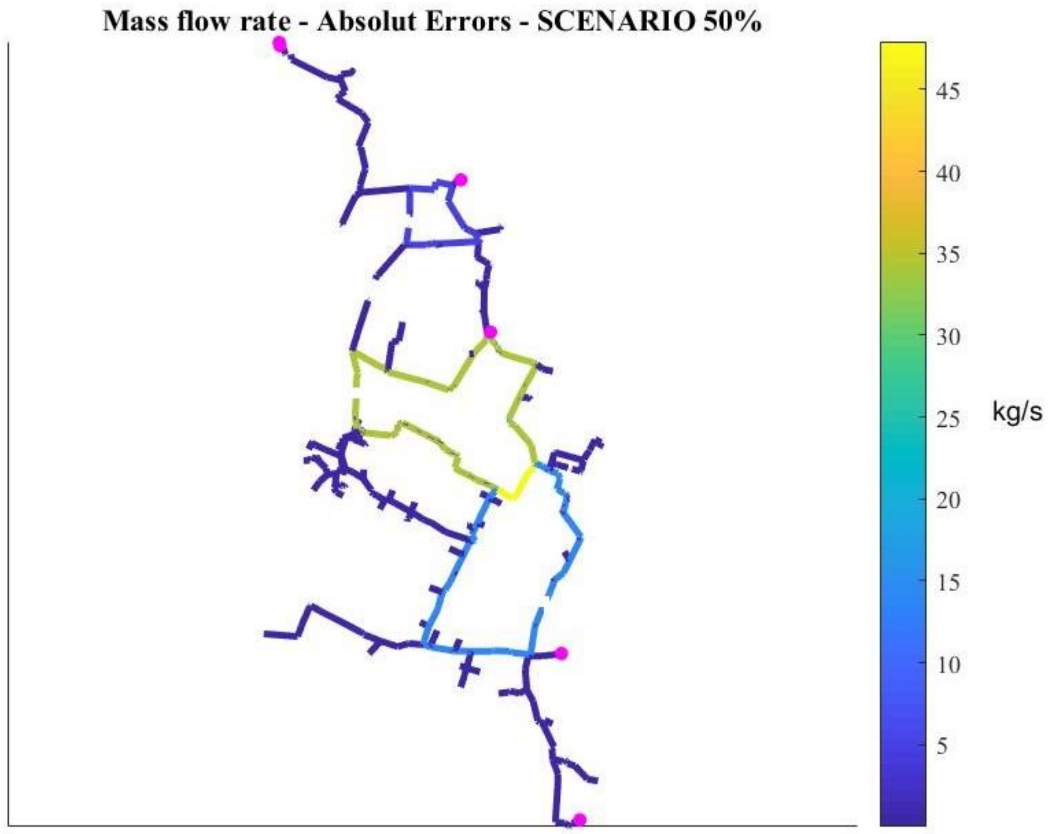

Figure 368 Absolute errors, SCENARIO 50%. Power plants nodes in magenta.

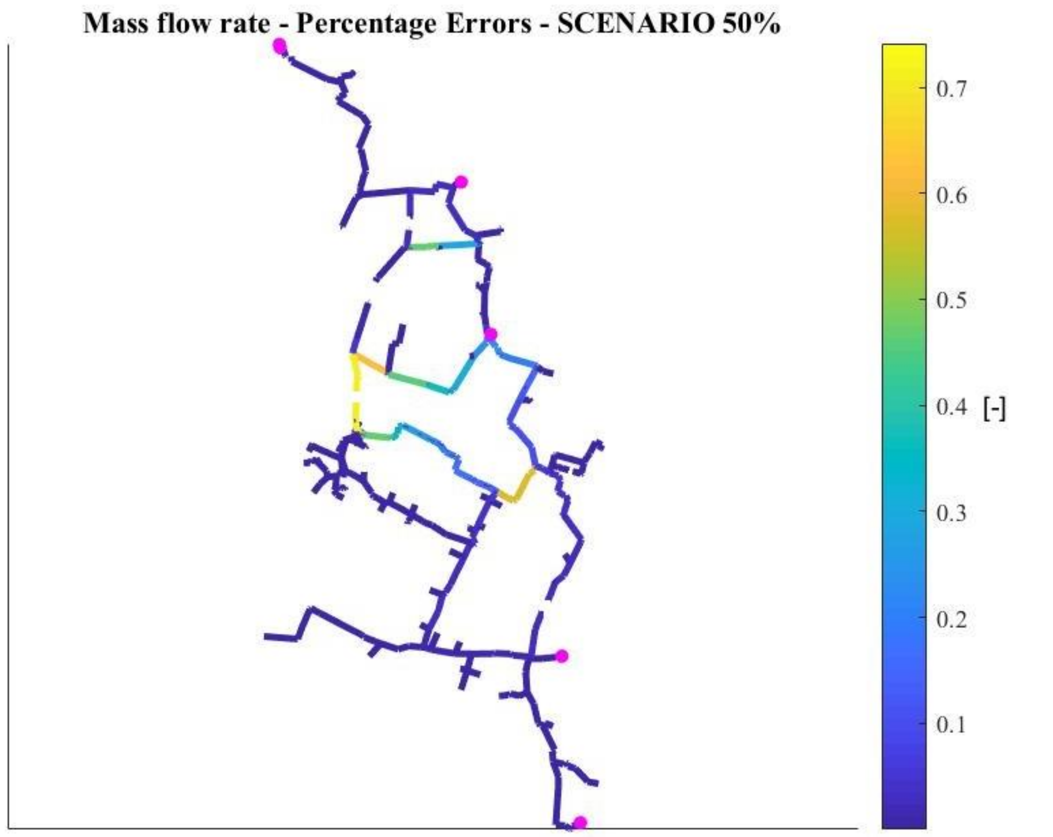

Figure 39 Relative errors, SCENARIO 50%. Power plants nodes in magenta.

Power Plants	**Temp. [K]** *Compact+ Thermal Model*	**Temp. [K]** *Full+Thermal Model*	**Temp. Errors %**	**Heat Flux[15] [MW]** *Compact+ Thermal Model*	**Heat Flux[16] [MW]** *Full+Thermal Model*
Moncalieri	324,2	324,1	0,03	180,00	180,260
TN	322,9	322,5	0,12	183,40	184,45
Politecnico	299,8	301,4	0,53	-	-
Martinetto (storages)	322,2	306,8	5,02	-	-
TN (storages)	299,0	301,2	0,73	-	-
BIT	299,8	300,8	0,33	-	-

Table 15

[15] Constants specific heat and supply temperature (Appendix G)

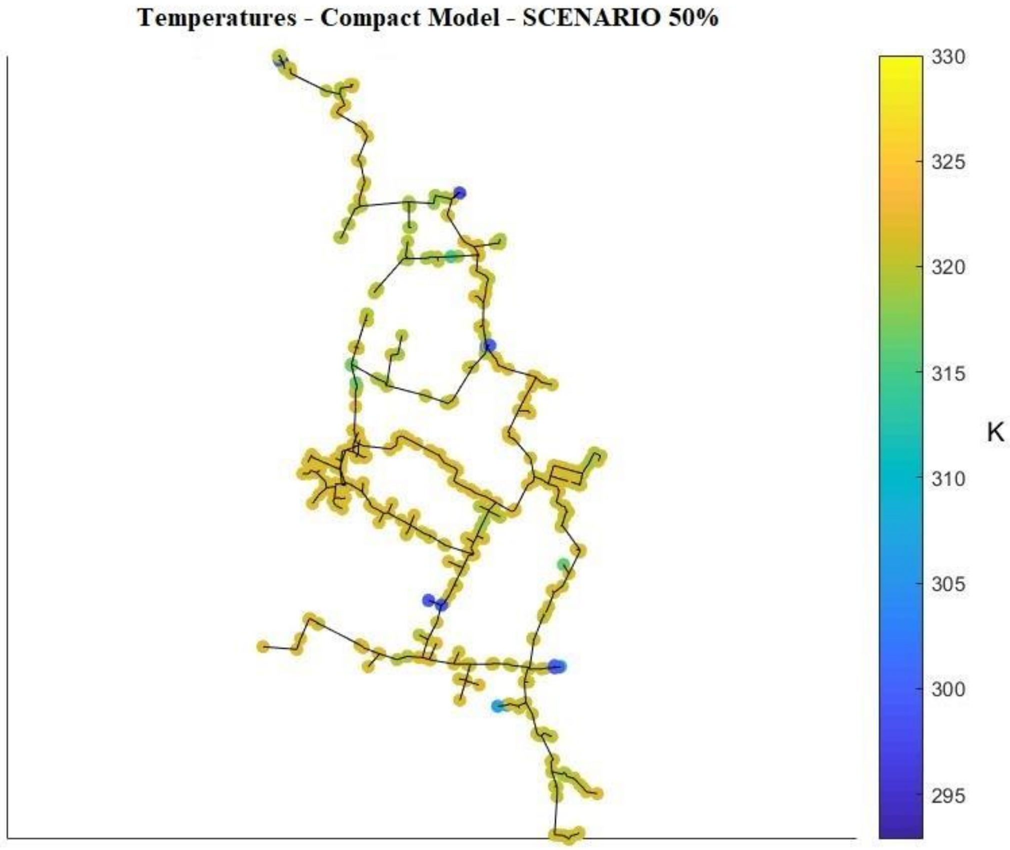

Figure 40 Temperature distribution from the *Compact+Thermal Model*

9.2.3 SCENARIO 75%

Power plants mass flow rate [kg/s]	***Moncalieri***	***TN***	***Politecnico***	***Martinetto (storages)***	***TN (storages)***	***BIT***
SCENARIO 75%	2000	800	500	0	0	500

Table 16 Mass flow rates at the power plants

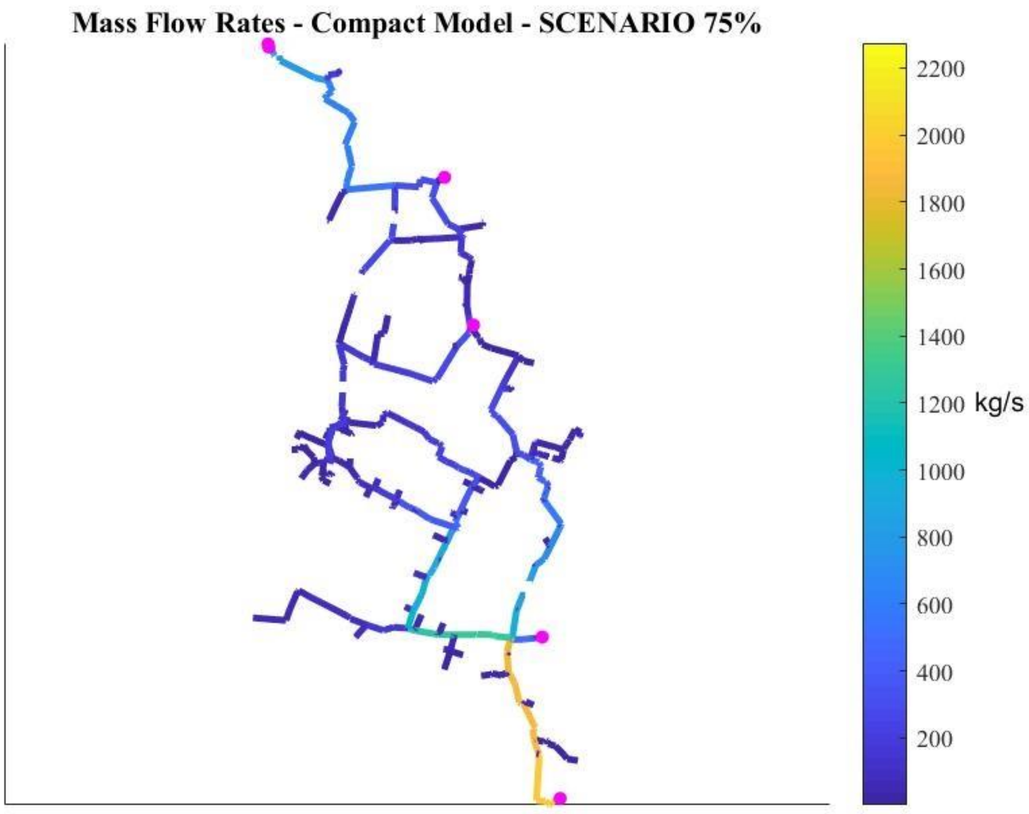

Figure 41 Mass flow rates, SCENARIO 75%. Power plants nodes in magenta.

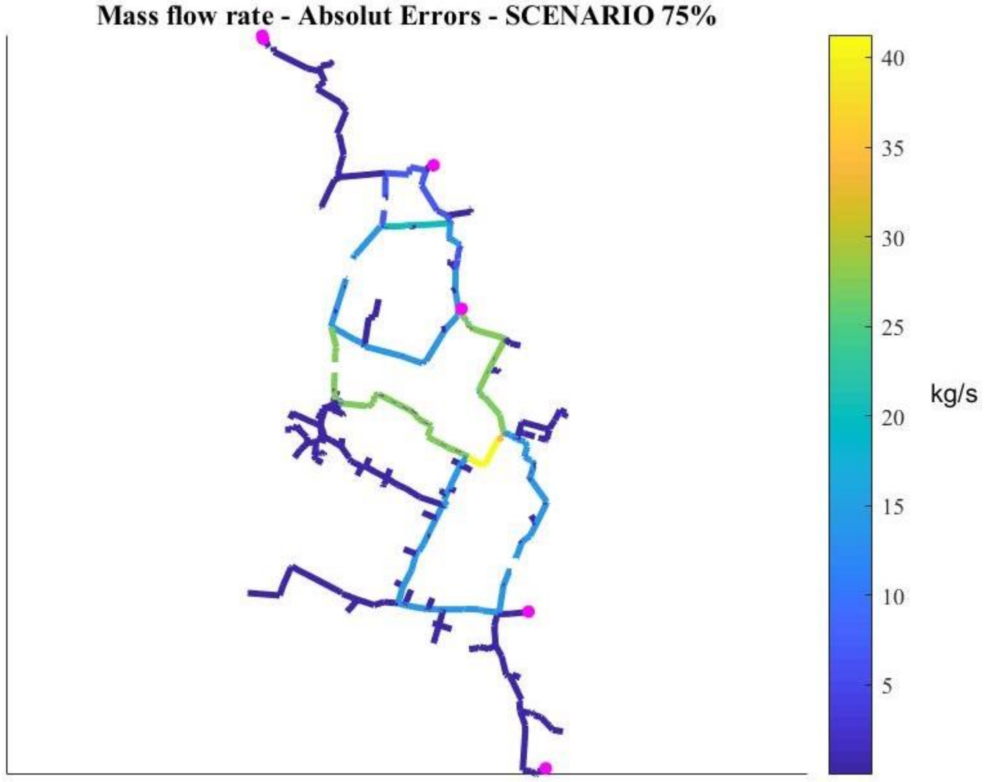

Figure 42 Absolute errors, SCENARIO 75%. Power plants nodes in magenta.

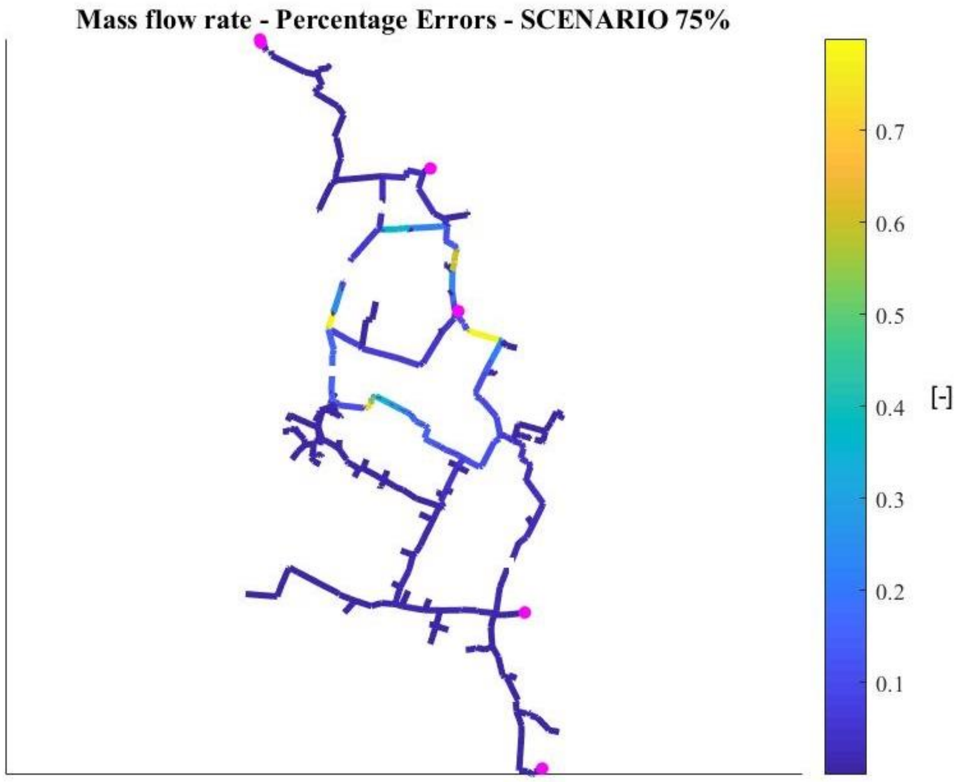

Figure 43 Relative errors, SCENARIO 75%. Power plants nodes in magenta.

Power Plants	**Temp. [K]** *Compact+ Thermal Model*	**Temp. [K]** *Full+Thermal Model*	**Temp. Errors %**	**Heat Flux[16] [MW]** *Compact+ Thermal Model*	**Heat Flux[17] [MW]** *Full+Thermal Model*
Moncalieri	327,8	327,9	0,03	545,22	545,44
TN	327,0	326,5	0,15	221,14	222,57
Politecnico	327,1	326,7	0,12	137,88	138,70
Martinetto (storages)	325,4	308,0	5,65	-	-
TN (storages)	299,0	301,3	0,76	-	-
BIT	327,9	327,9	0,00	136,19	136,22

Table 17

[16] Constants specific heat and supply temperature (Appendix G)

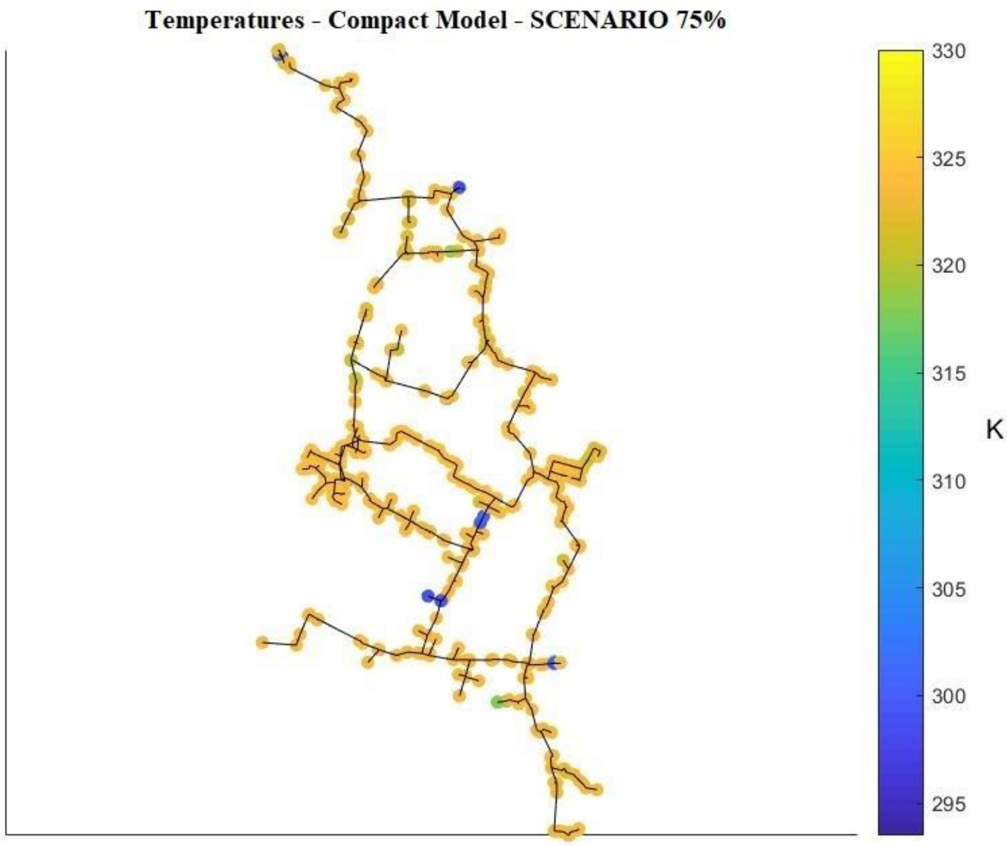

Figure 44 Temperature distribution from the *Compact+Thermal Model*

37

9.2.4 SCENARIO 100%

Power plants mass flow rate [kg/s]	***Moncalieri***	***TN***	***Politecnico***	***Martinetto (storages)***	***TN (storages)***	***BIT***
SCENARIO 100%	2000	800	410	690	690	410

Table 18 Mass flow rates at the power plants

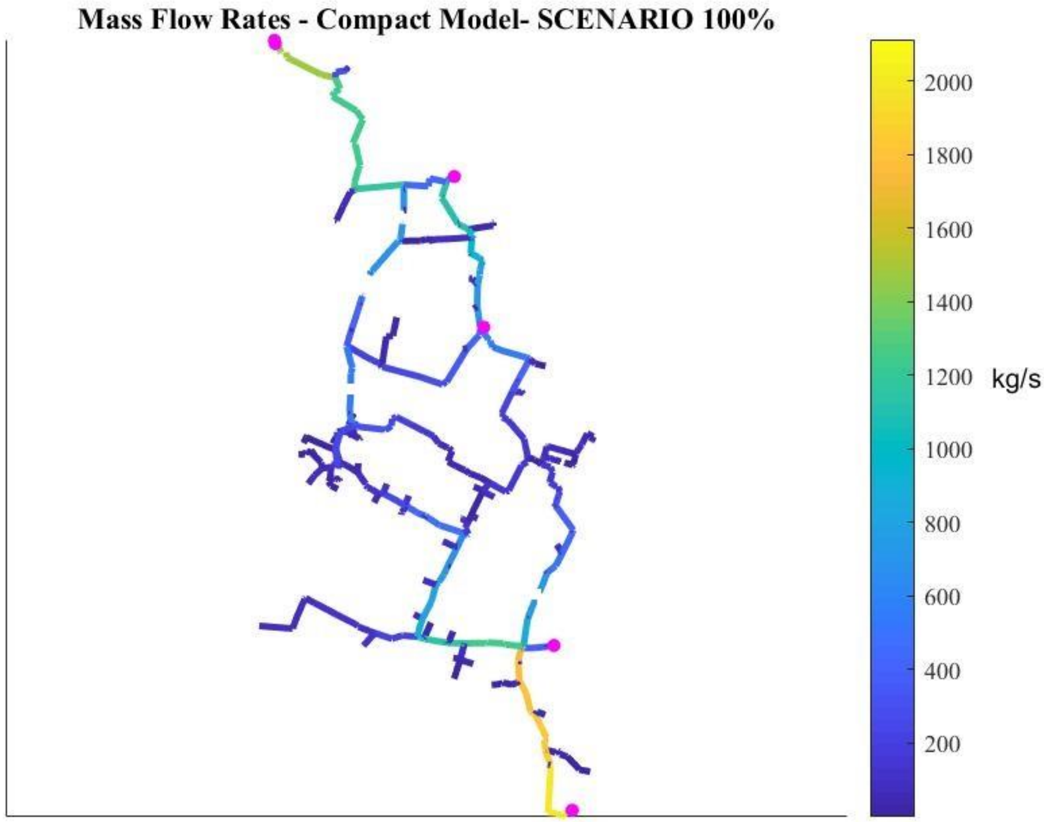

Figure 45 Mass flow rates, SCENARIO 100%. Power plants nodes in magenta.

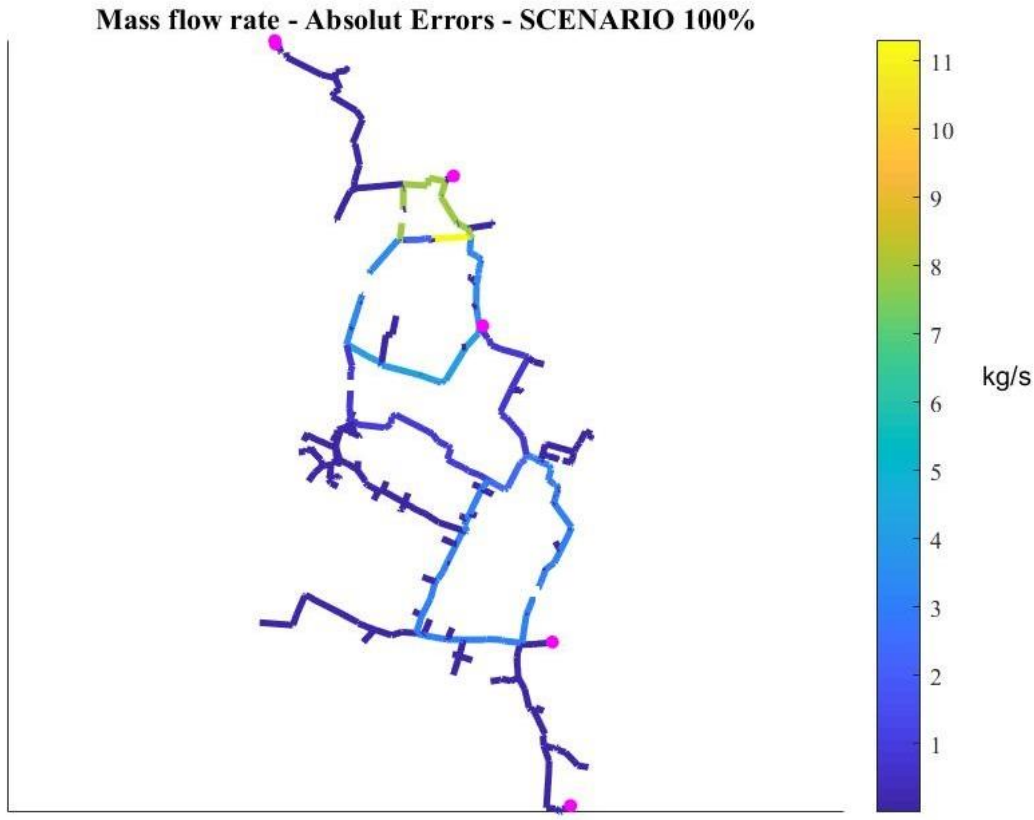

Figure 4638 Absolute errors, SCENARIO 100%. Power plants nodes in magenta.

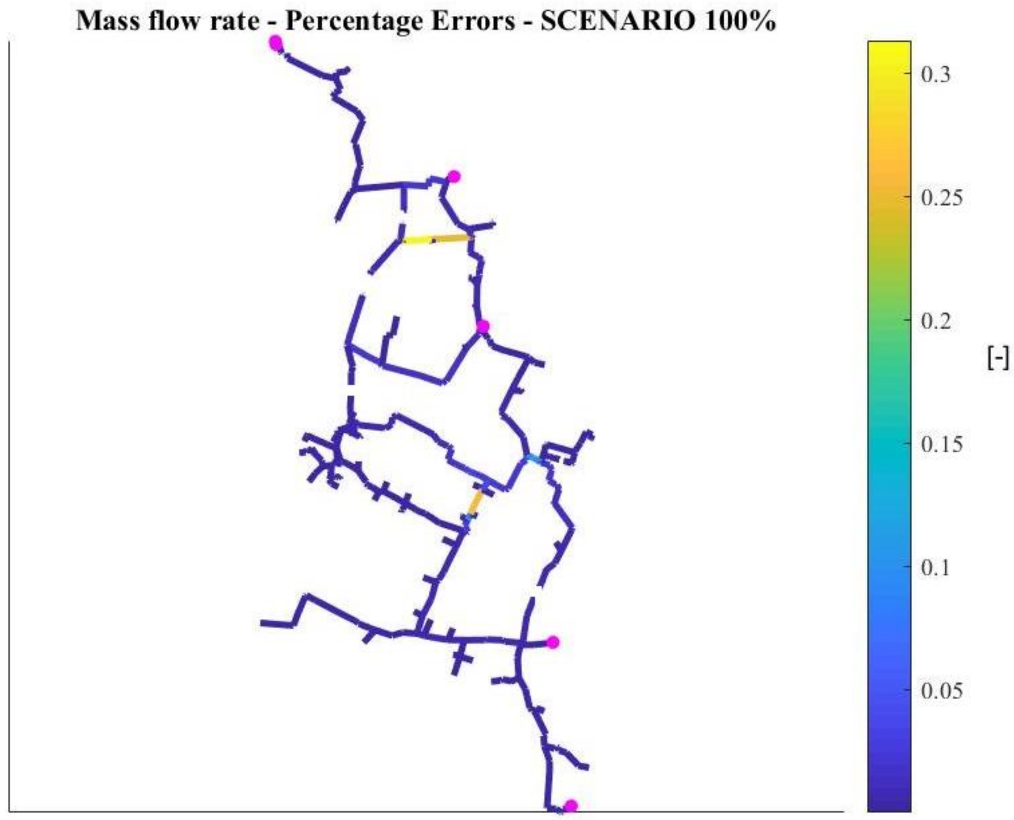

Figure 47 Relative errors, SCENARIO 100%. Power plants nodes in magenta.

Power Plants	**Temp. [K]** *Compact+ Thermal Model*	**Temp. [K]** *Full+Thermal Model*	**Temp. Errors %**	**Heat Flux[17] [MW]** *Compact+ Thermal Model*	**Heat Flux[18] [MW]** *Full+Thermal Model*
Moncalieri	331,3	331,3	0,00	516,76	516,87
TN	331,0	330,9	0,03	207,59	207,97
Politecnico	330,8	330,7	0,03	106,756	106,93
Martinetto (storages)	331,0	330,8	0,06	179,21	179,58
TN (storages)	331,0	330,9	0,03	179,05	179,37
BIT	331,3	331,3	0,00	105,90	105,88

Table 19

[17] Constants specific heat and supply temperature (Appendix G)

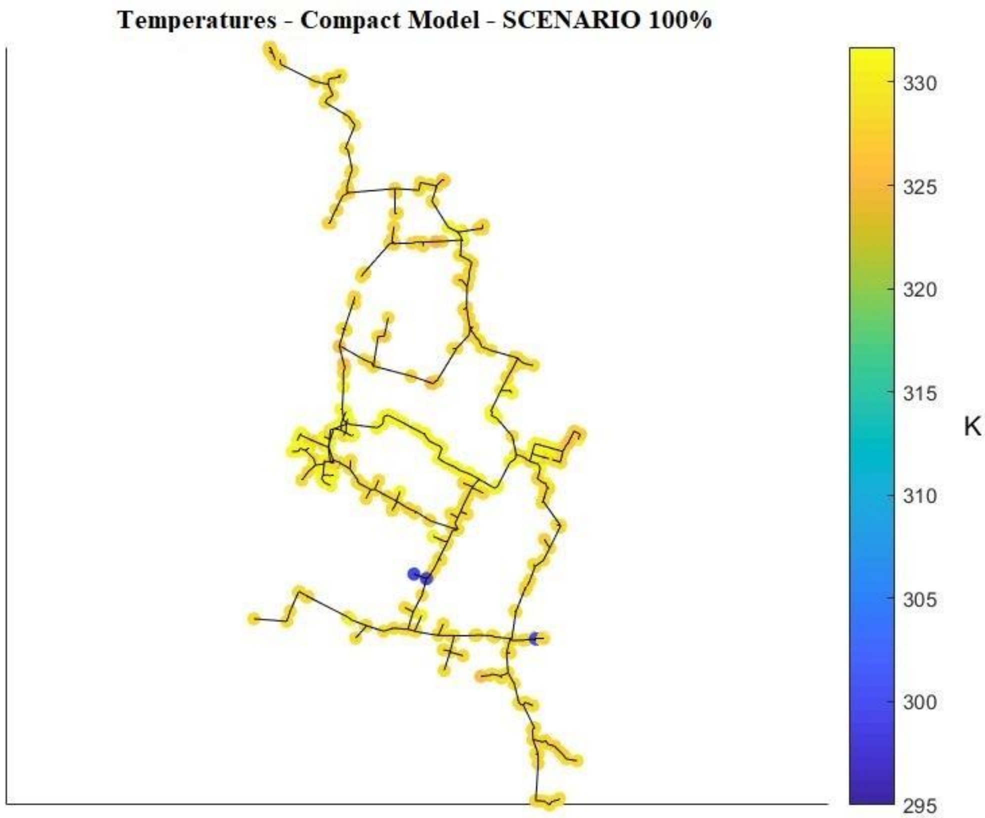

Figure 48 Temperature distribution from the *Compact+Thermal Model*

10.0 Conclusions

An alternative algorithm has been developed to the solution of fluid networks that present loops. The main novelty of this paper is the solution of the fluid dynamic of such networks in a short period of time, respect to the conventional tools. In this respect, a 60% decrease in computational time has been observed, mainly due to the substitution of the iterative resolution strategy with a direct one. Mapping the network is another feature of the presented algorithm: it allows one to observe the thermodynamic evolutions (mass flow rates, temperatures and computational errors) directly from the map.

The algorithm is able to predict the mass flow rate in each branch of the Turin district heating network with a good level of accuracy, as a unique function of the fluid supply at the thermal plants. Analysis of results coming from the new approach shows a mean error rate below the 15% to the comparison with the ‘traditional’ model, in up to 90% of the branches. The thermal power at the power station is also evaluated with a good level of approximation: average temperature errors due to the fluid dynamic alterations are below the 5% in all the power plants. Since a mean temperature evolution has been used for the simulations, a further in-depth analysis can be made using monitored data as boundary temperatures.

Considering future developments, availability and rapidity of the algorithm allows one to include this numeric scheme in thermo-fluid-dynamic software tools that require multiple simulations, in order to make dynamics analysis, network optimization and operation improvements.

List of Symbols

A *Incidence matrix*

A_tree *Incidence matrix* of the equivalent tree-shape network

α User's thermal request coefficient

B *A pp*-by-*NL* matrix of coefficients

b A *pp*-by-1 vector of coefficents

BC.b *A* 1-by-*NN* vector containig the boundary conditions of the network

CV Control volume

DHN District heating network

G Mass flow rates matrix evaluated in each branch of the network using the *Full Model*

Gb Vector of known mass flow rates exchanged at the barycenter nodes

G_full Generic row vector from matrix ***G***

G_ext Vector of external mass flow rates

G_Linear A 1-by-*NB* vector of unknown mass flow rates from the *Compact Model*

$\boldsymbol{G_{LTTB\_n}}$ A *n*-by-*NL* matrix of *LTTBs* mass flow rates from the *Full Model*

G_LTTB_linear A 1-by-*NL* matrix containing estimated mass flow rates values in each *LTTB*

Gpp A1-by-*pp* vector containing mass flow rates flowing at the power plants

i Row index

j Column index

k Thermal conductivity

n Number of observations (simulations)

NB Number of Branches

NL Number of Loops

NN Number of Nodes

P Total pressure

pp Number of power plants

Y Conductance

References

(s.d.). Tratto da Iren Energia: http://www.irenenergia.it/ChiSiamo/Attivita/Teleriscaldamento_Torino/piano_sviluppo.html

Batchelor, G. K. (1967). *An Introduction To Fluid Dynamics.* London: Cambridge University Press.

Elisa Guelpa, e. a. (2017). Thermo-fluid dynamic model of large district heating networks for the analysis of primary energy savings. *Energy*, 4. Tratto da http://dx.doi.org/10.1016/j.energy.2017.07.177

Sciacovelli, V. B. (2015). *Numerical Design of Thermal Systems - II edizione.* Torino: C.L.U.T.

Verda, V. (s.d.). Slides from the course of Numerical Design of Thermal Systems. *1D Thermo-Fluid-Dynamics Network Analysis*. Politecnic of Turin.

Appendix A - Empirical laws for pressure differences

Pressure Difference	Characteristic expression
ΔP_{FRICT}	$\frac{1}{2} f \frac{L}{D_h} \frac{G^2}{\rho\, S^2}$
ΔP_{LOCAL}	$\frac{1}{2} \sum_k \beta_k \frac{G^2}{\rho\, S^2}$
ΔP_{PUMP}	$a(v) + b(v_1) + c$

Where:

f is the friction factor, L the duct length, ρ density, D Diameter, S the cross section,G the mass flow rates, β local resistance factor, k is the number of local losses in a branch and a, b, c are coefficients for the characteristic curve of a pump.

Appendix B - Hydraulic Resistance

$R = \frac{1}{2}\frac{\left(f\frac{L}{D_h}+\sum_k \beta_k\right)}{\rho \cdot S^2}G$, in each branch, where friction and local losses occurs.

Appendix C - Nodes coordinates

Junction, barycenter nodes and power plants nodes are collect in a data array in which the x-y coordinates appear.

Node Name	x-coordinate [m]	y-coordinate [m]
NMN01	1391911,8	4988878,2
NMN02	1391829,2	4988914,2
NMN03	1391656,2	4988987,4
NMN04	1391509,2	4989053,2
NMN05	1391438,4	4989090,3
NMN06	1391452,9	4989117,2
NMN07	1391389,0	4988994,4
NMN08	1391913,1	4988896,6
NMN09	1391916,8	4988953,4
NMN10	1391922,0	4989022,8
NMN11	1391894,6	4989030,2
NMN12	1391832,6	4989056,4
NMN13	1391925,4	4989065,9
NMN14	1391930,7	4989135,2
NMN15	1391933,3	4989170,5
NMN16	1392001,1	4989191,4
NMN17	1392113,2	4989160,3
NMN18	1392114,9	4989288,8
NMN19	1392191,4	4989471,4
NMN20	1392121,7	4989155,8
NMN21	1392170,3	4989130,3
NMN22	1392159,4	4989071,7
NMN23	1392192,2	4989118,9
NMN24	1392192,3	4989194,8
NMN25	1392193,9	4989217,3
NMN26	1392199,2	4989289,1
NMN27	1392216,4	4989353,0
NMN28	1392288,2	4989069,3
NMN29	1392317,7	4989089,7
NMN51	1391837,8	4988650,2
NMN52	1391830,5	4988661,7
NMN53	1391830,3	4988609,7
NMN54	1391819,8	4988484,7
NMN55	1391812,1	4988421,0
NMN56	1391789,3	4988377,6
NMN57	1391830,5	4988310,5
NMN58	1391938,5	4988254,1
NMN59	1391861,3	4988429,0
NMN60	1391884,3	4988430,9
NMN61	1391915,0	4988417,0
NMN62	1391935,0	4988415,6
NMN63	1391943,3	4988408,3
NMN64	1391964,0	4988425,7
NMN65	1391966,6	4988414,2
NMN66	1391986,1	4988434,9
NMN67	1391747,9	4988597,4
NMN68	1391688,3	4988590,2
NMN69	1391670,0	4988685,8
NMN70	1391523,7	4988831,8
NMN71	1391582,5	4988869,5
NMN72	1391437,8	4988866,3
NMN73	1391410,5	4988817,2
NMN74	1391308,8	4988813,1
NMN75	1391643,6	4988548,3
NMN76	1391566,4	4988477,8
NMN77	1391465,2	4988340,9
TMNCAS	1391984,8	4988647,0
TMNCRE	1391982,8	4988647,1
AFCH1	1395408,6	4983065,3
AFDO1	1392282,9	4993415,5
AFPO1	1395762,0	4983820,3
AFS01	1395445,2	4984047,6
AFS02	1395273,5	4984253,7
AFS03	1394577,9	4985145,9
AFS04	1394325,3	4985790,9
AFS05	1394587,6	4989433,3
AFS06	1394366,0	4990651,3
AFS07	1392158,0	4990145,8
AFSA1	1395050,0	4984664,2
CA001	1395454,8	4983061,8
CA002	1395350,1	4983069,8
CA005	1395061,9	4984651,8
CA006	1395030,8	4984684,3
CA007	1394955,6	4984995,1
CA009	1395169,9	4986602,2
CA011	1395468,5	4988299,9

Node Name	x-coordinate [m]	y-coordinate [m]
CA012	1395439,8	4988292,4
CA014	1394588,5	4985785,1
CA016	1394309,2	4985786,5
CA017	1393915,6	4985787,0
CA018	1393723,1	4985819,4
CA020	1393332,6	4985887,0
CA021	1393152,1	4985894,7
CA022	1393290,9	4986181,0
CA023	1393439,1	4986449,4
CA024	1393557,3	4986759,1
CA025	1393566,6	4986777,9
CA026	1393831,7	4987276,9
CA027	1393949,8	4987525,7
CA029	1393574,9	4987675,8
CA030	1393547,7	4987692,3
CA031	1393237,5	4987865,4
CA032	1393202,6	4987883,9
CA034	1392418,2	4988281,4
CA035	1392386,5	4988318,1
CA037	1392807,7	4985858,2
CA038	1392269,5	4986049,0
CA039	1392261,5	4986064,0
CA040	1392217,3	4986092,4
CA041	1391408,6	4986496,0
CA042	1391215,7	4986020,7
CA045	1395101,6	4985711,0
CA046	1395152,0	4985718,9
CA051	1395462,5	4984062,6
CA052	1395706,6	4983874,2
CA053	1395811,7	4983757,3
CA055	1394591,3	4985153,4
CA056	1394556,3	4985133,9
CA061	1395383,8	4988530,5
CA062	1395350,0	4988607,4
CA063	1394983,7	4988772,6
CA064	1394975,7	4988692,7
CA065	1394579,5	4989406,1
CA066	1394598,4	4989464,0
CA067	1394093,9	4991631,7
CA068	1394051,4	4991632,5
CA069	1394213,9	4991690,5
CA070	1394219,2	4991772,6
CA071	1394255,0	4991921,6
CA072	1394198,5	4991968,0
CA073	1394224,4	4990780,2
CA074	1394209,8	4990733,4
CA075	1393670,1	4989975,0
CA076	1393619,0	4989929,6
CA077	1392581,1	4990282,1
CA078	1392483,9	4990325,4
CA079	1392446,6	4991690,0
CA080	1392477,3	4991747,7
CA082	1394382,2	4990643,6
CA083	1394351,9	4990659,0
CB001	1395986,5	4983727,5
CB005	1394407,1	4985116,1
CB006	1395263,8	4984635,2
CB007	1394746,2	4985089,0
CB009	1394892,7	4985502,9
CB011	1395307,5	4985760,5
CB012	1395271,2	4986958,3
CB013	1395451,2	4987368,6
CB014	1395653,8	4987610,1
CB016	1395413,2	4987971,2
CB017	1395456,4	4988133,5
CB019	1393789,8	4985977,5
CB020	1393791,0	4985551,9
CB021	1394112,1	4985454,8
CB023	1393804,6	4985214,4
CB024	1393755,5	4987031,9
CB025	1393432,3	4986116,8
CB026	1393159,3	4986249,0
CB027	1393308,2	4986798,9
CB028	1392350,4	4985746,3
CB029	1390677,9	4986062,8
CB030	1393624,9	4987418,4
CB031	1393320,2	4987799,0
CB033	1393079,1	4988152,8
CB034	1392952,7	4987844,8
CB035	1393907,5	4987788,4
CB036	1394181,1	4987783,8
CB037	1394118,0	4988295,1
CB038	1394446,5	4988125,7
CB054	1392520,8	4988039,7
CB055	1392727,7	4988339,9
CB056	1392372,5	4988315,6
CB057	1392266,7	4988670,9
CB06B	1395291,4	4984267,6
CB10B	1395132,8	4986530,7
CB15B	1395527,5	4988209,0
CB17B	1395337,2	4988374,1

Node Name	x-coordinate [m]	y-coordinate [m]
CB261	1392100,6	4995000,7
CB263	1392110,5	4995000,4
CB264	1392105,5	4995000,6
CB265	1392095,9	4995001,0
CB266	1392090,8	4995001,1
CB291	1392075,0	4995001,3
CB292	1392070,0	4995001,6
CB294	1392064,8	4995001,7
CB29B	1391546,6	4986417,8
CB401	1394921,5	4989060,5
CB402	1394666,1	4989361,5
CB403	1394594,3	4989395,6
CB404	1394571,0	4989475,2
CB406	1394830,6	4990032,2
CB410	1394920,2	4989776,2
CB413	1394956,7	4990366,0
CB418	1394213,3	4991009,5
CB419	1394120,6	4991145,7
CB420	1394011,6	4990513,8
CB422	1393589,7	4989933,8
CB423	1393691,7	4989968,0
CB424	1393261,9	4990047,6
CB426	1392884,2	4991011,4
CB429	1392336,4	4991245,3
CB430	1392191,3	4990803,5
CB431	1392083,5	4990548,1
CB432	1392324,0	4991355,3
CB433	1392129,1	4990826,4
CB440	1394268,8	4991913,5
CB441	1394054,2	4992045,8
CB442	1394039,6	4991634,1
CB443	1393462,0	4992192,4
CB445	1392982,0	4992216,4
CB447	1392501,6	4991749,6
CB456	1392103,9	4989506,0
CB462	1393887,3	4992507,1
CB463	1393622,5	4992915,0
CB480	1393808,0	4993267,6
CBV60	1392083,6	4994993,2
CBV90	1392095,5	4994967,3
CM001	1395274,8	4984076,7
CM002	1394797,1	4985149,2
CM003	1395709,0	4987571,6
CM006	1395496,7	4988217,4
CM007	1393966,1	4985765,5
CM008	1392508,4	4985957,3
CM009	1393809,6	4987335,0
CM010	1394389,9	4988351,6
CM011	1393707,1	4988697,3
CM012	1393696,5	4988918,2
CM013	1393320,9	4989182,8
CM014	1392682,2	4989209,8
CM015	1394598,9	4989395,4
CM016	1394570,8	4989471,9
CM019	1394384,9	4990616,9
CM021	1394505,8	4992808,3
CM022	1392274,8	4991275,8
CM024	1392153,1	4990258,4
CV001	1395253,9	4984238,0
CV002	1393334,3	4985853,5
CV003	1395338,8	4988369,8
CV004	1394379,1	4988353,3
CV005	1394682,5	4988239,4
CV006	1395019,9	4988753,7
CV007	1395096,9	4988727,9
CV008	1395214,4	4988665,3
CV009	1394925,3	4989061,1
CV010	1394942,1	4990201,4
CV011	1394744,7	4989815,9
CV012	1394013,3	4990513,8
CV013	1394012,7	4990510,5
CV014	1394012,1	4990512,2
CV015	1392644,4	4990208,0
CV016	1392641,0	4990205,9
CV017	1392641,9	4990208,1
CV018	1392081,1	4990547,5
CV019	1392081,3	4990543,7
CV020	1392079,9	4990546,9
CV021	1394210,9	4991662,3
CV022	1394096,7	4992279,3
CV023	1394111,7	4992279,1
CV024	1394088,5	4992332,6
CV025	1392962,1	4992234,8
CV026	1392948,0	4992295,5
CV027	1392972,5	4992234,8
CV029	1394959,8	4990365,3
CV030	1391119,3	4995178,2
CV031	1391907,7	4994942,5
CV032	1391847,7	4994552,6
CV033	1392221,7	4993064,2
CV034	1392222,2	4993067,7

Node Name	x-coordinate [m]	y-coordinate [m]
CV035	1392993,5	4993099,3
CV036	1393413,1	4993236,8
CV038	1393682,8	4993178,1
CV039	1394060,1	4992428,8
CV041	1392156,1	4989317,0
NC001	1394924,4	4989062,4
NC002	1394667,0	4989363,4
NC003	1394595,1	4989397,2
NC004	1394570,1	4989472,1
NC005	1394737,0	4989819,9
NC006	1394882,7	4989814,5
NC007	1394886,5	4989811,6
NC008	1394842,9	4990026,0
NC009	1395015,4	4990346,6
NC010	1395016,3	4990348,3
NC011	1395019,3	4990335,7
NC012	1395104,7	4990265,8
NC013	1394958,8	4990367,1
NC014	1394573,4	4990475,0
NC015	1394421,1	4990536,3
NC016	1394209,8	4990725,3
NC017	1394208,4	4990725,1
NC018	1394013,0	4990512,1
NC019	1394011,4	4990512,4
NC020	1393684,1	4989973,5
NC021	1393674,1	4989975,3
NC022	1393587,0	4989942,5
NC023	1393256,7	4990056,3
NC024	1392654,6	4990214,4
NC025	1392642,7	4990206,9
NC026	1392717,3	4990699,7
NC027	1392715,3	4990700,1
NC028	1392820,8	4990712,7
NC029	1392822,6	4990720,5
NC030	1392607,9	4990280,8
NC031	1392085,2	4990553,1
NC032	1392081,5	4990548,7
NC033	1392080,8	4990546,7
NC034	1392164,5	4990825,5
NC035	1392168,9	4990838,6
NC036	1392303,1	4991252,1
NC037	1392308,9	4991269,6
NC040	1392335,4	4991350,5
NC041	1392492,6	4991757,7
NC043	1392911,0	4992233,3
NC044	1392968,2	4992236,6
NC045	1392975,7	4992256,9
NC046	1392944,3	4992262,8
NC047	1394199,2	4991007,4
NC048	1394174,2	4991182,1
NC049	1394180,7	4991531,2
NC050	1394217,5	4991683,9
NC051	1394256,2	4991912,4
NC052	1394258,9	4991911,1
NC053	1394072,0	4992033,8
NC054	1394088,1	4992281,2
NC055	1394107,9	4992282,1
NC056	1394105,4	4992296,5
NC057	1394087,7	4992299,0
NC058	1394109,9	4992293,2
NC059	1393778,3	4992270,9
NC060	1393662,7	4992264,8
NC061	1393449,6	4992256,0
NC062	1393347,2	4992259,2
NC063	1393269,0	4992237,2
NC064	1392987,8	4992235,1
NC065	1392084,1	4990534,5
NC066	1392173,8	4990199,8
NN001	1391108,8	4995260,2
NN002	1391110,7	4995245,6
NN003	1391680,0	4994899,1
NN004	1391899,1	4994850,0
NN005	1392082,6	4994967,8
NN006	1391977,4	4994672,1
NN007	1391884,4	4994618,7
NN008	1391861,4	4994576,8
NN009	1392235,4	4994322,7
NN010	1392338,6	4994179,0
NN011	1392181,5	4993798,1
NN012	1392220,2	4993781,5
NN013	1392294,9	4993442,9
NN014	1392270,6	4993390,0
NN015	1392210,2	4993182,7
NN016	1392208,0	4993075,9
NN017	1394087,5	4992303,0
NN018	1394028,6	4992423,1
NN019	1394086,9	4992428,6
NN020	1394361,9	4992472,2
NN021	1394430,6	4992478,6
NN022	1394436,6	4992532,5
NN028	1393870,3	4992502,4

Node Name	x-coordinate [m]	y-coordinate [m]
NN029	1393603,6	4992930,6
NN030	1393673,9	4993180,1
NN031	1393776,9	4993284,8
NN032	1393568,0	4993203,7
NN033	1393391,0	4993110,0
NN034	1392994,3	4993136,0
NN035	1392945,0	4992274,7
NN036	1392951,0	4992313,3
NN037	1392978,1	4992506,5
NN038	1392973,2	4992507,3
NN039	1392995,8	4992724,0
NN040	1392997,1	4993063,0
NN041	1392139,4	4993018,0
NN042	1392022,8	4992789,8
NN043	1391924,2	4992574,1
NN044	1391920,2	4992565,5
NS001	1395309,2	4983073,0
NS002	1395349,4	4983681,5
NS003	1395350,3	4983834,1
NS004	1395266,0	4984072,0
NS005	1395429,5	4984033,9
NS006	1395482,6	4984046,4
NS007	1395501,3	4984004,5
NS008	1395617,2	4983967,9
NS009	1395288,2	4984265,7
NS010	1395104,1	4984645,4
NS011	1395136,9	4984690,0
NS012	1394854,0	4985175,7
NS013	1394732,1	4985121,5
NS014	1394830,0	4985502,9
NS015	1394878,9	4985701,0
NS016	1395306,6	4985731,7
NS017	1395306,9	4985729,8
NS018	1394982,4	4986176,0
NS019	1395145,9	4986590,3
NS020	1395216,0	4986703,6
NS021	1395300,4	4986924,8
NS022	1395435,5	4987026,9
NS023	1395537,4	4987225,5
NS024	1395716,4	4987597,4
NS025	1395430,5	4987994,5
NS026	1395422,9	4987997,0
NS027	1395415,9	4987980,7
NS028	1395469,8	4988124,8
NS029	1395494,3	4988209,0
NS030	1395511,8	4988213,7
NS031	1395337,9	4988365,5
NS032	1395210,2	4988651,0
NS033	1395227,3	4988709,6
NS034	1395250,6	4988790,0
NS035	1395328,1	4988753,1
NS036	1395351,6	4988741,7
NS037	1395412,0	4988727,8
NS038	1395437,6	4988719,9
NS039	1395513,3	4988697,9
NS040	1395575,8	4988680,3
NS041	1395618,3	4988667,4
NS042	1395630,0	4988664,1
NS043	1395704,6	4988642,9
NS044	1395708,9	4988631,6
NS045	1395292,3	4988933,3
NS046	1395293,2	4988936,7
NS047	1395304,5	4988940,6
NS048	1395385,6	4988918,1
NS049	1395453,8	4988899,1
NS050	1395574,1	4988865,5
NS051	1395575,1	4988867,7
NS052	1395680,2	4988835,6
NS053	1395745,0	4988818,7
NS054	1395807,8	4988912,2
NS055	1395852,8	4988977,9
NS056	1395888,3	4989044,1
NS057	1395939,8	4989147,7
NS058	1396011,9	4989030,4
NS059	1394985,7	4988774,9
NS060	1394630,0	4985763,4
NS061	1394342,3	4985795,5
NS062	1393970,4	4985786,3
NS063	1393970,3	4985782,7
NS064	1393904,6	4985531,3
NS065	1393901,1	4985519,3
NS067	1393709,0	4985789,6
NS068	1393705,7	4985811,1
NS069	1393313,6	4985859,9
NS070	1393316,2	4985868,3
NS071	1393209,5	4985892,4
NS072	1392531,9	4985948,3
NS073	1391563,3	4986429,8
NS074	1391424,4	4986508,9
NS075	1391275,7	4986192,9
NS076	1393293,0	4986169,6

Node Name	x-coordinate [m]	y-coordinate [m]
NS077	1393513,0	4986724,4
NS078	1393639,8	4986888,1
NS079	1393712,7	4987042,0
NS080	1393716,8	4987043,7
NS081	1393723,4	4987064,8
NS082	1393858,2	4987331,6
NS083	1393930,0	4987558,8
NS084	1393341,5	4987824,7
NS085	1393029,1	4987992,3
NS086	1392981,0	4987899,7
NS087	1392959,6	4987879,5
NS088	1393011,0	4988001,2
NS089	1393023,5	4988012,5
NS090	1393007,9	4988002,8
NS091	1392871,5	4988076,9
NS092	1392678,9	4988181,1
NS093	1392664,0	4988189,1
NS094	1392626,1	4988189,4
NS095	1392596,2	4988184,8
NS096	1392387,3	4988339,7
NS097	1392387,2	4988337,3
NS098	1392251,1	4988531,6
NS099	1392253,5	4988531,4
NS100	1392259,6	4988544,6
NS101	1392080,1	4988635,2
NS102	1391986,8	4988673,2
NS103	1391951,9	4988647,0
NS105	1393981,8	4987630,3
NS106	1394025,3	4987722,0
NS107	1394026,5	4987724,6
NS108	1393925,4	4987784,5
NS109	1394072,4	4987821,0
NS110	1394127,0	4987806,0
NS111	1394085,2	4987850,7
NS112	1394137,0	4987964,8
NS113	1394189,4	4988068,3
NS114	1394261,3	4988217,5
NS115	1394385,6	4988161,2
NS116	1394267,8	4988232,6
NS117	1394269,3	4988235,7
NS118	1394388,3	4988348,7
NS119	1394217,9	4988445,3
NS120	1394047,5	4988508,6
NS121	1393977,1	4988560,6
NS122	1393839,5	4988620,6
NS123	1393769,5	4988868,4
NS124	1393718,8	4988914,0
NS125	1393663,1	4988935,1
NS126	1393555,5	4988989,6
NS127	1393474,1	4989103,4
NS128	1393420,0	4989133,5
NS129	1393334,8	4989176,9
NS130	1393332,4	4989178,1
NS131	1393123,1	4989287,9
NS132	1393117,9	4989290,5
NS133	1393006,1	4989347,6
NS134	1392920,6	4989391,0
NS135	1392917,9	4989392,3
NS136	1392877,3	4989413,0
NS137	1392809,2	4989383,9
NS138	1392800,3	4989269,7
NS139	1392699,0	4989201,3
NS140	1392268,7	4989256,8
NS141	1392269,7	4989258,7
NS142	1392209,5	4989284,3
NS143	1392201,6	4989269,3
NS144	1391989,0	4989183,6
NS145	1391899,9	4988909,1
NS146	1391929,7	4988654,6
NS147	1396037,0	4989097,9
NS148	1395617,8	4988852,3
NS150	1394632,1	4988211,9
NS151	1394679,1	4988232,1
NS152	1394685,6	4988247,0
NS153	1394885,5	4988634,6
NS154	1392129,6	4989511,8
NS155	1392149,4	4989877,9
NS156	1392148,4	4989883,3
P002	1395307,7	4983843,3
P010	1394964,9	4986192,0
P015	1395420,4	4987979,3
P058	1391977,6	4988681,0
P061	1394221,3	4988460,0
P063	1393972,2	4988550,9
P065	1393838,1	4988617,9
P066	1393766,8	4988869,8
P067	1393716,8	4988910,2
P068	1393658,3	4988925,6
P06A	1395621,1	4983970,1
P070	1393484,9	4989117,7
P071	1393415,8	4989132,3

Node Name	x-coordinate [m]	y-coordinate [m]
P072	1393331,3	4989169,7
P073	1393334,9	4989182,9
P074	1393120,8	4989280,0
P075	1393121,6	4989294,8
P076	1392915,0	4989380,8
P077	1392923,7	4989403,2
P078	1392805,4	4989384,3
P079	1392696,5	4989196,5
P081	1392798,5	4989269,8
P082	1392874,6	4989409,8
P090	1394881,2	4988637,6
P091	1394629,8	4988207,4
P092	1394032,7	4987531,6
P094	1393007,3	4989341,8
P095	1393554,4	4988993,6
P097	1392278,5	4989256,4
P301	1395230,4	4988712,9
P302	1395327,2	4988761,1
P303	1395348,8	4988741,5
P304	1395413,2	4988729,5
P305	1395428,1	4988712,3
P306	1395527,7	4988707,2
P307	1395566,0	4988690,4
P308	1395621,9	4988659,4
P309	1395625,7	4988677,4
P310	1395707,4	4988625,6
P311	1395722,7	4988634,5
P312	1395288,6	4988931,4
P313	1395302,2	4988944,4
P314	1395459,4	4988902,2
P315	1395582,0	4988871,9
P316	1395678,9	4988850,8
P317	1395802,4	4988916,9
P318	1395857,5	4988980,0
P319	1395381,7	4988925,6
P320	1395563,6	4988872,3
P322	1395894,1	4989048,4
P325	1396002,7	4989013,4
P326	1396045,5	4989098,9
P329	1395618,6	4988848,1
P407	1394871,5	4989811,0
P408	1394882,3	4989829,4
P411	1395108,5	4990273,1
P412	1395269,8	4990228,3
P414	1394416,0	4990526,4
P415	1394207,1	4990724,8
P421	1393942,1	4990501,1
P425	1392828,6	4990710,6
P427	1392715,4	4990706,5
P457	1392111,1	4989871,0
P461	1394095,0	4992441,5
P464	1393034,5	4992734,5
P465	1393013,5	4993067,1
P467	1392046,5	4992780,9
P468	1391936,8	4992565,9
P469	1392124,6	4993020,5
P470	1391897,3	4992569,2
P490	1394369,5	4992483,2
P491	1394439,9	4992472,0
P492	1394448,6	4992539,6
PM001	1395269,4	4988770,1
PM002	1395253,5	4988799,5
PM003	1395380,4	4988919,5
PM004	1395698,6	4988644,6
PM005	1395716,4	4988656,2
PM006	1395753,7	4988807,3
PM007	1395760,7	4988830,8
PM008	1395737,3	4988820,9
PM009	1395849,8	4988966,0
PM010	1395951,9	4989141,5
PM011	1395944,7	4989156,7
PM012	1395018,8	4990345,6
PM026	1392486,8	4988249,7
R109	1394896,1	4985710,5
R110	1394903,5	4985734,6
R1BI	1394905,9	4985707,5
R1MO	1394888,1	4985712,9
R1OS	1394915,0	4985731,1
R1VI	1394892,0	4985738,1
R206	1394023,2	4987535,4
R207	1394031,1	4987531,9
R2IN	1394006,1	4987519,6
R2MN	1394015,4	4987539,0
R2TU	1394031,2	4987532,3
R3IN	1392978,6	4985909,5
R3US	1392965,9	4985907,9
R402	1392227,6	4993066,8
R4M3	1392227,2	4993063,8
R4R1	1392234,4	4993073,0
R4R2	1392244,3	4993071,7
R4TC	1392224,6	4993067,5

Node Name	x-coordinate [m]	y-coordinate [m]
R4TE	1392224,2	4993063,9
R4TN	1392225,5	4993074,1
RPN06	1394254,2	4990856,6
RPNU	1394225,1	4990855,4
RPO06	1394255,8	4990845,6
RPOU	1394226,7	4990844,4
RPS06	1394257,3	4990835,4
RPSU	1394228,1	4990834,2
TBI01	1395396,1	4985742,6
TBI02	1395395,5	4985747,5
TBI05	1395386,2	4985741,3
TBI06	1395376,3	4985740,1
TBICA	1395405,4	4985748,8
TBIU	1395366,3	4985738,8
TMN01	1391996,8	4988626,1
TMN03	1391982,6	4988637,1
TMN04	1391983,0	4988642,1
TMN05	1391991,9	4988626,4
TMN06	1391981,9	4988627,1
TMN07	1391928,4	4988636,0
TMNAL	1391928,6	4988638,5
TMNMO	1392006,8	4988625,3
TMNTS	1391930,9	4988635,8
TMO01	1395549,7	4983011,1
TMO02	1395686,5	4983086,8
TMO03	1395566,9	4983056,1
TMO04	1395544,8	4983013,7
TMO07	1395533,9	4983002,4
TMO08	1395525,1	4983007,1
TMOGT2	1395544,6	4983067,3
TMOGT3	1395697,6	4983108,9
TMOU	1395519,7	4983018,3
TP015	1394256,3	4990859,9
TPO01	1394279,8	4990854,1
TPO12	1394274,9	4990853,4
TPO13	1394269,6	4990854,7
TPO14	1394259,8	4990853,2
TPO16	1394255,2	4990850,1
TPO17	1394256,9	4990838,4
TPOCA	1394280,3	4990851,2
TTN01	1390944,9	4995463,2
TTN02	1390989,5	4995353,8
TTN03	1390938,5	4995393,3
TTN04	1390945,1	4995383,3
TTN05	1390951,7	4995373,3
TTN06	1391019,2	4995277,2
TTN07	1391014,2	4995273,9
TTN15	1391015,7	4995271,7
TTN16	1391017,1	4995269,5
TTN17	1391022,6	4995261,1
TTNCA	1390934,8	4995398,9
TTNCG	1390923,2	4995448,9
TTNU	1391028,1	4995252,8
CM023	1392147,2	4990108,6

Appendix D - Barycenters data

Limit mass flow rate values exchanged in each barycenter node are considered (Table ….) in order to find a linear relation between the global mass flow rate at the power plants and the user request.

Barycenter Node Name	**Gb_{max} [kg/s]**
NMN02	2,584
NMN03	4,276
NMN04	1,393
NMN06	2,399
NMN07	1,36
NMN08	8,248
NMN09	3,735
NMN11	2,761
NMN12	8,757
NMN13	3,735
NMN14	7,69
NMN15	8,207
NMN16	1,337
NMN18	1,195
NMN19	13,908
NMN20	2,59
NMN22	7,29
NMN24	1,192
NMN25	2,338
NMN26	2,597
NMN27	15,513
NMN29	27,746
NMN52	7,606
NMN54	0,16
NMN56	1,735
NMN57	1,71
NMN58	4,273
NMN59	1,974
NMN60	0,787
NMN61	1,839
NMN63	3,927
NMN64	1,574
NMN65	0,747
NMN66	1,47
NMN69	5,002
NMN71	3,514
NMN72	4,45
NMN73	2,28
NMN74	5,456
NMN75	1,887
NMN76	8,207
NMN77	53,644
CB001	16,272
CB005	11,318
CB006	28,364
CB007	37,525
CB009	34,176
CB011	45,041
CB012	203,517
CB013	63,056
CB014	80,045
CB016	56,634
CB017	17,819
CB019	26,665
CB020	31,631
CB021	22,812
CB023	16,985

Barycenter Node Name	Gb_{max} [kg/s]
CB024	81,175
CB025	43,578
CB026	85,849
CB027	82,81
CB028	122,566
CB029	57,414
CB030	69,062
CB031	51,369
CB033	123,174
CB034	54,434
CB035	89,948
CB036	46,821
CB037	20,35
CB038	64,214
CB054	44,144
CB055	91,469
CB056	53,076
CB057	31,422
CB06B	0,186
CB10B	39,466
CB15B	108,001
CB17B	43,934
CB261	16,375
CB263	21,443
CB264	9,713
CB265	23,687
CB266	0,615
CB291	135,592
CB292	37,209
CB294	26,431
CB29B	31,741
CB401	7,239
CB402	14,32
CB403	8,118
CB404	31,134
CB406	90,411
CB410	68,595
CB413	69,47
CB418	131,072
CB419	34,815
CB420	12,3
CB422	33,989
CB423	5,661
CB424	37,736
CB426	26,243
CB429	102,954
CB430	30,227
CB431	7,054
CB432	136,544
CB433	24,719
CB440	156,866
CB441	52,9
CB442	69,908
CB443	54,802
CB445	45,692
CB447	36,222
CB456	2,976
CB462	18,522
CB463	15,051
P002	136,954
P010	148,531
P015	14,823
P058	31,543
P061	3,511
P063	75,202
P065	6,902

Barycenter Node Name	**Gb$_{max}$ [kg/s]**
P067	19,704
P068	16,201
P06A	2,649
P070	59,702
P071	3,814
P072	20,681
P073	4,31
P074	15,568
P075	12,391
P076	12,774
P077	9,107
P078	17,564
P079	47,944
P081	18,775
P082	2,8
P090	4,97
P092	17,936
P095	14,211
P097	4,382
P301	8,912
P302	5,675
P303	2,808
P304	0,966
P305	2,522
P306	11,249
P308	2,977
P309	7,252
P310	8,275
P311	14,687
P312	8,22
P313	3,898
P314	0,811
P315	6,663
P316	3,072
P317	4,472
P319	8,869
P320	0,327
P322	11,799
P325	39,937
P326	1,404
P407	14,504
P408	43,949
P411	43,139
P412	17,312
P414	62,886
P415	1,705
P421	62,452
P425	13,111
P427	4,717
P461	7,103
P464	14,478
P465	7,655
P467	20,394
P468	21,562
P469	21,645
P470	13,727
P490	9,503
P491	14,838
P492	20,435

Appendix E - Power plants limit mass flow rate

Power Plants	**Gpp_max [kg/s]**
Moncalieri	2070
TorinoNord	876
TorinoNord-Storages	694
Politecnico	1015
Martinetto-Storages	694
BIT	1015

Appendix F - Temperature Boundary conditions

If the return network is considered, temperature in each barycenter node has to be set as boundary condition to solve the thermal problem. For the sake of simplicity, in a single scenario these temperatures are set equals to a unique value, that has been identified according to historic data provides by IREN. Temperatures of the mass flow rates injected in the barycenter nodes is reported in the Table below.

	Inlet Temperature [K]
SCENARIO 25%	322
SCENARIO 50%	325.2
SCENARIO 75%	327
SCENARIO 100%	331.7

Appendix G - Other Data

Specific Heat [J/kg K]	c_p	4186
Fluid Density [kg/m^3]	ρ	1000
Global Conductance [W/m^{2}K]	U	0.06
T Supply [K]	T_{sup}	393
T Environment [K]	T_{env}	280
Friction Factor [-]	f	0.001

Ringraziamenti

Ora riprendo finalmente il mio italiano per ringraziare tutti coloro che mi hanno aiutato, criticato, supportato, sopportato in questi mesi di lavoro per la tesi e in questi anni di università. Grazie, questo diploma di laurea è anche un po' vostro.

Un ringraziamento particolare va anzitutto al professor Vittorio Verda e all'ingegner Elisa Guelpa, miei relatori; guide fondamentali per la stesura di questa tesi, che mi hanno dimostrato grande gentilezza e disponibilità, con uno spirito sempre cordiale. A loro la mia gratitudine, a me la responsabilità per ogni errore.

Tra le persone a me care, ce ne sono alcune che non posso permettermi di dimenticare.

Grazie alla mia amica Sabrina, vero punto fisso fin dai tempi del liceo, per esserci sempre stata nonostante la distanza, per avermi sempre fatto ragionare. Ti auguro ogni bene.

Grazie a *le Caninese*, Anna, Martina e Valentina, e a mio cugino Diego, che mi ricordano ogni volta quanto è bello tornare a CASA.

Grazie a Giancarlo, mio matematico di fiducia. Il caldo umido dell'aula studio mi manca di già.

Grazie a Lorenzo, per avermi introdotto in questa città quando ero poco più che un turista.

Grazie a Giovanni, per il supporto di questi mesi; quello skyline nella presentazione della tesi è la tua firma.

Grazie agli indimenticabili Andrea, Francesco e Gabriele, amici di rara generosità, per il supporto negli anni intensissimi della triennale, per avermi sfamato con i vostri pacchi *da giù* (buoni), per avermi sempre fatto sentire uno di casa.

Un grazie speciale al mio fratellone Daniele: lui non lo sa ma, sette anni fa, ho avuto il coraggio di iniziare tutto questo soprattutto grazie al suo esempio. Ti voglio bene.

Infine il ringraziamento più grande di questa pagina, quello ai miei genitori Gianni e Wilma: per aver creduto in me, per avermi sempre dato il consiglio giusto, per non avermi mai lasciato solo. A voi devo TUTTO! GRAZIE!

E grazie a tutti!